



U.S. Department of Energy
**Energy Efficiency
and Renewable Energy**

Bringing you a prosperous future where energy
is clean, abundant, reliable, and affordable

ENERGY STORAGE RESEARCH & DEVELOPMENT

*Less dependence on foreign oil, and eventual transition to
an emissions-free, petroleum-free vehicle*

*FreedomCAR and Vehicle
Technologies Program*

**2004
ANNUAL
PROGRESS
REPORT**



Acknowledgement

We would like to thank all our program participants for their contributions to the programs and to all the authors who prepared the sections that comprise this report. In addition, we would like to express our sincere appreciation to Dr. Jack Deppe for compiling this report and to Sentech, Inc. for their artistic and technical contributions in preparing and publishing this report.

**U.S. Department of Energy
FreedomCAR and Vehicle Technologies Program
1000 Independence Avenue S.W.
Washington, D.C. 20585-0121**

FY 2004

**Progress Report for
Energy Storage Research and Development**

**Energy Efficiency and Renewable Energy
FreedomCAR and Vehicle Technologies**

**Edward J. Wall
Program Manager, FreedomCAR and Vehicle Technologies**

**Tien Q. Duong
Manager, Energy Storage R&D**

January 2005

TABLE OF CONTENTS

I.	INTRODUCTION	1
	I.A. FreedomCAR and Vehicle Technologies Program Overview.....	1
	I.B. Energy Storage Research & Development Overview.....	1
II.	BATTERY TECHNOLOGY DEVELOPMENT	3
	II.A. System Development	3
	II.A.1 Vehicle High-Power Energy Storage	3
	II.A.2 Electric Vehicle Battery Research and Development	16
	II.B. Technology Assessment	17
	II.C. Benchmark Testing	18
	II.D. Small Business Innovative Research (SBIR)	18
III.	APPLIED BATTERY RESEARCH	20
	III.A. Introduction.....	20
	III.B. More Accurate Life Predication	22
	III.B.1 Introduction	24
	III.B.2 Aging Characteristics of High-Power Cells	25
	III.B.3 Diagnostic Results on Aged Cells	28
	III.B.4 Electrochemical Modeling of Aged Cells	33
	III.B.5 More Accurate Life Prediction Methodology Development.....	35
	III.C. Understand and Enhance Low Temperature Performance	38
	III.C.1 Introduction	38
	III.C.2 Low-Temperature Performance Characteristics.....	40
	III.C.3 Low-Temperature Electrolyte Modeling.....	43
	III.D. Understand and Enhance Abuse Tolerance	47
	III.D.1 Introduction	48
	III.D.2 Thermal Abuse	49
	III.D.3 Overcharge Abuse	60
	III.E. Cell Level Cost Reduction	63
	III.E.1 Introduction	64
	III.E.2 Material Screening and Development	65
	III.E.3 Gel-Polymer Electrolyte Technologies	70
	III.E.4 Low-Cost Flexible Cell Packaging	72
IV.	LONG-TERM RESEARCH.....	77
	IV.A. LiNiCoMnO ₂ and Spinel Systems: Performance and Limitations	80
	IV.B. Electrolyte Limitations	91
	IV.C. New, High Energy Materials	96

IV.D. LiFePO ₄ System: Performance and Limitations	101
IV.E. Li/Polymer Component Limitations	109
APPENDIX: CONTRIBUTORS.....	119

I. INTRODUCTION

Our nation's energy security depends significantly on the efficiency of our transportation system and on which fuels we use. Transportation in the United States already consumes much more oil than is produced here at home. Domestic oil production has been dropping steadily for over 20 years, and by 2025 it is predicted that about 70% of our oil will be imported. Importing oil will remain a problem, because our petroleum resources are far away and found mostly in politically or environmentally sensitive areas. Another cloud on the horizon is the rapidly escalating worldwide demand for oil, especially in countries such as China and India, where the number of motor vehicles in use is growing much more quickly than here in the United States. The challenge is for the United States to work towards energy independence and market leadership while maintaining consumer choice and mobility.

I.A. FreedomCAR and Vehicle Technologies Program Overview

The U.S. Department of Energy (DOE) FreedomCAR & Vehicle Technologies (FCVT) Program¹ works with industry to develop advanced transportation technologies that reduce the nation's use of imported oil and improve its air quality. The program also maintains a diverse set of research and development (R&D) activities in light and heavy vehicle technologies. Some of the technologies being supported by FCVT include hybrid drive system technologies including advanced energy storage devices, power electronics, and motors; advanced structural materials; and advanced combustion and fuels.

Collaboration with automakers enhances the potential for success and the relevance of these programs. With this in mind, on January 9, 2002 the United States Department of Energy (DOE) and the United States Council for Automotive Research (USCAR) — representing DaimlerChrysler Corporation, Ford Motor Company, and General Motors Corporation — announced the creation of the FreedomCAR and Fuel Partnership.² This partnership is focused on funding high-reward/high-risk research that promises improvements in critical components needed for more fuel efficient, cleaner vehicles and provides ongoing guidance and expertise to FCVT activities.

I.B. Energy Storage Research & Development Overview

Energy storage technologies, including batteries as well as ultracapacitors, have been identified as critical enabling technologies for advanced, fuel-efficient, light- and heavy-duty vehicles. The Energy Storage Research and Development Effort within the FCVT Program is responsible for researching and improving advanced batteries for a wide range of vehicle applications, including hybrid electric vehicles (HEVs), battery electric vehicles (EVs), and fuel cell vehicles (FCVs). The office is working in close partnership with the automotive industry, represented by the United States Advanced Battery Consortium (USABC).³

¹ See <http://www.eere.energy.gov/vehiclesandfuels/>.

² For more information, please see http://www.uscar.org/Media/2002issue1/p1_freedomcar.htm, or www.eere.energy.gov/vehiclesandfuels/pdfs/program/fc_fuel_partnership_plan.pdf.

³ The USABC partnership was formed in 1991 between DaimlerChrysler, Ford, and General Motors to initiate a domestic advanced battery industry based on new technology.

The current effort is comprised of three major activities: battery technology development, applied battery research, and long-term exploratory research. A summary of the work done in each of these areas is presented below:

Battery Technology Development is subdivided into three closely related sets of activities: full system development, technology assessment, and benchmark testing.

- **Full System Development** — In cooperation with the USABC, efforts are focused on developing and evaluating lithium-battery technologies and designs for advanced vehicles. Specifically, this work is focused on the development of batteries for HEVs, 42-volt (42V) vehicle systems, and FCVs; and on the development of battery technologies to enable commercially competitive, full-function EVs.
- **Technology Assessment** — Technology assessments are conducted on newly emerging technologies prior to full system development. These 12-month projects assess a developer's overall capabilities and validate technical claims through independent testing. Current assessment projects include cells based on Li-ion gel technology, spinel-based chemistries, and a new LiFePO₄ cathode active material.
- **Benchmark Testing** — Benchmark testing of emerging technologies is important for remaining abreast of the latest industry developments. Working with the national laboratories, FCVT purchases and independently tests hardware against the manufacturer's specifications and the most applicable technical targets.

Applied Battery Research is focused on addressing the cross-cutting barriers that face Li-ion systems which are closest to meeting all of the energy and power requirements for vehicle applications. Five national laboratories participate in this activity, each bringing its own expertise to remaining critical barrier areas: life, abuse tolerance, low temperature performance, and cost.

Long-term Battery Research addresses fundamental problems of chemical instabilities that impede the development of advanced batteries. This research provides a better understanding of why systems fail, develops models that predict system failure and permit system optimization, and investigates new and promising materials. The work presently concentrates on research into several promising systems, including LiNiCoMnO₂, LiFePO₄, Li/Polymer, and new high power and energy materials such as composite cathodes and non graphitic anodes.

This report highlights the activities and progress achieved in the Energy Storage Research and Development Effort during FY 2004. We are pleased with the progress made during the year and look forward to continued work with our industrial, government, and scientific partners to overcome the challenges that remain to delivering advanced energy storage systems for vehicle applications.

Tien Q. Duong
Manager, Energy Storage Research and Development
FreedomCAR and Vehicle Technologies Program

II. BATTERY TECHNOLOGY DEVELOPMENT

Introduction

One of the primary objectives of the Energy Storage Effort is the development of advanced batteries and ultracapacitors for use in electric and hybrid electric vehicles. This activity is subdivided into four mission areas: (1) System Development, aimed at developing advanced battery systems for a wide range of vehicle applications; (2) Technology Assessment, to assess developers' current capabilities and validate technical claims; (3) Benchmark Testing of emerging technologies in order to remain abreast of the latest industry developments; and (4) Small Business Innovative Research (SBIR), that provides valuable support to electric vehicle (EV) and hybrid electric vehicle (HEV) battery development efforts.

II.A. System Development

System Development is divided into two programmatic areas: (a) Vehicle High Power Energy Storage, focusing on the development of batteries for hybrid electric vehicles (HEVs), 42-volt (42V) vehicle systems, and Fuel Cell Vehicles (FCVs); and (b) Electric Vehicle Battery Research and Development, that supports the development of battery technologies to enable commercially competitive, full-function EVs. All battery system development for light-duty vehicles is conducted in collaboration with industry through the United States Advanced Battery Consortium (USABC). All of the USABC subcontracts to develop advanced light vehicle batteries for hybrid and electric vehicles are awarded under a competitive process and are cost-shared.

II.A.1 Vehicle High-Power Energy Storage

Introduction

Vehicle High-Power Energy Storage research is part of a multifaceted effort within the Department of Energy's (DOE's) FreedomCAR and Vehicle Technologies (FCVT) Program to develop and perfect the technologies needed to encourage the adoption of cleaner, more fuel-efficient hybrid electric vehicles in the commercial marketplace. Lightweight, durable, and affordable high-power energy storage devices are one of the critical technologies essential for the continuing development of hybrid electric vehicles, 42V vehicular systems, and FCVs. Vehicle High-Power Energy Storage research focuses on overcoming the main technical barriers associated with commercialization of these advanced vehicles by concentrating on four major areas, namely:

Cost

The current cost of lithium-based batteries (the most promising high-power battery chemistry) is prohibitively high on a kW or kWh basis. The main cost drivers being addressed are the high cost of raw materials and materials processing, and cell and module packaging cost.

Performance

The barriers related to battery performance are the reduced discharge pulse power that is available at low temperatures and the loss of available power over time due to use and aging.

Abuse Tolerance

High power batteries are not intrinsically tolerant to abuse such as short circuits, overcharge, over-discharge, mechanical shock, vibration, crush, or exposure to fire and/or other high temperatures. Multiple strings of cells pose a problem for lithium-based technologies because they require overcharge and over-discharge protection at the cell level. In addition, challenging thermal management issues need to be addressed.

Life

Hybrid systems with conventional engines have a life target of 15 years, and battery life goals have been set to meet these targets. The cycle life goal of 300,000 cycles has been attained in laboratory tests and the calendar life of lithium-based batteries is estimated to be 15 years, according to reports from Saft America Inc.⁴

The Vehicle High-Power Energy Storage Program was created to develop solutions to these technical challenges by developing low-cost, high-power batteries that meet or exceed the energy storage requirements for hybrid electric vehicles, 42V vehicular systems, and fuel cell vehicles, as shown in Tables II-1 thru II-3, respectively. Note that these requirements have been developed in close coordination with industry through the USABC technical teams.

Specific objectives of the Vehicle High-Power Energy Storage activity include:

- By 2010, develop an electric drive train energy storage device with a 15-year life at 300Wh with a discharge power of 25 kW for 18 seconds and \$20/kWh cost.
- Reduce the production cost of a high-power 25-kWh battery (light vehicle) from \$3000 to \$750 in 2006 and to \$500 in 2010 (priority FCVT goal).
- Establish and continuously reaffirm performance and cost targets for batteries covering the full range of applications, including 42V systems, HEVs, and FCVs.
- Develop hardware for specific applications that can be tested against respective performance targets and used for subsystem benchmarking.

Two candidate battery chemistries have been identified as the most likely to meet these performance and cost targets: NiMH and lithium-based technology. NiMH batteries offer relatively good power capability as a result of the good ionic conductivity of the potassium hydroxide electrolyte. Lithium-based batteries offer excellent energy density that can be traded for higher power.

The USABC has supported development of these two technologies since the program's inception in 1997 by awarding subcontracts to a number of developers including Saft America (Li-ion and NiMH), VARTA (NiMH), Delphi (Li polymer), AVESTOR (Li polymer), Texaco-Ovonic (NiMH) and Electro Energy (bipolar NiMH). Contracts active in 2004 were with COBASYS (formerly Texaco-Ovonic, NiMH), Saft America (Li-ion), and CPI/LG Chem (Li-ion polymer).

⁴ K. Nechev, et al., Saft America, Inc., Improvements in Saft Li-Ion Technology for HEV and 42V Systems, 2nd Advanced Automotive Battery Conference, Las Vegas, February 2001.

Table II-1. Energy Storage Targets for High-Voltage, Power-Assist Hybrid Electric Vehicles

Characteristics	Minimum Value	Maximum Value
Pulse discharge power (kW)	25 (for 10 seconds)	40 (for 10 seconds)
Maximum regenerating pulse (10 s; kW)	20 (50 Wh pulse)	35 (97 Wh pulse)
Total available energy (kWh)	0.3	0.5
Round trip efficiency (%)	>90–25 Wh cycle	>90–50 Wh cycle
Cycle life for specified SOC increments (cycles)	300k 25-Wh cycle (7.5 MWh)	300k 50-Wh cycle (15 MWh)
Cold-cranking power at –30°C (three 2-sec pulses, 10-s rests between; kW)	5	7
Calendar life (years)	15	15
Maximum weight (kg)	40	60
Maximum volume (liters)	32	45
Production price @ 100k units/year (\$)	500	800
Maximum operating voltage (Vdc)	<400 maximum	<400 maximum
Minimum operating voltage (Vdc)	>0.55 × V _{max}	>0.55 × V _{max}
Maximum self-discharge (Wh/d)	50	50
Operating temperature (°C)	–30 to +52	–30 to +52
Survival temperature (°C)	–46 to +66	–46 to +66

Table II-2. Energy Storage Targets for 42V Systems: M-HEV^a and P-HEV^b

Characteristics	M-HEV Commercialization Goals	P-HEV Commercialization Goals
Pulse discharge power (kW)	13 (for 2 seconds)	18 (for 10 seconds)
Regenerative pulse power (kW)	8 (for 2 seconds)	18 (for 2 seconds)
Engine-off accessory load (kW)	3 (for 5 Minimum)	3 for 5 minutes
Available energy (Wh @ 3 kW)	300	700
Recharge rate (kW)	2.6 kW	4.5 kW
Energy efficiency on load profile (%)	90	90
Cycle life, profiles (engine starts)	150 k (450 k)	150 k (450 k)
Cycle life and efficiency load profile	Partial power assist (PPA)	Full power assist (FPA)
Cold cranking power @ –30°C (kW)	8 (21 V minimum)	8 (21 V minimum)
Calendar life (years)	15	15
Maximum system weight (kg)	25	35
Maximum system volume (liters)	20	28
Self discharge (Wh/day)	< 20	< 20
Maximum operating voltage (Vdc)	48	48
Maximum open circuit voltage (Vdc)	48 (after 1 sec.)	48 (after 1 sec.)
Minimum operating voltage (Vdc)	27	27
Operating temperature range (°C)	–30 to 52	–30 to 52
Selling price (\$/system @ 100-k units)	260	360

^a Mild hybrid electric vehicle (M-HEV)

^b Power-assist hybrid electric vehicle (P-HEV)

Table II-3. Energy Storage Targets for 42V Systems: M-HEV and P-HEV

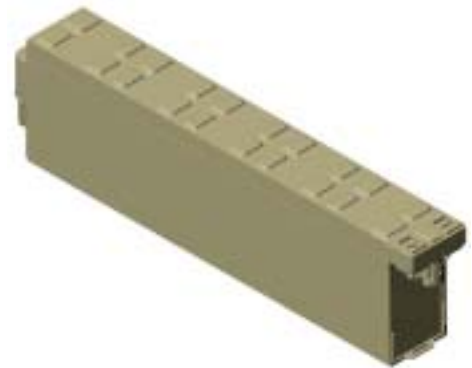
Characteristics	Minimum	Maximum
Pulse discharge power (kW)	25 (for 18 s)	75 (for 18 s)
Maximum regeneration pulse (kW)	22 (for 10 s)	65 (for 10 s)
Total available energy (kWh)	1.5	5
Round trip efficiency (%)	>90	>90
Cycle life (cycles)	TBD (15 year life equivalent)	TBD (15 year life equivalent)
Cold-start at -30°C (TBD kW for TBD min.; kW)	5	5
Calendar life (years)	15	15
Maximum weight (kg)	40	100
Maximum volume (liters)	30	75
Production price @ 100k units/year (\$)	500	1,500
Maximum operating voltage (Vdc)	≤ 440 maximum	≤ 440 maximum
Minimum operating voltage (Vdc)	≥ 0.5 × V _{max}	≥ 0.5 × V _{max}
Maximum self-discharge (Wh/d)	50	50
Operating temperature (°C)	-30 to +52	-30 to +52
Survival temperature (°C)	-46 to +66	-46 to +66

NiMH Battery Development

A multi-year, cost-shared contract with COBASYS (formerly Texaco-Ovonic Battery Systems) was completed in the second quarter of 2004. The focus of this effort was on developing high-power, low-cost, liquid-cooled, multi-cell modules designed to be assembled into full batteries. The module developed in this project is illustrated in Figure II-1 and its properties are presented in Table II-4.

Table II-4. Properties of TOBS NiMH Module

Characteristic	Value
Nominal voltage	12V
Nominal capacity	9 Ah
Nominal power	2.7 kW
Nominal energy (@ 1C rate)	125 Wh
Module weight	2.4 kg
Module volume	1.28 L
Energy density	52 Wh/L
Specific power	1125 W/kg
Power density	2100 W/L

**Figure II-1. COBASYS Series 1000 NiMH Monoblock Module**

Li-ion Battery Development

A contract with Saft to develop high-power cells and modules for the HEV application was also completed in the past year. Saft focused on material cost reduction and process and assembly optimization. The performance and life of the improved low-cost cells were validated in nominal 50-volt modules. At the conclusion of the contract, Saft delivered two full packs to DOE. The packs met all of the FreedomCAR HEV performance targets, except cost, as shown in Table II-5. Two battery packs have completed 300,000 HEV test cycles suffering less than 2% power fade.

Table II-5. Performance of High-Power Li-Ion Batteries (2003)

Performance	Current Li-ion	System target
Specific power (W/kg, 18-s discharge)	900 ⁵	625
Power density (W/L)	1,450	780
Specific energy (Wh/kg)	75	7.5
Cycle life (25-Wh cycles)	300,000 ⁶	300,000
Calendar (years)	15	15
Selling price (\$/system @ 100 k/year)	(Approximately 2–4 times the target value)	500

Twenty-four cells are undergoing testing to determine calendar life at the Idaho National Engineering and Environmental Laboratory (INEEL) at temperatures from 30 to 60°C. After over 600 days, the calendar life at 37.5°C, estimated from a data fit, was approximately 17 years. However, there was considerable spread in the data at test temperatures below 40°C, so a conservative estimated life of 12 years was arrived at by using data representing the lower end of the data band. Five cells are still on test at 30°C and have not shown any measurable power fade.

Li-ion 42-volt (42V) Battery Development

In 2004, the USABC/FCVT Program awarded a contract to Saft America to develop an inherently safe and affordable high power 42V automotive battery. Although the requirements are very challenging, Saft believes that the 42V FCVT Program objectives can be met without compromising any goals, thus providing a 42V battery that is affordable and can be used under extreme conditions both in terms of abuse behavior and performance.

The program objectives and accomplishments to-date are:

- Abuse Tolerance.** The Saft lithium ion battery system is considered safe with all the protection devices and electronics in place. There is room to improve the safety at the cell level in areas such as over-charge, radiant heating, short circuit, and crush. One of the major tasks of this program is to address these issues by evaluating improved cell design and abuse-resistant materials and ultimately developing an inherently safe cell. In this area, a new positive material has been identified for testing. Additionally, new promising hardware is in development.

⁵ Battery performance calculated from cell performance by applying a Burden Factor based on battery design.

⁶ K. Nechev, et al., SAFT America, Inc., Improvements in Saft Li-Ion Technology for HEV and 42V Systems, 2nd Advanced Automotive Battery Conference, Las Vegas, February 2001.

- **Battery Life and Prediction Modeling.** Saft is currently developing the appropriate modeling and verification to demonstrate a life of 15 years and 150,000 cycles. Accelerated testing in Cockeysville has shown that a usable life of more than 15 years is possible for HEV systems. Saft's objective for this program is to demonstrate that the USABC/FCVT Program target can also be met. A preliminary model is almost completed.
- **Discharge/Re-gen Power, Energy, and Cold Cranking.** Saft is developing both M-HEV and P-HEV packs to meet 42V requirements. An improved negative material has been selected for better charge acceptance and power.
- **Environmental Impact.** Saft is studying the environmental impact and concerns during manufacture and use of these lithium ion batteries. Recycling options, both in the US and Europe, will be identified.
- **Battery Price.** Saft is focusing on cost-effective design and processing at all levels of component and assembly, based on 100,000 units. As part of this effort, low-cost carbon and a low-cost separator are under evaluation.
- **Deliverables.** 34 full battery systems of each type (M-HEV and P-HEV) will be manufactured and made available for testing.

Li-ion Full Power Assist HEV Battery Development

In 2004, the USABC/FCVT Program awarded a contract to Johnson Controls, Inc. (JCI) to develop and design a Lithium ion 40 kW power assist hybrid battery system. As a major U.S. auto supplier, JCI provides significant promise to realize the aggressive objective of this contract, which is to commercialize a U.S./European based Li-ion battery technology that

- improves the competitive position of U.S. and European automotive OEMs in lithium technology, and
- achieves a U.S. position in key Li-ion technology for automotive use.

As part of this activity, and to achieve the above objective, JCI is designing and building a new cell container that will provide greater abuse tolerance, and internal components that will ultimately become the basis for a 10 Ah cell earmarked for use in the final battery module deliverable.

In addition, JCI with its subcontractor, TIAX, is testing two generations of proprietary cathode materials and a separator material using existing anodes and binders. This new cathode material, originally designed as a high energy material, promises improved abuse tolerance behavior.

JCI will assess the abuse tolerance of a ~10 Ah cell, packaged as modules of approximately 200 Wh of energy. These abuse tolerance tests will evaluate the new chemistry, the new cell design, and ultimately, the integrated module safety approach being used to supplement the chemical and cell level abuse tolerance features. Based on the results of these assessments, JCI will modify its cell and/or module design and then provide 500 Wh modules to Sandia National Laboratories for abuse tolerance validation testing.

To date, JCI has determined that manufacturing efficiency is a critical component of developing and selling a Li-ion battery. Although base materials cost (and safety) continue to be critical barriers that Johnson Controls is addressing, JCI is working in parallel to develop a high-volume, low-cost manufacturing capability that will enable the mass marketing of a competitive Li-ion HEV battery.

Li-ion Polymer Battery Development

In February 2004, Compact Power, Inc. (CPI)/LG Chem was awarded a program to develop Li-ion polymer cell technology for HEV applications using a LiMn_2O_4 spinel-based cathode. This program is a follow-up to a benchmarking study of CPI/LG Chem's cells by the USABC.

LiMn_2O_4 spinel is an attractive cathode for HEV batteries due to the fact that Mn is abundant, environmentally benign, and potentially much more abuse-tolerant than cathodes based on LiCoO_2 , LiNiO_2 , or their analogs. The problem that has hindered the widespread introduction of spinel-based cells is instability at elevated temperatures. Although there is no universal agreement on the exact reason for this, a number of factors have been identified which lead to this degradation. A major issue is leaching of Mn^{2+} into the electrolyte due to attack by HF from the LiPF_6 in the electrolyte. The leached Mn^{2+} also adversely affects the performance of the carbon anode in a full Li-ion cell.

The primary focus of this program, therefore, is to combat this calendar-life issue. Additional major tasks include attainment of the FCVT Program targets of 300,000 cycles, sufficient cold-cranking power at -30°C , and improved abuse-tolerance. This work will be supplemented by studies on module fabrication and development of algorithms to predict state-of-charge (SOC) and state-of-health (SOH) of the spinel-based batteries.

CPI/LG Chem is using a combination of approaches including doping, coating, and the use of additives to enhance the calendar-life of the spinel cells. The experiments are in their early stages and there are good indications that a number of these approaches are yielding results which will significantly improve the calendar life of the spinel cells.

The cycle-life of the baseline cells was determined to be about 160,000 cycles using the Partnership for a New Generation of Vehicles (PNGV) cycling protocol. The cell chemistry has been modified and these modifications have resulted in considerable improvement in cycle life. Although the cycling has not been completed as yet, based on the initial results, the cycle-life is expected to exceed the target of 300,000 cycles.

Thermal and electrochemical abuse studies of spinel-based cells have been initiated in order to improve upon the abuse tolerance of cells, as well as on cathodes and anodes in contact with the electrolyte and its components. The reaction between the carbon anode and EC seems to be the principal contributor to the thermal runaway reactions. These reactions are critically dependent on the SOC of the cell. Efforts are underway to minimize and mitigate the extent of these reactions. Studies with various separators (single or trilayer) indicate that the thermal shutdown separators do not provide the expected protection in high power cells during thermal runaway. The overcharge behavior, on the other hand, depends on the applied current and voltage. Below 8 V, the cells do not exhibit any hazardous behavior irrespective of the current applied (up to 60 A).

CPI is using the Kalman Filter to model the spinel-based cell in order to predict its SOC over the temperature range of -30 to +55°C to an accuracy of $\pm 3\%$. Preliminary data indicate that the model will be capable of predicting the SOC within $\pm 3\%$, a significant improvement over SOC prediction in NiMH batteries.

Low-Cost Separator Development

Studies at the national laboratories have shown that the cost of non-active material components in high-power batteries (packaging, current collectors, and separator) can equal or exceed the cost of the active materials, and the cost of the separator ($\sim \$2/\text{m}^2$) dominates the cost of the non-active materials. The Department of Energy (DOE), in conjunction with the USABC, is supporting research and development to create novel, low-cost materials and to improve processing techniques so that currently available materials may be produced in a less costly manner.

The goal of these tasks is to produce acceptable separators at a cost of $\$1/\text{m}^2$. Contractors engaged in this activity include Celgard, Inc., Advanced Membrane Systems (AMS), and Ultimate Membrane Technologies (UMT). All three contracts have an industry cost-share of at least 50%.

The goal is to develop a direct replacement for current materials having the following properties:

- Thickness: < 25 microns
- Wettability: Complete Wet Out in Electrolytes
- Puncture Strength: $> 300\text{g}/25.4\text{microns}$
- Permeability: MacMullin Number of < 11
- Pore Size: < 1 micron
- Moisture Content: < 50 ppm
- Chemical Stability: Stable in Battery for 10 Years

In addition, the separator should have the capability of shutting down at a temperature of 100–110°C and have structural stability to 200°C.

Some highlights of the FY 2004 Research and Development activities are presented below.

- **Celgard, Inc.** reports that significant progress has been made and that nearly all the specifications listed above have been met. A great deal of valuable knowledge was learned about the process, and information from laboratory studies should lead to simplification of the production process and broaden raw material selection. Unfortunately, a specialty chemical supplier stopped supplying a key material needed in this project, and work is underway to mitigate this issue.
- **AMS** reports that the Phase I effort was successfully completed and yielded a shutdown separator sample with good melt integrity (shutdown behavior of $\sim 110^\circ\text{C}$ and melt temperature of $\sim 175^\circ\text{C}$). Samples were sent to a national laboratory for testing and these results agreed with the AMS claims. AMS is in the process of signing a Phase II, 18-month 50/50 cost-shared contract with the USABC. The objective of this new contract will be further development work to meet the safety, affordability and other HEV cell requirements.

- **UMT** has the goal to develop low-cost micro-porous membrane separators, and to demonstrate the feasibility of scaling up their laboratory process. In this phase, UMT has developed a manufacturing technology for making low-cost micro-porous membrane separators and successfully demonstrated its feasibility on a large scale. The focus of efforts in this second phase will be on low-cost low-temperature shutdown separators for rechargeable lithium batteries based on an innovative non-conventional process.

High Energy Li-S Battery Development

The USABC PolyPlus Li/S Battery Development Program has been extended to March 2005 to develop metallic Li anode, anode protection barrier, electrolyte, and sulfur electrodes. In the first phase, the focus was on the development of adequate protection of the Li metal anode and scale up. Since the protected anode development was delayed the scale up was put on hold and a no cost extension was provided. The extension will permit PolyPlus to develop glass/ceramic anode protection and validate >99% Li cycling.

The production of the Li-ion conducting glass/ceramic barrier has to be pinhole free and easy to laminate with Li metal electrode without damage. The integrity of the barrier will be verified by testing for Li recycling efficiency in the cell or with a reference electrode. The main goal of this remaining program is to develop anode stabilization barrier to prevent soluble polysulfide reacting with the metallic Li anode. The other criterion shall be cost, performance, cycle/calendar life, abuse tolerance and manufacturability.

There are several “Go/No-Go” milestones that are a part of this extended program. The most critical milestone is the Li cycling efficiency. In this phase, 10 cells will be delivered to Lawrence Berkeley National Laboratory (LBNL) for Li cycling verification testing.

Ultracapacitor Development Program

The Maxwell ultracapacitor development program is a two-year program to develop affordable ultracapacitors for automotive applications. Maxwell is currently using a proprietary technology based on a symmetric carbon-carbon electrode with tetraethylammonium tetrafluoroborate (TEATFB) salt in acetonitrile as solvent.

Although the existing Maxwell technology meets most of the requirements for the automotive use, it needs improvements in the areas of weight and volume, energy content, but most importantly cost reduction in the amount of one to two orders of magnitude in order to become economically competitive.

Program Goals. The main goals of this program are to develop Carbon-Carbon (C-C) ultracapacitors that meet the FCVT Program 42V Stop-Start requirements (see Table II-6). Chief among the objectives are:

1. **Cost Reduction.** The cost reduction is addressed in a multi-pronged approach that aims at developing large scale production of activated carbons at or below \$10/kg. Mead-Westvaco is Maxwell’s partner in the activated carbon development. In addition to reducing cost of key materials, design for manufacturing, reduction of part counts by integrating smaller parts,

and process design and improvement, are other methods that will be employed for cost reduction.

2. **Increase Energy Content.** Currently the low energy content of the ultracapacitors leads to a total system size that exceeds FCVT Program volume and weight constraints. Maxwell is using several techniques to address this problem. Chief among these methods are:
 - a. Use of impurity-free activated carbons to allow raising the voltage bar without affecting life.
 - b. Use of asymmetrically designed C-C electrodes.

Table II-6. Ultracapacitor Requirements

FCVT Program Energy Storage Goals		Ultracapacitors ⁷		
Parameter	Unit	12V Start- Stop	42V Start- Stop	42V Transient Power Assist
Discharge Pulse Power	kW	4.2 for 2 sec	6 for 2 sec	13 for 2 sec
Regen Pulse Power	kW			8 for 2 sec
Recharge Rate	kW	0.4	2.4	2.6
Cold cranking power @ -30°C (3 pulses)	kW	4.2 @ $\geq 7V$ for 2 sec	8 @ $\geq 21V$ for 2 sec	
Available Energy	Wh	15 @ 1 kW	30 @ 1 kW	60 @ 1 kW
Calendar Life	years	15		
Cycle Life	cycle	750k cycles for 150k miles		
Energy Efficiency (on Cycle- Life/Load Profile)	%	95 for UC10 ⁸		
Maximum Self-discharge	var.	4% (72 hours from V_{max})		
Maximum Operating Voltage	Vdc	17	48	
Minimum Operating Voltage	Vdc	9	27	
Maximum System Weight	kg	5	10	20
Maximum System Volume	liter	4	8	16
Operating Temperature Range	°C	-30 to +52		
Survival Temperature Range	°C	-46 to +66		
Selling Price @ 100,000 units/year	\$	40	80	130

Milestones. There are several key milestones in the program. The first milestone involves characterizing the baseline cells and modules from performance and abuse tolerance perspectives. 24 baseline cells and five modules will be delivered and subsequently tested at Idaho National Engineering and Environmental Laboratory (INEEL) and Sandia National Laboratories (SNL) to establish the baseline technology. Later, high voltage cells will be delivered as stated in the program goals. The move to higher voltage cells will be initially from 2.5 to 2.75 volts and then later to 3.0 V to assess the impact on cell life. The delivery of 3.0V cells and validation of life and abuse tolerance are scheduled for the early part of 2006.

⁷ FreedomCAR Ultracapacitor Test Manual, Revision 0, DOE/NE-ID-11173, September 2004.

⁸ UC10 is a life cycle test that results in cycles of 10% depth-of-discharge (DOD) @ 100°C rate, please see the FreedomCAR Ultracapacitor Requirements at <http://www.uscar.org/consortia&teams/consortiahomepages/con-usabc.htm>.

Battery Thermal Management

Thermal management of energy storage devices such as batteries is critical to achieve life, performance, cost, and safety target/goals for vehicle applications under the FCVT Program. Poor thermal management could lead to 30% reduction in battery performance and thus a substantial increase in cost, reduced life by five years, and increased chance of poor abuse response. This activity is aimed at addressing issues related to battery thermal control and improving the thermal performance of energy storage devices through thermal characterization and testing, modeling, analysis, and management. The objectives of this research activity include:

- Benchmark and evaluate energy storage technologies.
- Perform electro-thermal analysis to improve the performance and life of cells
- Measure thermal properties.
- Design a new calorimeter for future 42V batteries.
- Thermally model modules and packs.

Electro-Thermal Battery Modeling. The electro-thermal approach has been used to develop the first-ever process/model for analyzing the thermal performance of energy storage devices such as batteries and ultracapacitors. This approach permits the prediction of thermal performance from the electrical behavior of a cell. In this process, the physical details of a cell or module are captured in a finite element modeling software program that can analyze the electrical and thermal behaviors of components and materials. Cell geometry, material properties, and resistances are used to calculate the heat generated in the cell and to predict temperature distributions based on external boundary conditions and power load. This analysis is then used to evaluate the thermal performance of a variety of cell and module technologies.

Thermal Improvement of Lithium-ion Cells. The electro-thermal model was used to evaluate the thermal performance of two proposed Li-ion cell designs by Saft America. Electro-thermal analysis was used to find hot spots in the mile hybrid electric vehicle (M-HEV) cells under transient and steady-state high-power profiles (Figure II-2). Recommendations were made to Saft on which design provided better thermal performance and had fewer hot spots during high transient loads. Also, recommendations were made on how to improve temperature uniformity and thermal design for future Saft cells.

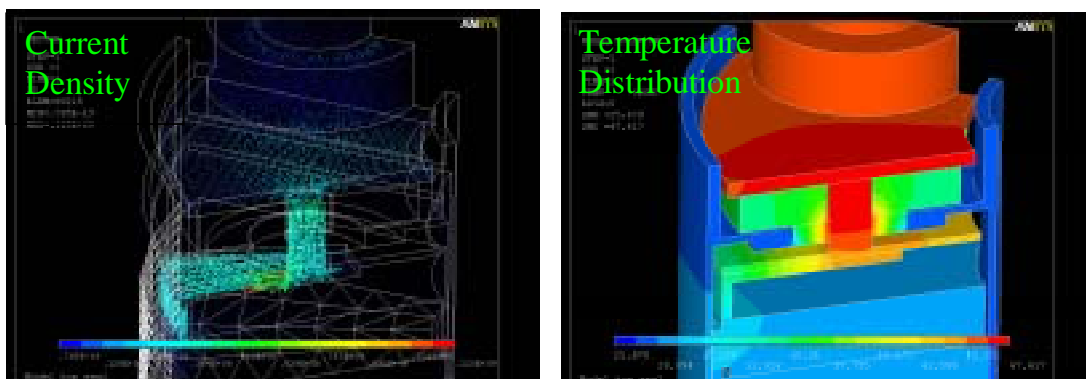


Figure II-2. Electro-thermal analysis of a cell showing current density and temperature distribution

Thermal Benchmarking of a State-of-the-Art NiMH Module. The latest Panasonic NiMH battery module from the Toyota Prius 2004 was tested and the results were compared to the previous generation battery. Both modules were about 7.2 V and 6.5 Ahr. The new module has ~30% more power, and it was found that the new module has a much better thermal signature, less heat generation, and better temperature uniformity than the previous generation (Figure II-3). This was attributed mainly to improved cell-to-cell interconnections, which result in lower local resistance and thus better current density distribution.

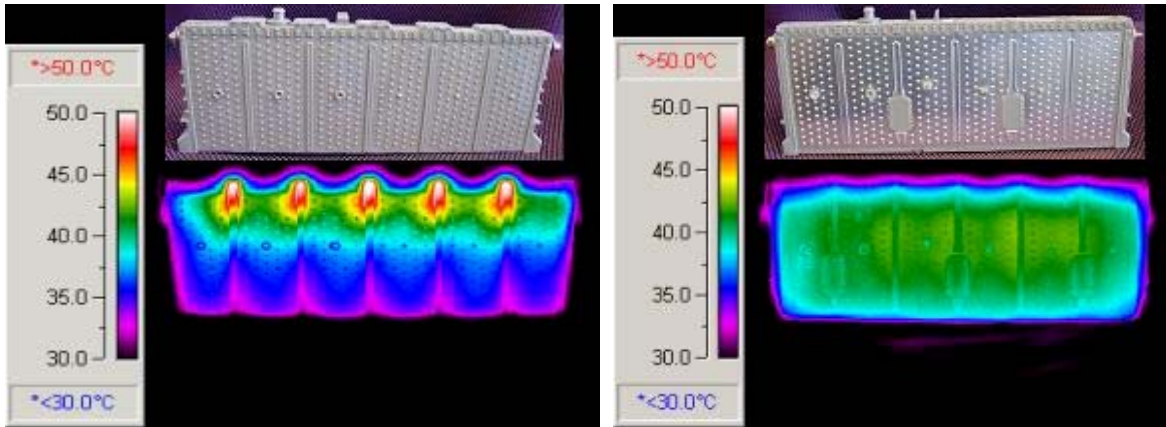


Figure II-3. Thermal Images of the new NiMH module (right) show much-improved temperature uniformity over the previous generation under the same 100 Amp-hour constant discharge.

Thermal Evaluation of Liquid-Cooled 42V Battery Module. A liquid-cooled 42V battery module that consists of 12 cylindrical Li-ion cells (a Saft America deliverable to the FCVT Program) has recently been tested. The tests consisted of measuring the temperature of various cells in the module under the FreedomCAR 25 Wh and 50Wh Life Cycle Test Profiles. The results were compared to a similar (but air-cooled) module previously delivered by Saft (Figure II-4). The comparison indicated that the liquid-cooled module had slightly better thermal performance (lower maximum temperature

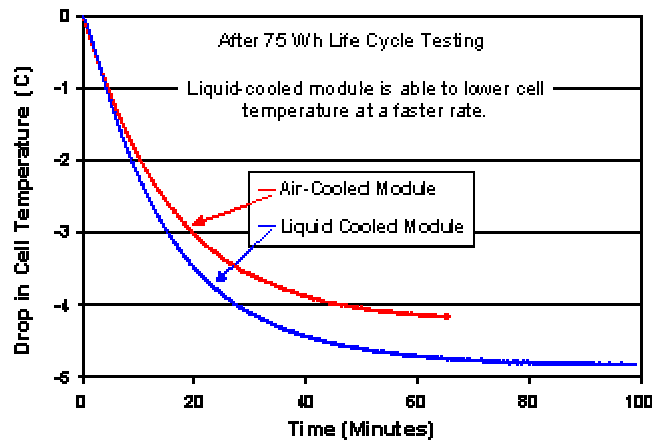


Figure II-4. Comparison of a Saft liquid-cooled and air-cooled modules

and temperature gradient) than the air-cooled module for similar parasitic power for moving air or liquid through the module. The design of the liquid cooled module appears to keep cells below 52°C under aggressive Life Cycle Test Profiles with a coolant below 45°C.

Designing an Improved Calorimeter. Measuring heat generation from high-power energy storage devices is important for designing improved thermal management systems. To thermally characterize future 42V modules, a calorimeter has been designed that allows the testing of large, liquid-cooled 42V modules with improved accuracy. The calorimeter (which measures heat loss and efficiencies) will be able to submerge the test chamber below its isothermal bath and provide a fluid to cool the module at the same time. The calorimeter's margin of error is expected to be less than 2%. When built, this equipment will give the Program a new capability for benchmarking, evaluating, and designing energy storage modules.

Thermal Characterization of Batteries. Researchers collaborated with engineers from Korea Automotive Research Institute and Kokam Engineering (a Korean battery developer) to characterize the performance of two Li-ion polymer cells (one high-energy 100 Ah cell suitable for electric vehicles and one high-power 11 Ah cell for HEVs). The thermal images of the 100Ah cell were obtained under a 200 A discharge and the heat generation from the 11Ah cell was measured under FreedomCAR test procedures at temperatures between -15°C and +30°C. In addition, the two cells were measured under a hybrid pulse power characterization (HPPC) test profile at various temperatures to develop an equivalent circuit model of the technology for ADVISOR™. The results show that this technology has good capacity, power, and efficiency at room temperatures, but needs improvement at cold temperatures.

Energy Storage Simulations

Ultracapacitor Models Developed for Test Manual. An equivalent circuit and electrochemical impedance spectroscopy model was developed for inclusion in the FreedomCAR Ultracapacitor Test Manual. The equivalent circuit model is being designed to be simple, easily accessible, and user friendly, and will help industry perform automated test analyses and characterizations for ultracapacitor simulations from standard test procedures.

Improved NiMH Battery Model. A new battery model with nonlinear behavior was developed and incorporated into ADVISOR™ to better estimate NiMH batteries' state of charge (SOC). NiMH batteries exhibit a more pronounced nonlinear open-circuit voltage than lithium batteries. The model is based on the original resistive/capacitive (RC) battery model, but it uses both open circuit voltage behavior and amp-hour integration to improve SOC predictions. The implementation of this algorithm resulted in ten times better SOC prediction accuracy over repetitive US06 Supplemental Federal Test Procedure (US06) drive cycles. With this model, researchers can have more confidence in the vehicle simulation studies done to estimate the energy storage requirements of FCVs.

Energy Storage Requirements of Fuel Cell Vehicles. An analysis of FCV energy storage requirements was completed for the USABC and the FreedomCAR Energy Storage Technical Team. Based on the optimum combination of fuel economy and cost, the analysis indicated that a midsize hybrid FCV would need an energy storage system with 250 Wh of usable energy and should be able to handle a 20-kW discharge for 12 seconds and 25 kW of regen power for 5 seconds. The study also highlighted that hybridization with energy storage could increase fuel economy by 20%–30%,

depending on the fuel cell system attributes. The FreedomCAR energy storage technical team is recommending these requirements for initial discussion with other technical teams.

Future Directions

The Vehicle High-Power Battery activity will continue to research low cost separators, define energy storage requirements for heavy hybrids, ensure that new materials are made available to manufacturers, and promote information exchange among the various participants in the program. In the thermal analysis area, work will continue to improve the thermal performance of batteries and develop models that enable the evaluation for advanced energy storage concepts for EVs and HEVs.

II.A.2 Electric Vehicle Battery Research and Development

Introduction

Electric vehicle (EV) Battery Research and Development (R&D) supports the development of battery technologies that would enable commercially competitive EVs. The advantage of EVs over other vehicles is that they use no petroleum fuels and produce no emissions. The EV Battery Research and Development activity has had several major successes, including the development and introduction of the NiMH battery for EV use. Over 1000 NiMH battery EVs have been put into service in the past several years. The activity conducts extensive benchmarking studies of advanced batteries from the U.S. and abroad. The technical requirements for the batteries in full-function EVs are defined in Table II-7.

Lithium/Sulfur Battery Development

Lithium/sulfur rechargeable batteries offer several advantages over the current Li-ion rechargeable cells. Because sulfur is inexpensive relative to the lithiated metal oxides used for the cathodes in lithium/ion systems, the lithium/sulfur system has the promise of significantly lower cost per unit energy. In addition, the use of a metallic lithium anode in these cells may allow for improved energy density relative to the lithium/ion system that must use a non-reactive matrix material, such as carbon, for the anode. The complex chemistry of the lithium/sulfur cell may also provide a “shuttle mechanism” that would allow the cell to be overcharged without significant safety problems or other adverse effects. Unfortunately, the lithium/sulfur system is not mature enough for these potential advantages to be demonstrated in commercial cells.

The Department of Energy (DOE), in conjunction with the United States Advanced Battery Consortium (USABC), is supporting research and development on this technology through a long-term contract with PolyPlus, Inc., of Berkeley, CA. The design parameters that affect the charge and discharge performance of a Li/S cell, methods to form encapsulated electrodes having glass protective layers, the formation of thermodynamically stable lithium solid electrolyte interface (SEI), and the use of Li_3N precursor to dramatically improve the performance of the Li/LiPon interface were highlighted as major accomplishments to-date.

Table II-7. U.S. Advanced Battery Consortium (USABC) Goals for Electric Vehicle Batteries

Primary Criterion	Long-term goals ⁹ (2005–2008)
Power Density, W/L	460
Specific Power, W/kg (80% depth-of-discharge [DOD]/30 sec)	300
Energy Density (Wh/L) (C/3 discharge rate)	230
Specific Energy, Wh/kg (C/3 discharge rate)	150
Life (years)	10
Cycle life (cycles)	1,000 (80% DOD) 1,600 (50% DOD) 2,670 (30% DOD)
Power and capacity degradation ¹⁰ (% of rated spec)	20%
Ultimate price ¹¹ (\$/kWh) (10,000 units @ 40 kWh)	<\$150 (desired to 75)
Operating environment	-30°C to 65°C
Recharge time	< 6 hours
Continuous discharge in 1 hour (no failure)	75% (of rated energy capacity)
Secondary Criteria	Long-term goals (2005–2008)
Efficiency (C/3 discharge and C/6 charge ¹²)	80%
Self-discharge	<20% in 12 days
Maintenance	No maintenance. Service by qualified personnel only.
Thermal loss	Covered by self-discharge
Abuse resistance	Tolerant. Minimized by on-board controls.
Specified by contractor: Packaging constraints, Environmental impact, Safety, Recyclability, Reliability, Overcharge/over-discharge tolerance	

Future Activities

Over the next year, Electric Vehicle Battery Research and Development will focus on testing and demonstrating the performance of the lithium/sulfur cells against the USABC requirements.

II.B. Technology Assessment

Technology assessments are conducted in order to validate a developer's technical claims by means of independent testing and to gauge the developer's ability to deliver a full-scale, fully packaged battery. The tests are performed both at the developer's facilities and at the DOE national laboratories in order to familiarize the developer with vehicular requirements and USABC testing procedures. The companies also share in the cost of the testing.

FY 2004 assessment tasks include contracts with Compact Power, Inc. (CPI), a company closely tied to LG Chem of Korea, Valence Technologies, Lithium T Corporation/GAIA, and Hitachi/Shin Kobe. The technologies assessed include cells based on Li-ion gel technology, a Li-ion system using a spinel-based chemistry, and a new LiFePO₄ cathode active material.

⁹ For interim commercialization (reflects USABC revisions of September 1996).

¹⁰ Specifics on criteria can be found in *USABC Electric Vehicle Battery Test Procedures Manual, Rev. 2*, DOE/ID 10479, January 1996.

¹¹ Cost to the original equipment manufacturer.

¹² Roundtrip charge/discharge efficiency.

II.C. Benchmark Testing

Benchmark testing of emerging technologies is important for remaining abreast of the latest industry developments. The FreedomCAR and Vehicle Technologies (FCVT) Program purchases and independently tests hardware against the manufacturer's specifications and the most applicable technical targets. During FY 2004 benchmark testing was performed on a 'sealed' lead-acid 42V battery from Japan Storage Battery (JSB) and a number of ultracapacitors.

II.D. Small Business Innovative Research (SBIR)

The Small Business Innovation Research (SBIR) program was created by the Small Business Innovation Development Act of 1982 (Public Law [P.L.] 97-219) and has been reauthorized until September 30, 2008. The SBIR program was designed to stimulate technological innovation, strengthen the technological competitiveness of small businesses, and use small businesses to meet federal research and development needs. DOE's SBIR funds were used to support projects in 234 small businesses in 34 states. Phase I awards of up to \$100,000 each for about nine months are used to explore the feasibility of innovative concepts. Phase II is the principal research or R&D effort, and the awards are up to \$750,000 over a two-year period.

Over the past several years, SBIR/STTR contracts have provided valuable support to EV and HEV battery development efforts. Phase II contracts (~\$750K ea.) active in FY 2004 are listed below:

- **Eltron Research, Inc.** Novel Lithium Ion Conducting Polymer Electrolytes for Lithium Ion Batteries
- **MER Corp.** Low-Cost Carbon Anodes for Li-ion Batteries
- **T/J Technologies, Inc.** A Novel Cathode Material for High-Power Lithium Rechargeable Batteries
- **Yardney Technical Products, Inc. (Lithion)** Development of Low-Cost Salts for Lithium-Ion Rechargeable Batteries
- **A123 Systems, Inc.** An Advanced Cathode Material for Li-ion Batteries
- **Optodot Corp.** Low-Cost Nanoporous Sol Gel Separators for Lithium-Based Batteries
- **Farasis Energy, Inc. (Previously Called Redox Control)** Stabilized Lithium Manganese Oxide Spinel Cathode for High-Power Li-ion Batteries
- **TIAX, LLC.** LiFePO₄ Cathode Material Designed for Use in Lithium-ion Batteries

The following Phase I Proposals were funded in FY 2004:

- **Enrev Power Solutions.** High Cycle Life Rechargeable Magnesium Batteries for Possible EV Applications
- **EVIONX, Inc.** Nanostructured Non-Carbonaceous Anode and Separator for High Energy and Power Density Rechargeable Li-Ion Batteries
- **Farasis Energy, Inc.** High Energy Density Intermetallic Anode Material for Li-Ion Batteries and Redox Stabilized Li-Ion Rechargeable Cell
- **Foster-Miller, Inc.** Environmentally Benign, High Specific Power Manganese Dioxide-Carbon Pseudocapacitors for Hybrid Vehicles
- **Materials and Systems Research, Inc.** Composite Anode Interlayers for Lithium Batteries with Stable Anode-Electrolyte Interfaces Under High Charging Current Densities
- **Microcoating Technologies, Inc.** Anode Electrolyte Nanocomposites as Alternative to Carbonaceous Anode Materials
- **Phoenix Innovation, Inc.** Polythiophosphonate Electrolytes for Rechargeable Magnesium Batteries
- **TDA Research.** Lithium ion-Channel Polymer Electrolyte for Lithium Metal Anode Rechargeable Batteries

III. APPLIED BATTERY RESEARCH

III.A. Introduction

The Applied Battery Research program is being conducted in support of the FreedomCAR and Fuel Partnership, which is targeting more fuel efficient light duty vehicles that can reduce U.S. dependence on foreign petroleum and reduce emissions, without sacrificing performance across a broad range of vehicles. So, there is an emphasis on developing and improving critical component technologies needed for more fuel efficient and cleaner vehicles. Advanced energy storage technologies are one of these critical components. As has been demonstrated by several commercially available hybrid electric vehicles (HEVs), energy storage devices can help level the load on the prime power source — enhancing efficiency of the prime power source — and can recapture regenerative braking energy to produce more fuel efficient and cleaner vehicles. In order to expand commercial markets for vehicles of this type, better energy storage systems are needed. This program focuses on assisting the industrial developers of high-power Li-ion batteries to overcome key barriers to the commercialization of this promising energy storage technology for light-duty vehicle applications of this type.

The energy storage requirements for HEVs, 42-volt (42V) systems, and fuel cell electric vehicles are presented in Section II. For high-power Li-ion batteries, the key barriers are:

- 15-year calendar life
- Operation between -30°C and $+52^{\circ}\text{C}$
- Selling price of \$20/kWh and
- Adequate abuse tolerance for use in on-road light-duty vehicles

This applied battery research program, denoted the Advanced Technology Development (ATD) program, was initiated to understand the factors that limit calendar life, abuse tolerance, and performance over the desired temperature range of high-power Li-ion cells so that improvements can be made in these three key areas. It addresses cost at the cell level through the identification and/or development of lower-cost cell materials, components, and technologies. The program seeks to understand the cell-level phenomena that control calendar life, abuse tolerance, and operational performance at low temperatures and to improve the cell chemistry to be more chemically, structurally, electrochemically, and thermally stable, as well as being less expensive than those currently used. Conventional Li-ion batteries, of the type used in consumer electronics, employ electronic control circuitry to limit their exposure to abusive conditions, but this program focuses on enhancing the inherent abuse tolerance of the cell chemistry.

This year the program had four focus areas listed below, each associated with one of the barriers:

- more accurate life prediction,
- understanding factors that limit low-temperature performance.
- understanding factors that limit inherent abuse tolerance and enhancing abuse tolerance of cell chemistry, and
- identifying and developing lower-cost cell-level materials, components, and technologies.

The main activities associated with each of these four focus areas are shown in Figure III-1.

Five Department of Energy (DOE) national laboratories collaborate in the execution of this program. Argonne National Laboratory (ANL) is the lead laboratory and provides coordination of the program activities for DOE. The other four participating laboratories are Brookhaven National Laboratory (BNL), Idaho National Engineering and Environmental Laboratory (INEEL), Lawrence Berkeley National Laboratory (LBNL), and Sandia National Laboratories (SNL). Also, the U.S. Army Research Laboratory (ARL) develops advanced low-cost electrolytes for high-power applications. As part of this program, ANL researchers maintain close communications with a large number of international material suppliers, through which they gain access to the latest advanced electrode and electrolyte materials for evaluation in these high-power applications.

In recent years, the program has thoroughly studied and characterized its own Gen2 baseline high-power cell chemistry. Also, it has studied and is studying two variations on the Gen2 chemistry. These three chemistries are listed in Table III-1. The variant carbon (C) cells differ from the baseline cells only in terms of the level of aluminum dopant in the positive electrode (10% vs. 5% for the baseline positive electrode). Both materials were made by the same manufacturer, using the same processes and process conditions. The GDR graphite cells differ from the baseline cells only in terms of the type of graphite employed in the negative electrode. Mag-10 is a synthetic graphite that possesses a flaky morphology, while GDR graphite is a round-edge natural graphite with an amorphous carbon surface coating. All of the extensive accelerated aging and detailed diagnostic studies (to be reported in this section) relate to one or more of these cell chemistries.

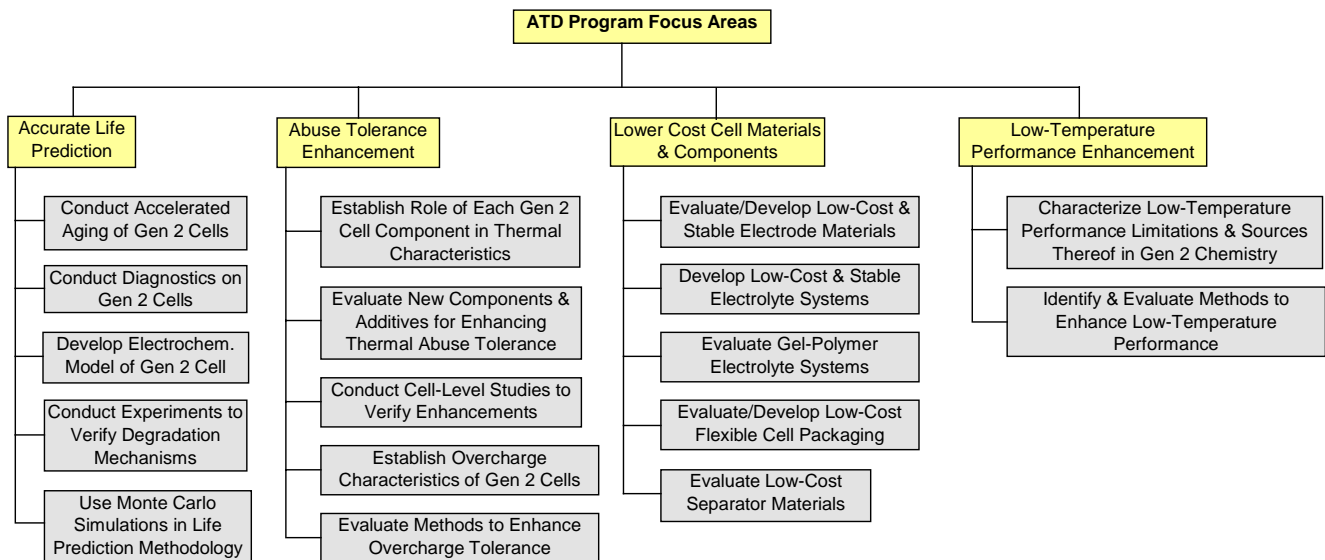


Figure III-1. Diagram of the activities conducted as part of the Applied Battery Research program

Table III-1. Components of the Gen2 Cell Chemistries

Component	Gen2 Baseline Cells	Gen2 Variant C Cells	Gen2 GDR Cells
Positive Electrode	84 wt% $\text{LiNi}_{0.8}\text{Co}_{0.15}\text{Al}_{0.05}\text{O}_2$ 8 wt% PVdF binder 4 wt% SFG-6 graphite 4 wt% carbon black	84 wt% $\text{LiNi}_{0.8}\text{Co}_{0.10}\text{Al}_{0.10}\text{O}_2$ 8 wt% PVdF binder 4 wt% SFG-6 graphite 4 wt% carbon black	84 wt% $\text{LiNi}_{0.8}\text{Co}_{0.15}\text{Al}_{0.05}\text{O}_2$ 8 wt% PVdF binder 4 wt% SFG-6 graphite 4 wt% carbon black
Negative Electrode	92 wt% Mag-10 graphite 8 wt% PVdF binder	92 wt% Mag-10 graphite 8 wt% PVdF binder	92 wt% GDR graphite 8 wt% PVdF binder
Electrolyte	1.2M LiPF_6 in EC:EMC (3:7)	1.2M LiPF_6 in EC:EMC (3:7)	1.2M LiPF_6 in EC:EMC (3:7)
Separator	25 μm thick polyethylene	25 μm thick polyethylene	25 μm thick polyethylene

The following subsections provide technical highlights and progress on the Applied Battery Research program for FY 2004. The information provided is representative only, detailed information is available upon request.

III.B. More Accurate Life Predication

Objectives

- Age Li-ion cells under controlled conditions for diagnostics evaluation, analyze performance.
- Help identify and quantify the factors responsible for power and capacity fade.
- Develop aging protocols and explore new tests, analyses, and modeling methodologies related to calendar and cycle life and provide results to battery developers and other laboratories.
- Develop life models and correlations to gain understanding of fade mechanisms.
- Develop Technology Life Validation Tool (TLVT) methodology, tool, and manual.

Approach

- Continue accelerated aging tests and thoroughly analyze accelerated life test data on Gen2 cells.
- Continue thorough diagnostic studies on Gen2 cell components from new and aged cells.
- Refine and apply cell model to link diagnostic findings to observed performance degradation.
- Employ Monte Carlo simulations in the development of more accurate life predictions.
- Document methodology for the more accurate life prediction of Li-ion cells in TLVT manual.

Accomplishments/Findings

- Completed performance analysis of all available Gen2 characterization and life-testing data.
- Determined that impedance growth at the cathode appears to be the greatest contributor to power fade, and that lithium loss at the anode contributes to capacity fade.
- Refined models to explain the impedance growth with time.
- Completed draft TLVT manual.

Future Studies

Power and Capacity Fade

- Complete life testing and data analyses for the Gen2 Baseline and Variant C cells.
- Provide guidance to aid in the selection of next generation chemistries for analysis by the program.
- Develop phenomenological hypotheses to explain performance degradation and power fade.
- Continue to develop predictive models for calendar life and cycle life.

TLVT Manual

- Solicit developer input and concurrence on TLVT testing methodology.
- Establish the test protocols and number of cells needed to validate the TLVT. Validate TLVT by performing life testing on sample developer cells and performing TLVT testing on them.
- Publish final TLVT manual.

Selected Publications

1. "Overview of Performance Testing of the Advanced Technology Development Program Gen2 Cells," T. Murphy, C. Motloch, J. Christophersen, R. Wright, K. Gering, C. Ho, I. Bloom, S. Jones, G. Henriksen, V. Battaglia, T. Duong, and J. Barnes, Proceedings of the 204th Meeting of The Electrochemical Society, Orlando, FL, October 12–17, 2003, No. 233.
2. "Performance Evaluation of the Advanced Technology Development Program Gen2 Cells," J. Christophersen, K. Gering, C. Motloch, R. Wright, C. Ho, I. Bloom, S. Jones, V. Battaglia and T. Duong, Proceedings of the 204th Meeting of The Electrochemical Society, Orlando, FL, October 12–17, 2003, No. 234.
3. "EIS of ATD Gen2 Lithium-Ion Cells," I. Bloom, S. Jones, G. Henriksen, V. Battaglia, C. Motloch, J. Christophersen, J. Belt, C. Ho, and R. Wright, Proceedings of the 204th Meeting of The Electrochemical Society, Orlando, FL, October 12–17, 2003, No. 235.
4. "Implications of dV/dQ for the Analysis of Performance Fade in Li-Ion Batteries," I. Bloom, S. Jones, G. Henriksen, V. Battaglia, C. Motloch, J. Christophersen, J. Belt, C. Ho, and R. Wright, Proceedings of the 204th Meeting of The Electrochemical Society, Orlando, FL, October 12–17, 2003, No. 236.
5. "Effect of Cathode Composition on Capacity Fade, Impedance Rise and Power Fade in High-Power, Lithium-Ion Cells," I. Bloom, S. Jones, V. Battaglia, G. Henriksen, J. Christophersen, R. Wright, C. Ho, J. Belt, and C. Motloch, *J. Power Sources*, 124 (2003) 538–550.
6. "Differential Voltage Analyses of High-Power, Li-Ion Cells 1: Technique and Application," I. Bloom, A. Jansen, D. Abraham, J. Knuth, S. Jones, V. Battaglia, and G. Henriksen, *J. Power Sources*, in press.
7. "Differential Voltage Analyses of High-Power Lithium-Ion Cells 2: Applications," I. Bloom, J. Christophersen and K. Gering, *J. Power Sources*, in press.
8. "Advanced Technology Development for Lithium-Ion Batteries. Battery Technology Life Verification Test Manual," H. Haskins, V. Battaglia, J. Christophersen, I. Bloom, G. Hunt and E. Thomas, INEEL/EXT-04-09186, June 2004 (draft).

III.B.1 Introduction

This subsection provides highlights and progress on the work that is focused on developing more accurate life prediction methodologies. Since this program began, it has been conducting accelerated aging and diagnostic studies on high-power cells to understand the factors that control the cycle and calendar life. In recent years, these activities have been supplemented by the development and application of an electrochemical cell model to help link the results of the diagnostic studies to the aging characteristics of the cells. This year these studies continued and efforts were initiated to use information developed on the Gen2 Baseline cells as the basis for developing methods for more accurately predicting the life of high-power Li-ion cells.

The Gen2 variant carbon (C) cells were built at the same time as the Gen2 Baseline cells and both groups of cells have been subjected to extensive accelerated aging tests and thorough diagnostic studies. The long-term aging characteristics of these two groups of cells differ significantly and part of the goal is to understand the reasons for their different aging characteristics, via the diagnostic and modeling studies.

The accelerated aging of Gen2 GDR graphite cells was initiated in the third quarter of this year and most of these cells are being used to study and refine features of the testing protocols that will be published in the Technology Life Validation Tool (TLVT) manual. The TLVT manual uses the life test data on the Gen2 Baseline cells, as well as the knowledge gained on the factors that impact on the life of these cells, to develop methodologies for more accurately predicting the calendar life of high-power Li-ion cells that employ the Gen2 Baseline cell chemistry. Monte Carlo simulations are used to provide a higher degree of confidence in the life predictions.

Figure III-2 provides a schematic diagram of how the activities in this focus area relate to each other, while Table III-2 provides a summary of how the five Department of Energy (DOE) laboratories contribute to this focus area.

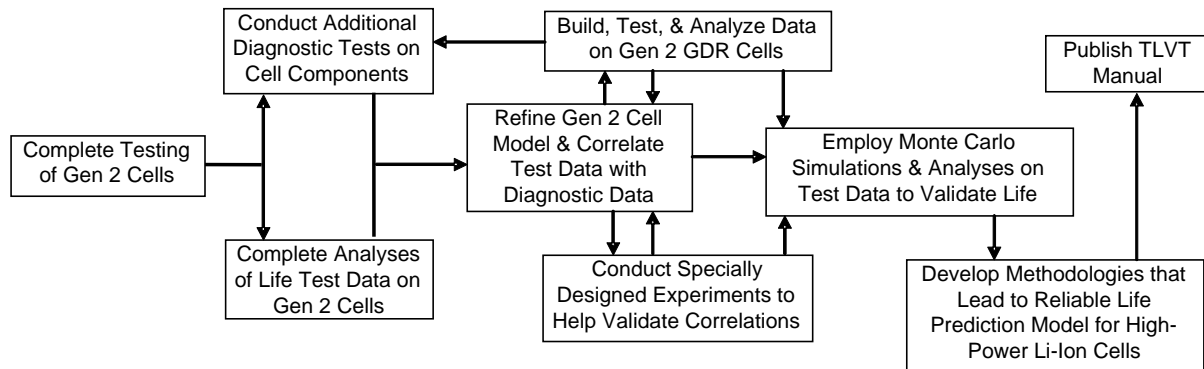


Figure III-2. Diagram of activities conducted in the “More Accurate Life Prediction” focus area

Table III-2. Summary of How the Five DOE National Laboratories Contribute to this Focus Area

	ANL ^a	BNL ^b	INEEL ^c	LBNL ^d	SNL ^e
Accelerated Cell Aging	X		X		X
Cell Component Diagnostics	X	X		X	
Cell Transport Modeling	X				
Statistical Analyses and Simulations	X		X	X	X
TLVT Manual Development	X	X	X	X	X

^a Argonne National Laboratory (ANL)

^b Brookhaven National Laboratory (BNL)

^c Idaho National Engineering and Environmental Laboratory (INEEL)

^d Lawrence Berkeley National Laboratory (LBNL)

^e Sandia National Laboratories (SNL)

III.B.2 Aging Characteristics of High-Power Cells

A summary of the cell test matrix is given in Table III-3. There were two aging schemes used: life cycle and calendar aging. These testing protocols are described in the Partnership for a New Generation of Vehicles (PNGV) Test Procedures Manual. The baseline cells were tested at 60% state-of-charge (SOC) and three temperatures, 25, 45, and 55°C. The Variant C cells were tested at the same SOC but at 45°C only.

Table III-3. Summary of Test Matrix

Cell Chemistry	Temperature		
	25°C	45°C	55°C
Baseline	15 cycle life	15 cycle life 2 calendar life	15 calendar life
Variant C		14 cycle life 10 calendar life	

Most of Gen2 cell aging is complete. There are two 25°C Baseline life cycle cells, two 45°C Variant C life cycle cells and one 45°C Variant C calendar aging cells still on test. Additionally, the cell aging teams used some of the results from these experiments to generate a draft Technology Life Validation (TLVT) manual (see Section III.B.5).

Sample Experimental Results. As the cells age, the C/25 capacity fades. A plot of the average C/25 capacity versus time for the cells along with the least squares fit to $at^{1/2} + d$ is given in Figure III-3. From the values of r^2 , 0.96 to 1.00, the fits are excellent. The order of C/25 capacity fades is 55°C calendar life > Baseline cycle life at 45°C \approx baseline calendar life at 45°C > Variant C calendar life at 45°C \geq Variant C cycle life at 45°C \approx 25°C cycle life. The fact that all the curves can be fit to a $t^{1/2}$ -dependent equation (parabolic kinetics) indicates that there is a common, diffusion-controlled, lithium-consuming reaction occurring in both chemistries. Further analysis of the C/25 voltage vs. time data indicate that the major source of capacity fade was due to side reactions at the anode.

Additionally, as the cells age, area-specific impedance (ASI) increases. Plotting the ASI values at 60% SOC vs. time shows that there are cathode-dependent (i.e., Al content) differences in the way

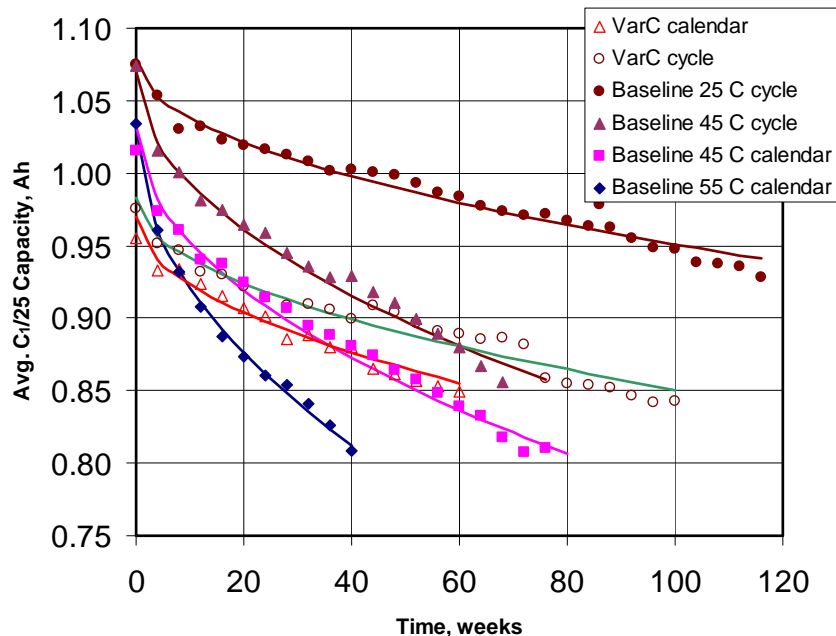


Figure III-3. Average C/25 capacity vs. time

ASI increases, as shown in Figure III-4. The Baseline chemistries follow a two-step mechanism that depends on $t^{1/2}$ at first then on t at later times. In this experiment, temperature controls only where the change from $t^{1/2}$ to t occurs. On the other hand, the data from the Variant C cells shows that ASI depends only on t over this time period.

Since the only difference between the two cell chemistries is the composition of the cathode, reactions at the cathode are the most likely source of impedance rise. The fact that the Variant C cells do not show t dependence suggests that the additional Al prevents this cathode degradation process or delays it until a later time.

Fitting the ASI vs. time data to a nonlinear equation, such as $at^{1/2} + Ic(t-t_0)$, $Ic=0$ when $t < t_0$, shows that there is a statistically significant difference in the a coefficient for both groups of cells calendar- and cycle-life tested at 45°C. This difference can be attributed to the additional stress that cycling puts on the cells.

As expected, power decreases with aging time, as shown in Figure III-5. Since power, P , is inversely proportional to ASI, the trend in $1/P$ versus time should be similar to that seen in the ASI. Indeed, that is the case (Figure III-6).

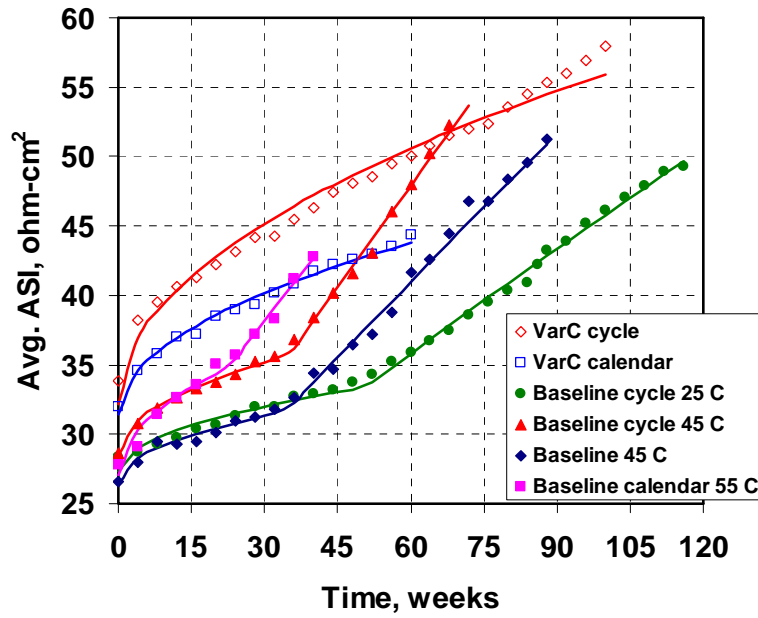


Figure III-4. Average ASI vs. time. At 86 weeks, the cycle life cells were moved to new testing channels, causing a deviation from previous trend.

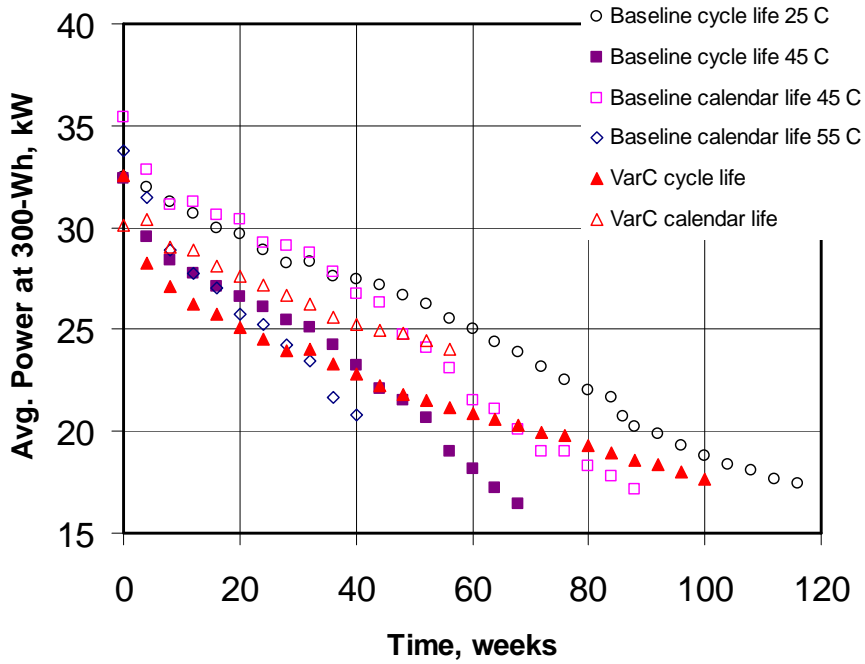


Figure III-5. Average power vs. time for both cell chemistries

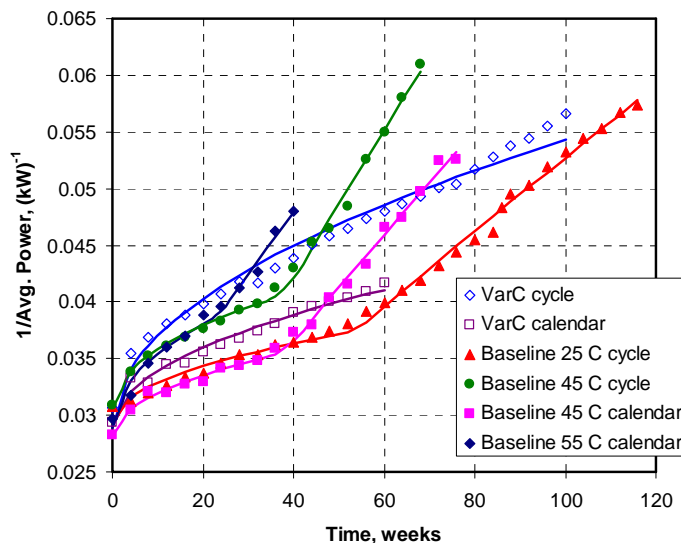


Figure III-6. 1/(average power) vs. time for both cell chemistries

III.B.3 Diagnostic Results on Aged Cells

Electrochemical Diagnostics. In an effort to identify the sources of capacity fade and impedance rise, electrochemical tests are being conducted on electrodes harvested from 18650-cells that showed varying levels of performance degradation. Planar-type cells, incorporating micro-reference electrodes, are used to isolate the individual positive and negative electrode contributions to cell impedance. These data have shown that the positive electrode is the main contributor to early-life (up to ~ 8 weeks) and mid-life (up to ~32 weeks at 45°C) cell impedance rise. Furthermore, the main increase of the positive electrode impedance is observed at the mid-frequency semicircular arc, which is usually associated with charge-transfer and mass-transfer processes at the electrode-electrolyte interface. The data provide fairly strong evidence that the same phenomena are controlling the cell impedance rise throughout much of the useful life (up to ~30% power fade) of these cells.

In the past year, impedance data were obtained with electrodes from highly-aged 18650 cells. These data showed significant Warburg impedances in the alternating current (AC) impedance spectra of the positive electrode (see Figure III-7) in addition to increases in the mid-frequency arc. The higher Warburg impedances indicate that late in the life of these cells it becomes increasingly difficult to transport lithium through the positive electrode, which may be the result of (a) an increase in Li^+ diffusion length through the electrode, and/or (b) a decrease in the Li^+ diffusion coefficient of the oxide particles.

Coin cells (2032-type) assembled with samples punched from the harvested electrodes and lithium-metal counter electrodes were used to determine the effect of aging on capacity. These data have shown that the capacities of both the positive and negative electrodes decrease with increasing age. In addition, significant hysteresis was observed for positive electrode samples from the highly-aged cells (see Figure III-8), which indicates that the Li^+ delivery-rate capability of the electrode

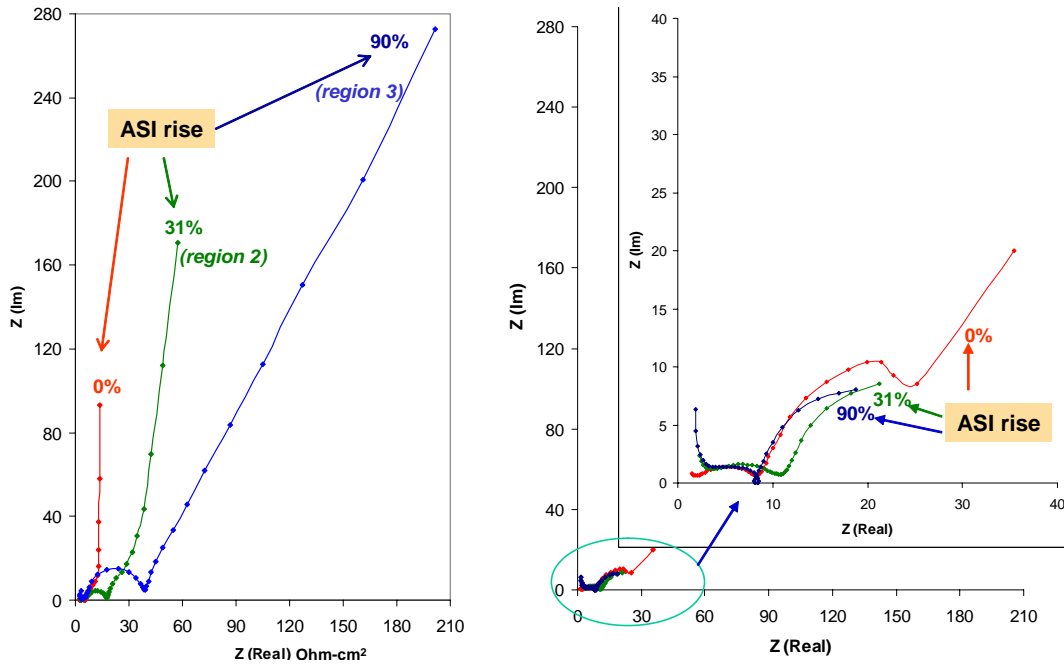


Figure III-7. AC impedance data from positive (left) and negative (right) electrodes harvested from 18650-cells that showed varying levels of impedance rise. The frequency ranges for the positive and negative electrodes are 100 kHz – 0.00025Hz and 100 kHz – 0.0004Hz.

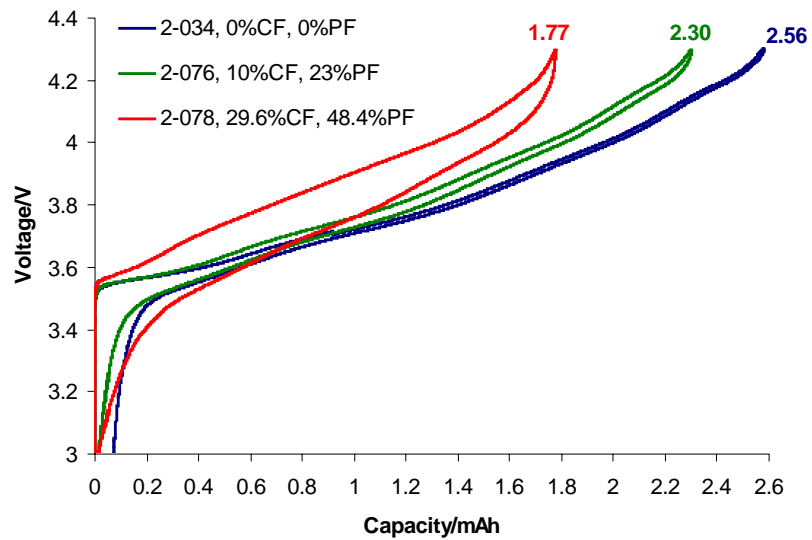


Figure III-8. Charge-discharge cycling plots from positive electrodes harvested from 18650 cells. The capacities decrease with increasing electrode age.

decreases with age. Cycling these cells at lower rates increases cell capacity which is, however, still lower than the capacity of a fresh electrode. The positive electrode capacity decline data could be the result of several factors that may include (a) oxide particle changes resulting from oxygen loss, (b) partially insulating films on the oxide surface that impede lithium motion into the particles, (c) breakup of secondary particles into fragments that are not in contact with the carbon (electronic conduction) media, and (d) retreat of carbon away from the particles.

Graphite particle isolation caused by electronically insulating surface films produced from the electrolyte is probably responsible for the negative electrode capacity decline because these electrodes regain capacity after being rinsed in solvents such as dimethyl carbonate (DMC). The positive electrodes, however, did not regain capacity after gentle-rinsing. But electrodes that were ultrasonically washed with DMC and pressed (to reduce electrode thickness by 15%) before assembly in Swagelok cells showed capacities that were comparable to those of fresh electrodes. These data (see Figure III-9) highlight mechanical and contact issues that might contribute to cell capacity and power fade.

Physicochemical Diagnostics. Most of the physicochemical diagnostic studies were focused on the positive electrode in an effort to identify phenomena that can cause the observed impedance rise. With transmission electron microscopy-energy dispersive X-ray (TEM-EDX) analysis, a correlation between oxygen loss from the oxide particle surfaces and cell power fade was established. X-ray diffraction (XRD) data showed that the c-axis parameter was greater for oxide from the aged cells, which is consistent with lithium loss from the oxide during aging. There was no indication of significant oxide damage or disorder in the XRD data. However, ex situ XRD on samples from a highly-aged (52% power fade [PF]) cell showed data that was consistent with particle isolation. Following a C/1 charge, about a third of the $\text{LiNi}_{0.8}\text{Co}_{0.15}\text{Al}_{0.05}\text{O}_2$ remained in the as-received SOC, while the rest was at a higher state-of-charge (SOC). The total SOC was equal to that expected from coulometry. Any mechanism offered to explain the observed particle isolation must account for the bimodal distribution of active and inactive particles.

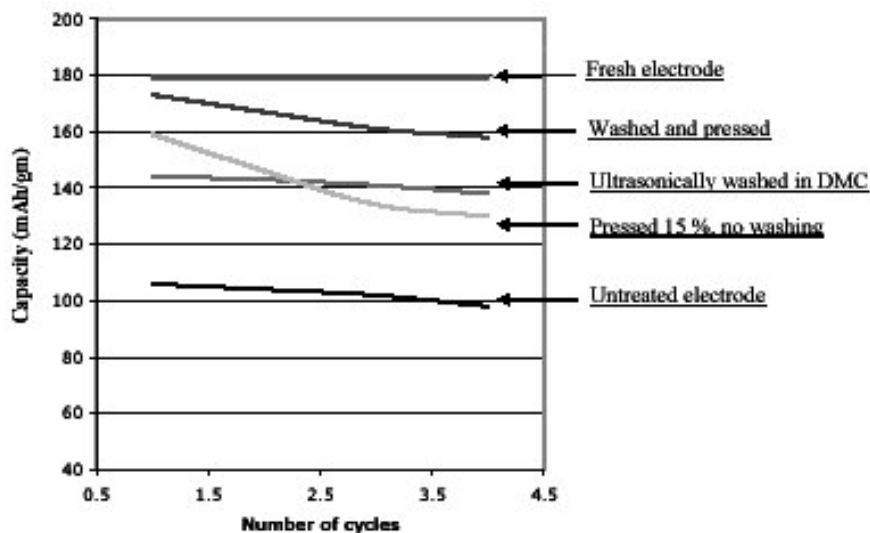


Figure III-9. Effect of electrode treatment on capacity of positive electrode harvested from an 18650 cell (~50% power fade). Cells were cycled between 2.5–4.2 V at a ~C/20 rate.

Micro-Raman imaging also showed that the local SOC of cathode particles removed from tested cells was never uniform despite the slow discharge of the cells prior to disassembly. Controlled experiments with samples of cathodes from cells showed that individual oxide particles charged and discharged at different rate as if they were partially or even fully disconnected from the conductive carbon matrix and current collector. The inconsistent kinetic behavior of the individual oxide particles can be attributed to degradation of the electronic conductance matrix in the cathode upon aging. Raman microscopy images have shown that the $\text{LiNi}_{0.8}\text{Co}_{0.15}\text{Al}_{0.05}\text{O}_2$ /elemental-carbon surface concentration ratio at the surface and in the bulk of the cathode increases monotonically with increasing cell power loss, up to an apparent break point at about 20% cell power loss. A non-uniform current distribution pattern could develop in the cathode during cycling/aging, which may lead to local overcharging of the oxide. Overcharged oxide particles could undergo further degradation through oxygen loss and/or induced mechanical stress that may lead to disintegration of the secondary oxide particles (observed in scanning electron microscopy [SEM] images of some highly aged samples) and consequent electronic isolation of primary particles.

Fourier transform infrared-attenuated total reflection (FTIR-ATR) analysis of electrodes harvested from 18650 cells, detailed in the paper by Song et al.¹³ has failed to identify any film formation chemistry which correlates directly with power/capacity fade. However, related experiments with Gen2 cathodes and electrolyte in Swagelok cells have produced results which allow the formulation of a mechanism for power/capacity fade. Truly in situ experiments with Gen2 electrolyte on inert cathodes such as Au, Pt and glassy carbon failed to show any solvent oxidation below ~5.5 V. With Gen2 cathodes, an oxidation product is observed beginning at 4.2 V (and higher), but not at any lower potential. Further experiments with other nickel oxide cathode materials, as well as other results in the literature, indicate that Li stoichiometry, not electrode potential, is the critical parameter initiating solvent oxidation. The reaction is oxygen transfer from the oxide lattice to the solvent at the point where x in $\text{Li}_{(1-x)}\text{Ni}_{0.8}\text{Co}_{0.15}\text{Al}_{0.05}\text{O}_2$ is > 0.6 . This result agrees quantitatively with thermochemical results from Manthiram's group¹⁴ on the instability of lattice oxygen in these cathode materials at high states of charge, e.g., $x > 0.65$ in the Ni-Co oxide w/o Al.

The relation of this chemistry to 18650 cell power and capacity fade requires some extrapolation. The nominal state of charge for the cell is 60 %, corresponding (initially) to a nominal $x = 0.5$. It is known (from the XRD data) that the active material in the cathode is not utilized uniformly, and that the nominal state of charge represents the average of high and low states of charge, i.e. some oxide particles may be at $x = 0.7$ and an equal number are at $x = 0.3$. Hence, some particles will react with electrolyte even when the nominal state of charge is 60%. As the cell ages and if some Li is consumed at the anode, the mean value of x in the cathode will increase with time, i.e. the "electrode slippage" phenomenon described by Abraham et al.¹⁵ At a loss of ~20 % of the initial cyclable Li, the nominal value of x in the cathode active material at 3.7 V would increase above the critical value of 0.6. It seems possible that close to $x = 0.6$ and at 45–55°C there is a slow loss of oxygen (on a time scale of 10^3 hrs.) from the cathode material that cannot be seen on the time scale of the FTIR experiment. The probable consequence of the reaction is the change in the oxide particles due to loss of oxygen, e.g. shrinkage resulting in particle isolation. This mechanism of power fade will become

¹³ *J. Electrochem. Soc.* **151**(2004) A1162-A1167.

¹⁴ *Electrochem. Solid State Lett.*, 6 (2003) A9.

¹⁵ *Electrochem. Acta* **49** (2004) 4763.

more dominant as the cell loses capacity, i.e., it could be the dominant mechanism in mid- and late-life cells, but is probably not associated with the initial impedance rise in the cathode.

Positive electrode surface films observed on the oxide particles by microscopy techniques could also contribute to electrode capacity loss (by isolating oxide particles) and impedance rise (by increasing resistance to Li-ion transport). These surface films have been identified by various techniques including nuclear magnetic resonance (NMR), soft X-ray absorption spectroscopy (XAS), X-ray photoelectron spectroscopy (XPS) and time-of-flight secondary ion mass spectrometry (TOF-SIMS). XPS data have indicated that these surface films contain a mixture of organic and inorganic constituents that include lithium alkyl carbonate, LiF, Li_xPO_y and $\text{Li}_x\text{PO}_y\text{F}_z$ species. Phosphorous K-edge XAS data have also shown the presence of insoluble phosphates in the electrode that cannot be removed by repeated washing. Proton NMR has suggested the presence of polymeric species on the electrodes. ^{19}F and ^{31}P NMR measurements have showed the presence of fluorophosphate species in electrolytes from highly-aged cells (see Figure III-10). ^{31}P NMR data obtained from the cathodes also show the presence of fluorophosphates (OPF_2OR , $\text{OPF}(\text{OR})_2$) which may transform to organophosphate compounds during cell cycling and aging.

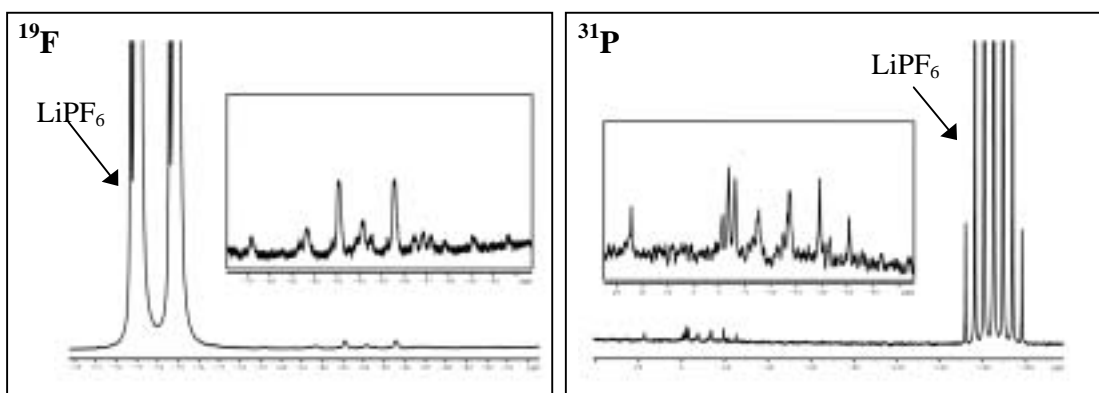


Figure III-10. ^{19}F and ^{31}P NMR spectra of the electrolyte taken from a Gen2 cell. Electrolyte decomposition leads to the formation of fluorophosphates (OPF_2OR , $\text{OPF}(\text{OR})_2$) as shown in the insets.

The long-chain phosphate compounds are similar to commercially available surfactants manufactured by Rhone-Poulanc (Rhodafac). It is easy to understand how the phosphate group may acquire a charge and strongly interact with the electrode and separator surfaces. In the case of the cathode, the nano-sized carbon black particles will be impacted by surface-active compounds and easily converted to a colloidal dispersion. This process would be completely consistent with the carbon “retreat” phenomenon observed by micro-Raman imaging. The generation of dispersions of nano-particles within the composite cathode will impact the transport properties of the electrolyte within the electrode. An increase in molecular weight (MW) of the phosphate compounds in combination with the presence of nano-particles will lead to increased viscosity, lower salt diffusion coefficients, and an increase in tortuosity in the positive electrode. These property changes may play an important role in the cell power fade and increased impedance.

III.B.4 Electrochemical Modeling of Aged Cells

The electrochemical modeling effort is aimed at examining the impedance rise in Gen2 cells. The overall goal of this work is to associate changes that are seen in the post-test diagnostic studies with the loss of electrochemical performance, as measured by the hybrid pulse power characterization (HPPC) tests on 18650 cells. The approach taken in this effort is to develop a model based on the analytical diagnostic studies, establish the model parameters, and conduct parametric studies with the model. The parametric studies are conducted to gain confidence with the model, examine degradation mechanisms, and analyze cell limitations. To accomplish these tasks two versions of the model have been developed. One version simulates the cell response from alternating current (AC) impedance studies, and another model version is utilized for examining HPPC tests. Both of these experimental techniques are extensively used in the program to quantify the cell's and its components' electrochemical performance. The underlying basis for both models is the same, as well as their parameter set. While both electrodes have been examined, the modeling effort has concentrated on the positive electrode because of its importance in the cell's overall impedance rise

The general methodology for the electrochemical model follows the work of Professor Newman at Berkeley. Concentrated solution theory is used to describe the transport of salt in the electrolyte. Volume-averaged transport equations account for the composite electrode geometry. Electrode kinetics, thermodynamics, and diffusion of lithium in the oxide active particles are also included. The detailed theoretical description of the oxide active material/electrolyte interface, commonly referred to as the solid electrolyte interface or SEI, is based on post-test analytical diagnostic studies. The SEI region is assumed to be a film on the oxide and an oxide layer at the surface of the oxide. The film on the oxide is taken to be an ill-defined mixture of organic and inorganic material through which lithium ions from the electrolyte must diffuse and/or migrate across to react electrochemically at the surface of the oxide. The lithium is then assumed to diffuse through the oxide surface layer and into the bulk oxide material. Capacitive effects are incorporated into the model at the electrochemical interfaces and a localized electronic resistance between the current carrying carbon and the oxide interface can also be included.

Besides the development of the electrochemical model and determining its parameters, previous years' highlights under this program include: examining the interfacial impedance rise of the positive electrode during aging, correlating AC impedance studies with HPPC tests, and examining the change in positive electrode impedance with electrode thickness. The study of the interfacial impedance rise of the positive electrode was particularly important because of its relevance to the overall cell aging. Electrochemical impedance spectroscopy (EIS) studies on the aging of Gen2 technology cells indicate that the interfacial impedance of the cells grow all through its life. Furthermore, the low-frequency Warburg diffusional impedance tail also begins to increase late in life. Reference electrode cell studies on harvested electrodes indicate that most of the cell impedance growth can be associated with the positive electrode.

Electrochemical model simulations identified three possible sources for the positive electrode interfacial impedance increase without a significant change in the diffusional impedance. First, an interfacial impedance increase could result from a degradation of the ionic pathway for lithium ions between the electrolyte in the electrode pores and the bulk oxide active material. This could result from changes in the electrolyte/oxide interfacial structure, composition, and/or properties and would

have a direct impact on the positive electrode's interfacial impedance. Second, a loss of positive electrode capacity, particularly isolation of the finer oxide particles would also cause the interfacial impedance to increase. Finally, an interfacial impedance increase would result from a degradation of the electronic pathway between the carbon matrix and the oxide active material provided the carbon matrix has a significant double layer capacitance associated with it.

Simulations of HPPC tests were used this year to show that capacity fade is only a minor contributor to the impedance rise observed in Gen2 18650 cells. The change in the positive electrode impedance was calculated assuming that all the 18650 cell capacity fade, as measured by C/25 rate cycling, was the result of oxide active material particle isolation. Figure III-11 compares the calculated positive electrode impedance rise to the overall 18650 cell impedance rise. Two cases are considered, one where the isolation of oxide particles is not biased according to size and another where only the fine particles are isolated. Obviously the finer particles have a greater impact in the impedance because of their higher surface area. The higher impedance rise curve (i.e., fine particle loss curve) can be considered an upper bound for the impact of the capacity loss resulting from the isolation of the oxide active material.

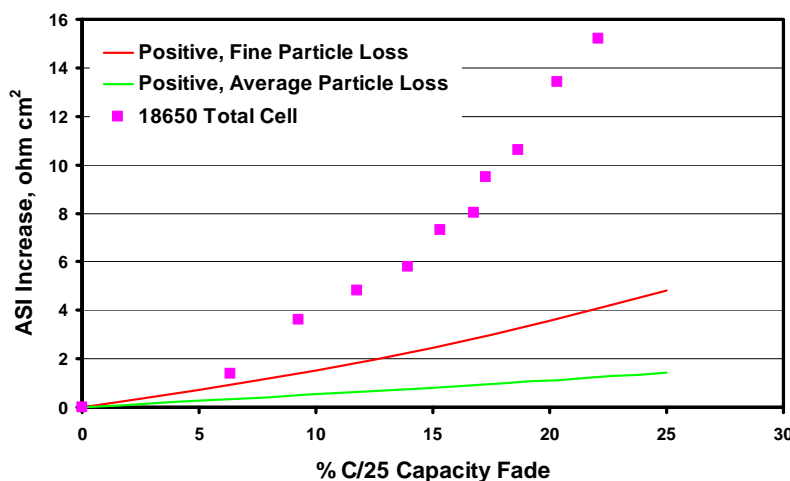


Figure III-11. HPPC area-specific impedance increase for 18s 5C discharge pulse

Also this year, the model was used to examine aging effects late in the cell's life, as the diffusional impedance starts to grow. The model simulations indicate that other positive electrode aging phenomena can contribute to the cell's impedance rise. These include a slowing of lithium diffusion through the oxide, a loss of electrochemically active area, degradation of electrolyte properties, and a change in electrode microstructure. Degradation of lithium diffusion through the oxide could be caused from changes in the oxide structure (e.g., micro-cracks), but also could result from changes in the intra-granular region between primary particles. A degradation of the intra-granular region and the loss of electrochemically active area are both consistent with an extensive general degradation of the oxide primary particles' interfaces. The degradation of electrolyte transport properties and/or a change in electrode microstructure that affects the electrode's tortuosity can produce an electrode impedance similar to those observed in the laboratory, but these degradation mechanisms are not commonly supported by post-test diagnostic studies.

III.B.5 More Accurate Life Prediction Methodology Development

In order to support the rapid and accurate assessment of Li-ion cell/battery life, the Advanced Technology Development (ATD) program has developed a Technology Life Verification Test (TLVT) Manual. The manual provides detailed guidance to battery developers and other interested users regarding approaches for life test matrix design, reference performance testing, and life test data analysis. A life test simulation tool has been developed to support optimization of the life test matrix.

Life Test Matrix Design. The suggested approach for designing the life test matrix is based on well-established statistical experimental design principles that will minimize life test program cost and maximize confidence in the resulting life predictions. The overall strategy involves both calendar-life and cycle-life accelerated aging under prescribed conditions with a variety of stress factors. Recommended stress factors to be considered include (a) temperature, (b) state of charge (SOC), (c) rate of discharge energy throughput, and (d) discharge and regenerative pulse power levels. It is suggested that the core life testing be conducted using separate factorial designs for calendar-life and cycle-life. In addition, it is recommended that some cells be tested under sequential combinations of calendar life (non-operating) and cycle life (pulse-mode operation) to assess the path-independence of life. This will use the highest levels of stress conditions, applied in complimentary sequences of calendar/cycle and cycle/calendar time blocks. Other recommended supplemental life tests will assess the capability of the technology for periodic cold-cranking and low-temperature operation within specified regenerative pulse current limits without impacting cell life.

Reference Performance Testing. At fixed time intervals during life testing, each cell will be subjected to a reference performance test (RPT) to measure its cumulative deterioration at its specified stress levels. In contrast to previous life test protocols, the specified RPT procedure minimizes the time spent off-test and possible reduction in life due to irrelevant stresses induced by the RPT. More extensive RPTs will be conducted on supplemental life test cells (outside the core life test matrix) to assess deterioration in such performance parameters as rated capacity and cold-cranking power. The minimum RPT primarily will measure power at a reference temperature (30°C) and specified minimum operating SOC. Power at the maximum operating SOC, as well as capacity from the maximum SOC to the minimum SOC, will also be measured. The RPT power measurements will be adjusted to account for measured cell temperatures that differ from the reference temperature. The area-specific impedance (ASI) is viewed as a very useful measure of the state of the health of a cell to be used in predicting cell life.

Life Test Simulation Tool. A life test simulation tool has been developed using Microsoft Excel and its integrated Visual Basic for Applications (VBA) programming language to support optimization of the core life test matrix. This tool uses the Monte Carlo approach to simulation, in which a simulated sample of cells is subjected to the life test, wherein the true response of the simulated cells is corrupted with specified noise levels induced by test measurement errors and cell-to-cell manufacturing variability. Numerous trials are simulated, each corresponding to a replication of the life test at the specified acceleration factor. Each Monte Carlo trial results in simulated cell performance deterioration from which the life on test can be estimated. The variation in estimated life on test across the set of trials provides a basis for developing confidence limits for life on test for

a particular experimental condition. The objective of the simulation tool is to estimate the number of cells required at each test condition for the core life tests to demonstrate that the technology can meet the 15-year, 150,000-mile life with 90% confidence given that the simulations accurately reflect actual cell performance and testing. To facilitate this optimization process, a spreadsheet analysis tool is also provided to give preliminary, approximate estimates of the number of cells required at each test condition for the core life tests.

Another important use of the simulation tool is to verify by statistical analysis of the data that the test measurement and manufacturing noise levels are no greater than those assumed in the original core test matrix optimization. If the measurement and manufacturing noise levels are greater than those assumed, then the test matrix may need to be modified, for example by increasing the number of cells at some of the critical stress conditions.

Life Data Analysis. The life test simulation tool, as it stands, implements one of many possible life models that can be used for analyzing both simulated and actual experimental data. The model chosen was based on analysis of ATD Gen2 cycle life data and can be represented as:

$$ASI_{true,k} = \beta_0(\beta_1^k - 1)/(\beta_1 - 1) + \beta_1^k ASI_0,$$

where $k = (\text{test time})/(\text{RPT interval})$, β_0 and β_1 are constants and ASI_0 is the true area-specific impedance at time = 0. Provisions were made in the tool for the user to enter different technology-specific model equations.

The simulated (or experimental) ASI data, from one or more cells, are then statistically analyzed using robust orthogonal regression¹⁶ to estimate the values of β_0 , β_1 and ASI_0 . The predicted life-on-test is given by

$$\hat{L}_{TEST} = \Delta t_{RPT} \ln \left\{ \frac{\hat{\beta}_0 + ([\hat{\beta}_1 - 1] A\hat{S}I_0) / (1 - PF)}{\hat{\beta}_0 + [\hat{\beta}_1 - 1] \times A\hat{S}I_0} \right\} \frac{1}{\ln \hat{\beta}_1},$$

where $\hat{\beta}_0$, $\hat{\beta}_1$, and $A\hat{S}I_0$ are the parameter estimates and PF is the allowable power fade at the end of life.

In the case of analyzing simulated data, the tool repeats the complete simulation numerous times in order to assess the uncertainty in life-on-test and the model parameters. In the case of experimental data, uncertainties in $\hat{\beta}_0$, $\hat{\beta}_1$, $A\hat{S}I_0$, and \hat{L}_{TEST} are estimated by using a resampling technique known as the Bootstrap¹⁷ to estimate the lower 90% confidence limit for the life-on-test.

Figure III-12 shows experimental ASI data from the Variant C cells and the estimated regression line. From the regression analysis, the estimated values of β_0 , β_1 and ASI_0 are 3.32, 0.94 and 32.46, leading to a 90% lower confidence limit for life-on-test of 1.22 years, assuming 30% power fade.

¹⁶ L. Amman and J. Van Ness, ACM Transactions on Mathematical Software, 14 (1988) 76–87.

¹⁷ *An Introduction to the Bootstrap*, Efron, B., and Tibshirani, R. J., 1993, New York, Chapman and Hall.

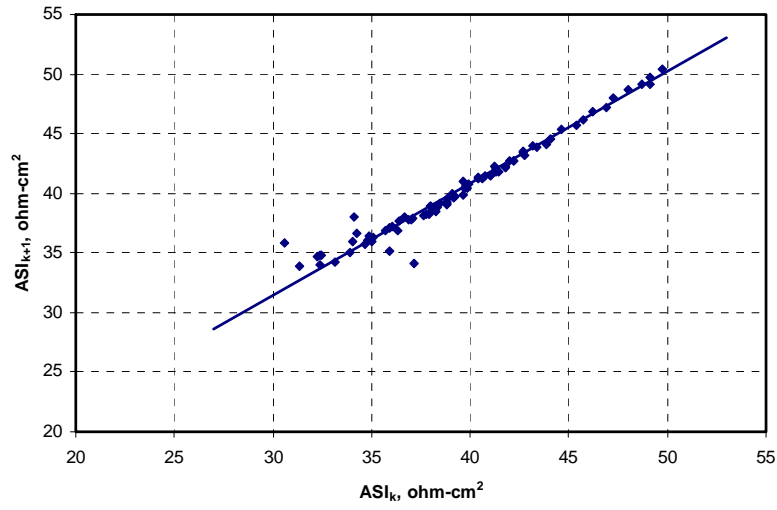


Figure III-12. ASI_{k+1} vs. ASI_k and the calculated regression line from the statistical analysis

III.C Understand And Enhance Low-Temperature Performance

Objectives

- Understand factors that limit low-temperature performance and identify approaches to enhance performance at low temperature.
- Develop a model of low temperature behavior of electrolytes specifically and Li-ion cells generally.
- Thoroughly characterize the Gen2 cell chemistry at low temperatures, study issues of
 - lithium plating during regenerative braking recharge, and
 - dramatic power loss during high-current pulse discharge.

Approach

- In order to characterize the Gen2 chemistry at low temperatures:
 - use reference electrode cells to isolate problem as arising at the anode or cathode,
 - use electrochemical impedance spectroscopy (EIS) to identify potential sources of the problems, and
 - use diagnostics and modeling to aid in identifying sources of problem.
- Based on the above information, identify potential methods for enhancing low-temperature performance and evaluate them experimentally.

Accomplishments/Findings

- Determined that the positive and the negative electrode interface contribute nearly equally to the low-temperature impedance rise. The responsible phenomenon may be independent of active material.
- Discovered that the negative electrode impedance is dominated by a single mechanism throughout the temperature range tested. Whereas, the positive electrode impedance has two major components, one that dominates above -10°C and another that dominates below -10°C .
- Determined that impedance growth of the electrolyte alone is not sufficient to explain the overall cell impedance rise, thus indicating a possible interfacial affect.
- Modeling studies show that the bulk of the activation energy assigned to electrolyte performance is due to the lithium desolvation process.

Future Studies

- Continue testing hard carbons, alternative cathode and electrolytes for use at low temperatures.

III.C.1 Introduction

This subsection provides highlights and progress on the work that is focused on understanding the factors that limit the low-temperature performance of the Gen2 Baseline cell chemistry and the use of this information to identify methods of enhancing low-temperature performance through cell material and component changes. This was a new focus area for the Applied Battery Research program and efforts this year were directed at understanding the factors that limit low-temperature performance. The performance limitations occur in the areas Li^0 plating on the negative electrode,

during regenerative braking, and a major loss of discharge power below -10°C , which can not be explained by the conductivity vs. temperature characteristics of the electrolyte.

Figure III-13 provides a schematic of how activities in this focus area relate to each other, while Table III-4 provides a summary of how the five Department of Energy (DOE) laboratories contribute to this focus area.

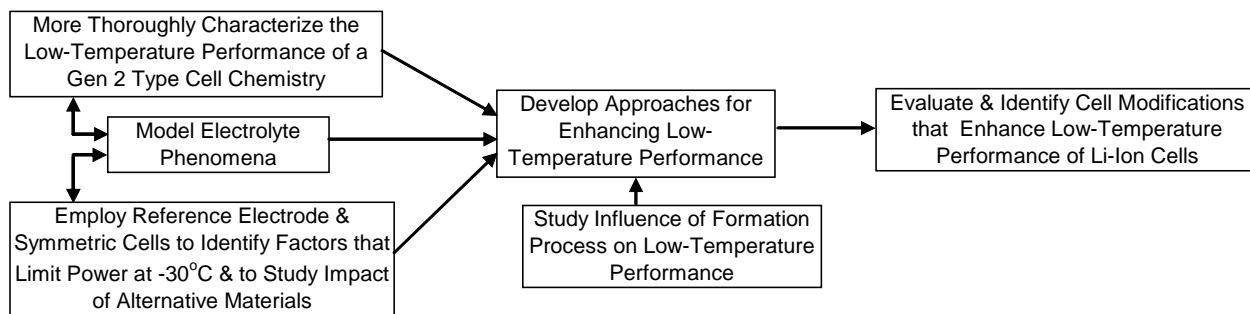


Figure III-13. Diagram of activities conducted under this “Understand and Enhance Low-Temperature Performance” focus area

Table III-4. Summary of How the Five DOE National Laboratories and the U.S. Army Research Laboratory Contribute to this Focus Area

	ANL ^a	ARL ^b	BNL ^c	INEEL ^d	LBNL ^e	SNL ^f
Thoroughly Characterize Gen2 Cells	X			X		
Reference Electrode Cells	X					
Beaker Studies	X					
Diagnostic Studies	X		X		X	
Electrolyte and Cell Modeling	X			X		
Electrolyte Development	X	X		X		

^a Argonne National Laboratory (ANL)

^b U.S. Army Research Laboratory (ARL)

^c Brookhaven National Laboratory (BNL)

^d Idaho National Engineering and Environmental Laboratory (INEEL)

^e Lawrence Berkeley National Laboratory (LBNL)

^f Sandia National Laboratories (SNL)

III.C.2 Low-Temperature Performance Characteristics

The rate capability and impedance of the Gen2 Li-ion cell system was determined over a wide temperature range of 40°C to -30°C. It was determined that the cell performance suffered significantly below -10°C. The cell impedance increased over an order of magnitude upon lowering to -30°C. Constant voltage charging improved the capacity utilization, but the C/1 capacity at -30°C was only 60% of its room temperature value (see Figure III-14).

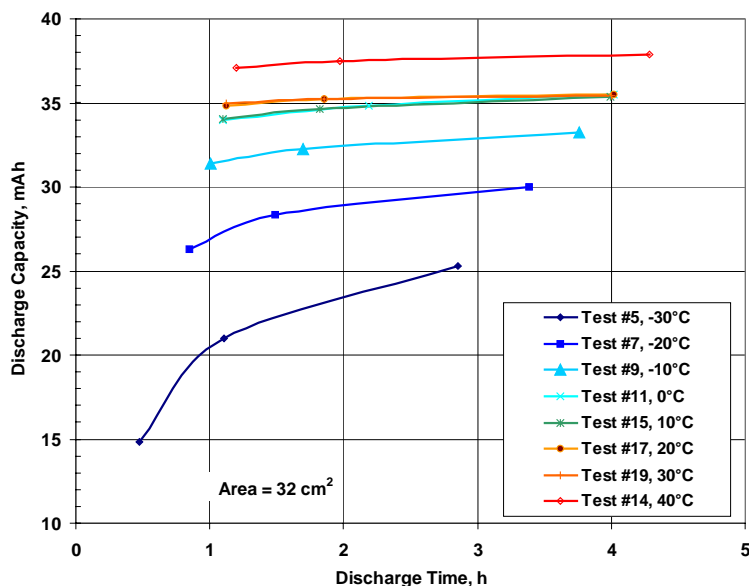


Figure III-14. Discharge capacity vs. discharge time with temperature as a parameter for the Gen2 cell system (following constant voltage charge at 4.1 V)

Impedance Study Using Reference Electrode. Reference electrode studies were conducted to determine the reason for the high impedance rise at low temperature. These were in situ full-cell experiments with lithiated tin on a 25- μm copper wire, which was developed earlier in the diagnostics effort. The most surprising finding from this work was that the impedance rise at low temperature was nearly the same in the positive and negative electrodes (Figure III-15). This meant that a phenomenon was responsible that is independent of the active material, most likely an electrolyte effect. An anomaly was observed in this data that further supports the belief that the electrolyte is playing a major role in the low-temperature impedance rise. Namely, the positive electrode impedance did not increase significantly until the temperature was below -10°C. Whereas, the negative electrode impedance, which is much lower than the positive electrode impedance at room temperature, rose steadily with decreasing temperature, as can be seen in Figure III-16. This suggests that the negative electrode impedance is dominated by a single mechanism throughout the temperature range tested. Whereas, the positive electrode impedance has two major impedance components, one that dominates above -10°C and another process that dominates below -10°C. The latter impedance component most likely has the same mechanism as in the negative impedance component, which displays near Arrhenius behavior.

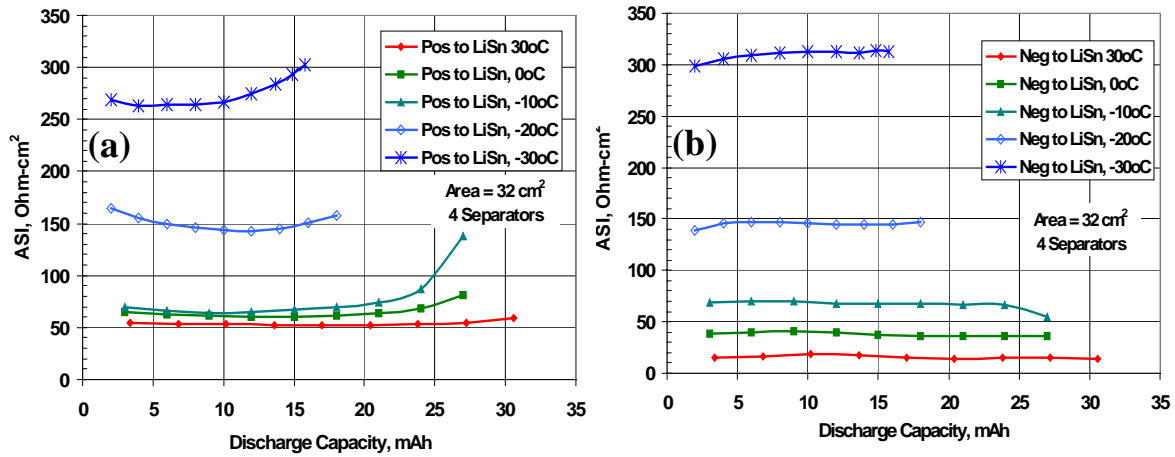


Figure III-15. Area-specific impedance (ASI) from 10-sec hybrid pulse power characterization (HPPC) discharge pulse with temperature as a parameter for (a) positive electrode and (b) negative electrode

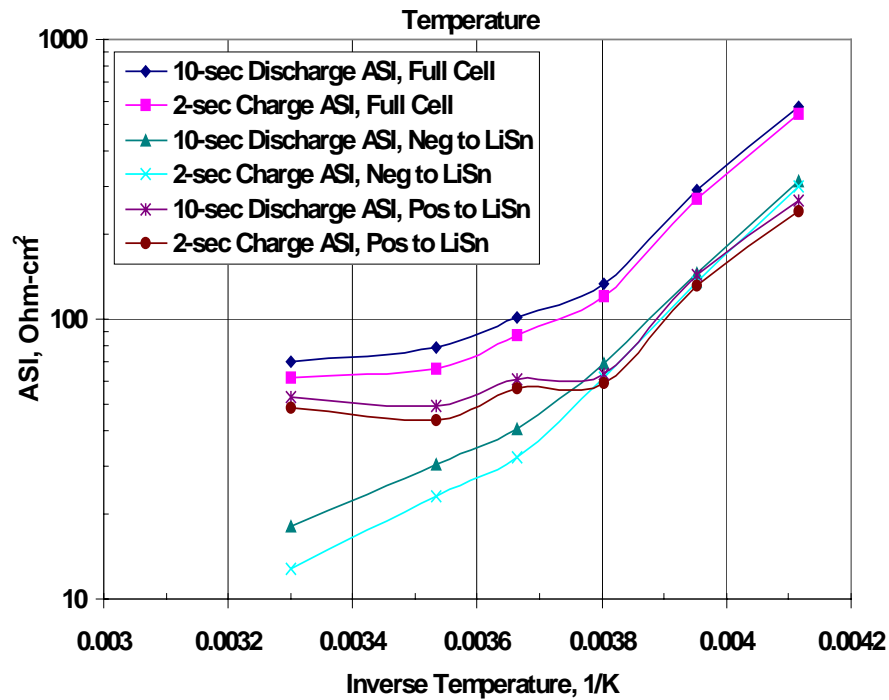


Figure III-16. ASI from HPPC test evaluated at 10-mAh discharge capacity

Electrochemical impedance spectroscopy (EIS) studies were performed on these cells over a frequency range of 60 kHz to 2 mHz. The high frequency impedance data indicate that the electrolyte conductivity does decrease as the temperature is lowered, as expected, but is not the dominant cause of the impedance rise. The main rise in impedance occurs in the mid frequency range of the spectrum as can be seen in Figure III-17. Processes that occur in this frequency range are generally interfacial in nature.

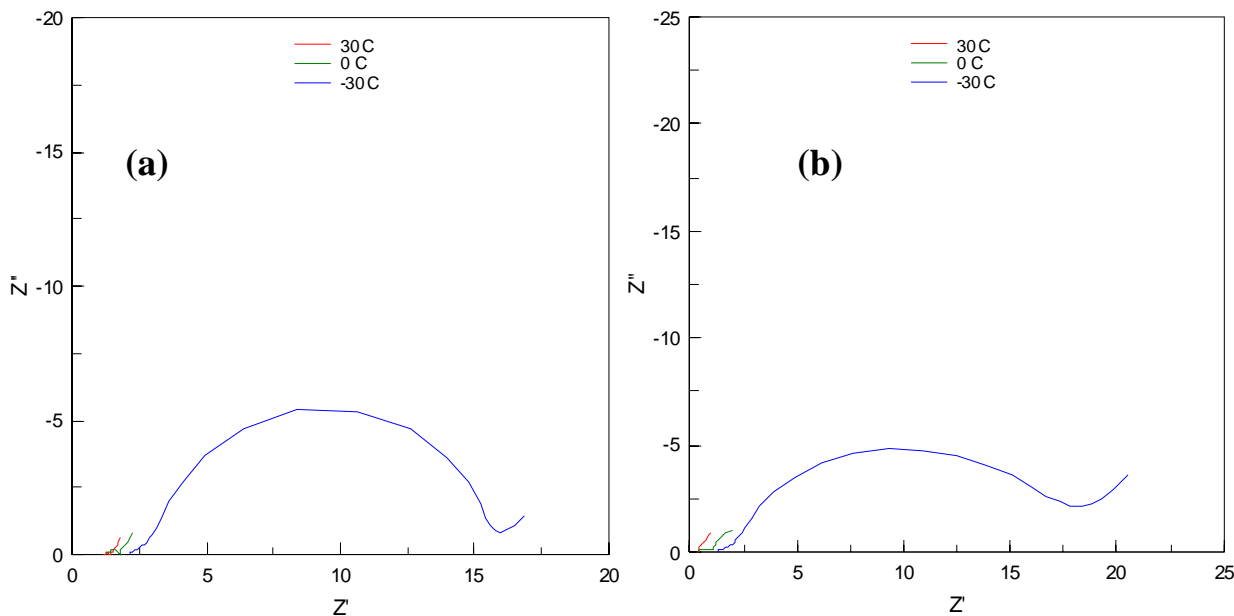


Figure III-17. Imaginary impedance plotted versus real impedance with temperature as a parameter for (a) positive electrode and (b) negative electrode, in a Gen2 cell system

Lithium Plating. Concern exists that lithium metal might plate on the graphite electrode during regen pulses. Full cells were constructed with two reference electrodes: a lithiated-tin on copper wire between the positive and negative electrodes and a small lithium ingot in a region exterior of the cell electrodes. In this manner the true potential of the Li_ySn reference electrode could be measured versus the electrochemically fixed lithium potential (Li_ySn has several voltage plateaus).

Hybrid pulse power characterization (HPPC) tests were performed on this four-electrode Gen2 cell at decrements of 10°C down to -30°C with a widened cell voltage window of 1.5 to 4.6 V during the pulse segments (to guarantee a complete data set for analysis). The potential of the graphite negative electrode was measured versus the lithium reference electrode and is plotted in Figure III-18, the cell voltage is listed below each charge pulse. It is readily apparent that the graphite potential does dip below lithium potentials during charge pulses with the cell voltage window expanded to 4.6 V. If the cell voltage is limited to 4.1 V, the potential for all of the charge pulses was above lithium potential. However, the graphite potential remained below lithium potential during a portion of the constant voltage charge, as indicated in Figure III-18. This suggests that it is necessary to lower the cell cutoff voltage on low temperature charges to a value less than 4.0 volts.

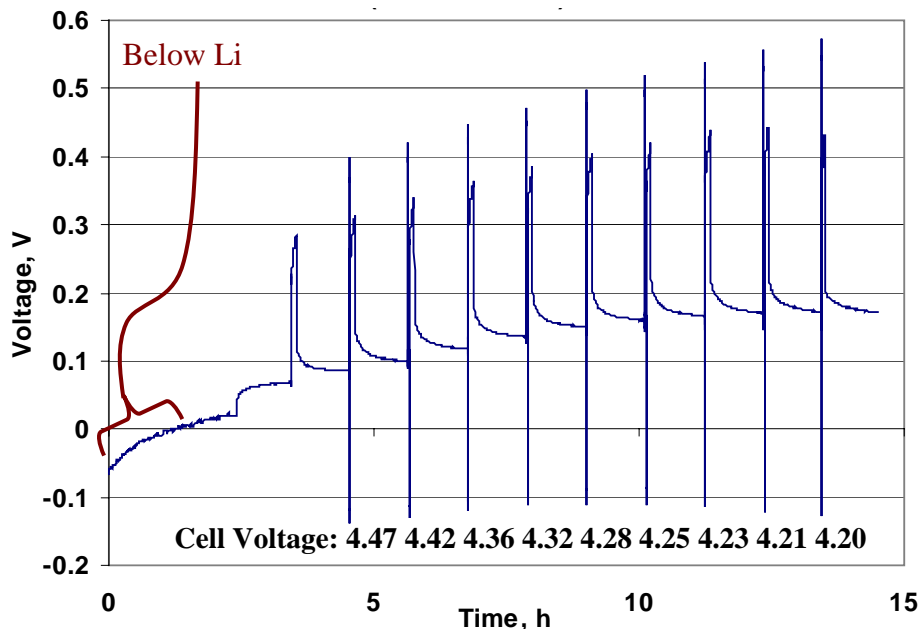


Figure III-18. Potential of the graphite negative electrode versus a lithium reference electrode during a HPPC test on the Gen2 cell system at -30°C .

A similar cell was built with hard carbon as the negative electrode versus a Gen2 positive electrode in Gen2 electrolyte. At no point in the charging process or the HPPC pulse charges did the hard carbon electrode potential go below lithium potential even though the cell voltage pulsed up to 4.4 V. This is because the hard carbon operates at potentials 200 to 800 mV above lithium potential than graphite, which has a long voltage plateau only 100 mV above lithium potential.

Precipitation of Electrolyte Component(s). Electrolyte compositions that represent the Gen2 system were stored at low temperatures to determine their precipitation point. No signs of precipitates were observed at -30°C . Precipitates did form at -60°C that are believed to be ethylene carbonate (EC)-rich. They did not re-dissolve until the temperature was raised to -10°C . This suggests that a liquid two-phase region may exist at low temperature, but this needs to be explored further to confirm.

III.C.3 Low-Temperature Electrolyte Modeling

Battery performance in general is a consequence of several contributing factors (Figure III-19). Li-ion cell performance is made complex by the dynamic process of lithium desolvation which must occur for lithium intercalation into either electrode (Figure III-20). Static electrolyte properties alone (conductivity, diffusivity, etc.) are insufficient to describe the effect of temperature on lithium transport. Thus, a more rigorous tool is required to understand the role of the electrolyte in cell performance. This work has produced a modeling tool that enables selection of electrolytes for use in Li-ion batteries. One application of the model in 2004 has been to investigate low-temperature performance of candidate electrolytes.

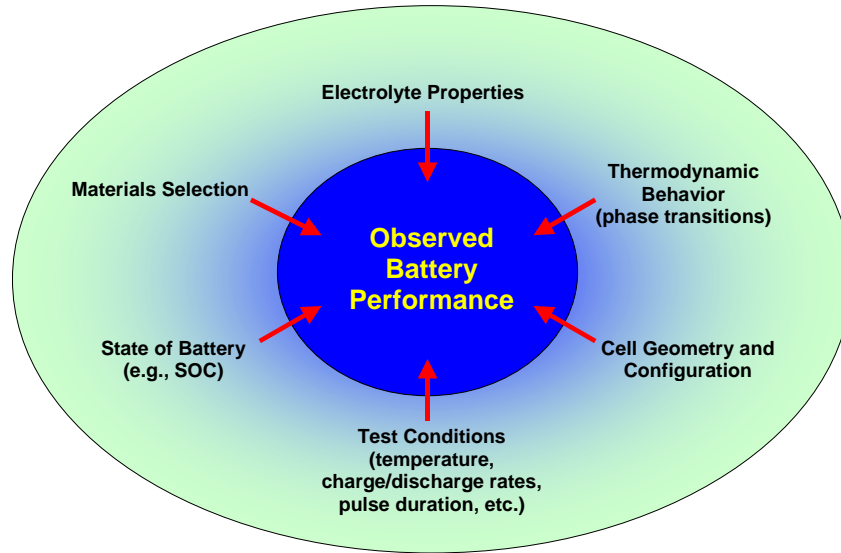


Figure III-19. Performance of batteries on test depends on a multiplicity of factors

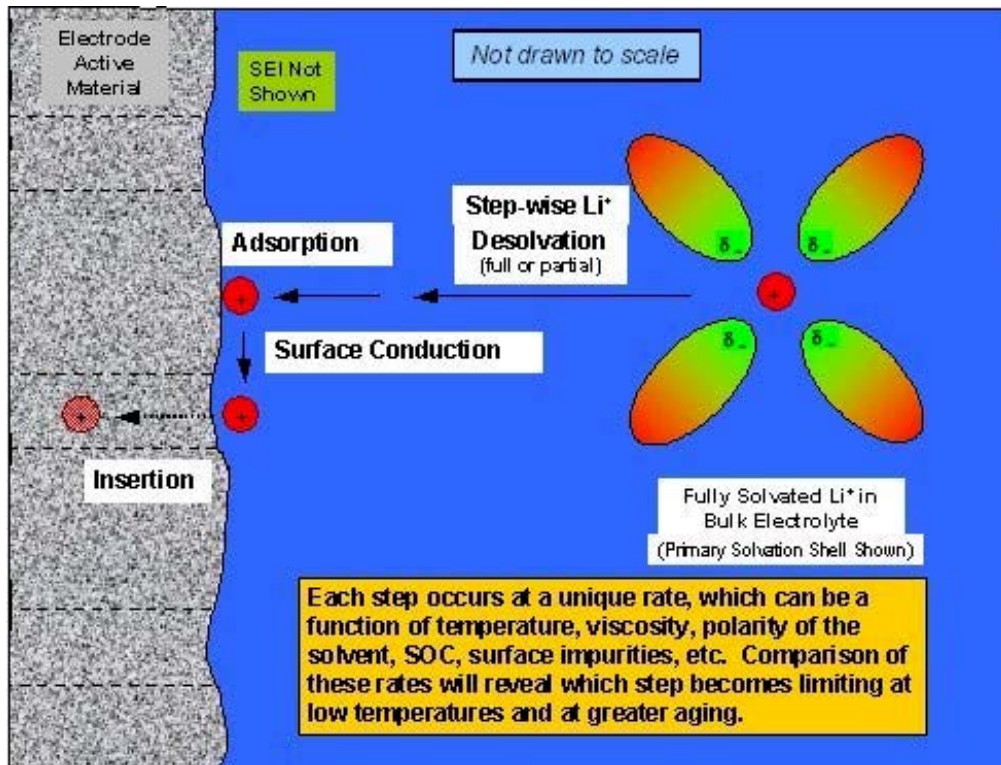


Figure III-20. Idealized rendering of the lithium desolvation/intercalation process

To facilitate a thorough investigation of Li-ion electrolyte behavior as a function of temperature, a new method has been developed and applied to representative electrolyte systems. This method yields a bulk parameter denoted as Li-STEP (Lithium Solvation and Transport Electrolyte Parameter), which incorporates five essential quantities for considering the role of transport properties and lithium desolvation prior to cation intercalation: electrolyte conductivity, lithium transference number, solvent-lithium binding energy (BE), average solvent residence time around lithium ions, and the lithium solvation number. Figure III-21 summarizes the function and parameters of the Li-STEP method. This method can also be used to describe the activation energy of lithium charge transfer from the bulk electrolyte to the surface of an electrode particle through a step-wise Arrhenius approach.

Key systems were tested by this approach (EC-EMC-LiPF₆ and PC-EA-LiBOB) to see how the activation energies differ, and with that obtained from cell performance data (polarization resistance of Gen2 cells under cold-crank testing). Arrhenius plots of Li-STEP values are shown in Figure III-22, wherein the LiBOB system exhibits better overall performance due to its higher Li-STEP values and lower activation energies. Also shown are the Arrhenius plots of the conductivity component of Li-STEP, indicating that the bulk of the activation energy assigned to electrolyte performance is due to the lithium desolvation process. This result is significant in that it shows that the greatest impedance component arising from the electrolyte at lower temperatures is due to the lithium desolvation process, which can involve energies generally between 400–500 kJ/mole to decouple all the solvent molecules from a lithium ion prior to intercalation.

Note that electrolyte performance must be considered in tandem with cell test conditions. Jointly, these will have a profound effect on concentration polarization (e.g., at near proximity to cathode particles) and the phase separation of one or more electrolyte component due to a Gibbs Adsorption process. The general Li-STEP approach is utilized as a screening tool to determine which electrolytes have a minimal impact on the activation energy of lithium charge transfer. Supporting the Li-STEP approach are a number of quantities also predicted by the analytical electron microscopy (AEM), including concentration-dependent solvent and solution permittivities, Gibbs Free Energy of ion solvation, and ion association terms (concentrations of free ions, ion pairs, and triple ions).

Lastly, Large-Scale Simulations (LSS) were performed on key LiBOB-based electrolytes to determine optimal solvent proportions, using conductivity as the optimization parameter. These systems included EC-PC-DMC-LiBOB, EC-PC-EMC-LiBOB, and EC-PC-DEC-LiBOB. Also, final LSS were performed on the system EC-DMC- γ BL-EA-LiBOB. Results from these LSS have enabled other researchers to optimize electrolytes used in materials screening studies.

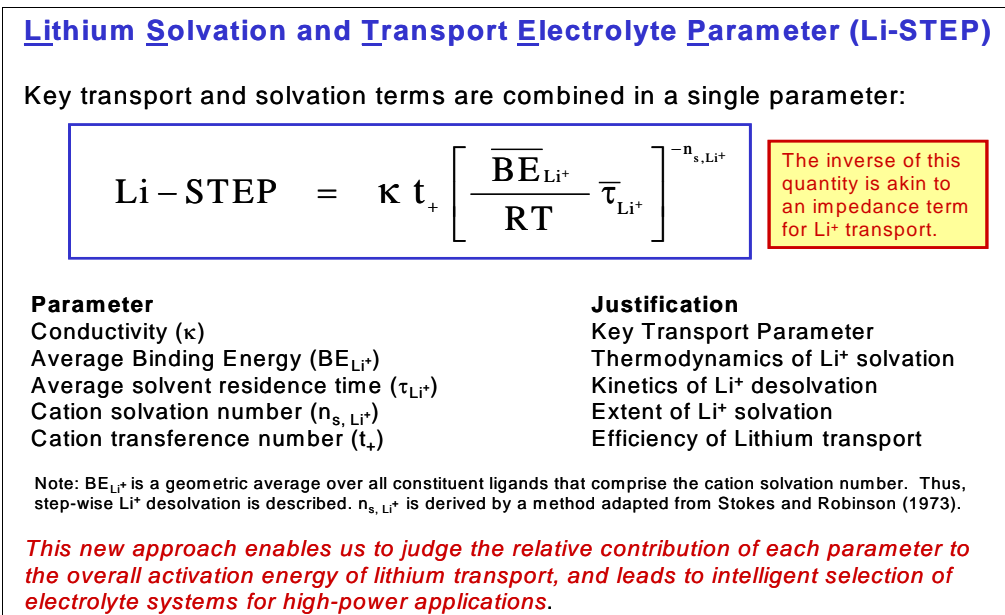
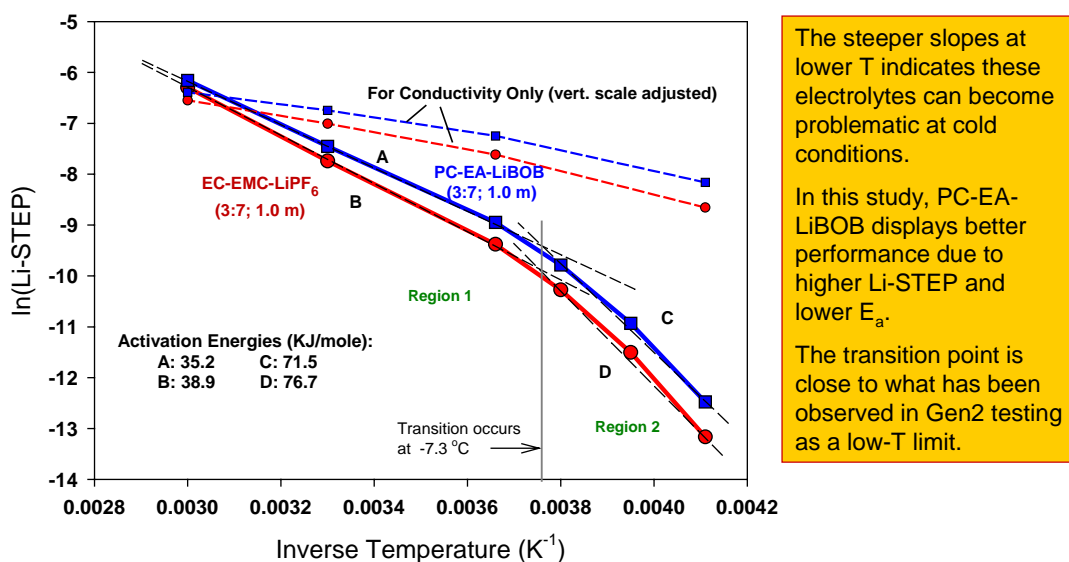


Figure III-21. Summary of Li-STEP expression and related parameters

Arrhenius Plots of Li-STEP for Li-ion Electrolytes



Two Regions are seen where the activation energies double after the transition.

Figure III-22. Comparison of Li-STEP Arrhenius plots for EC-EMC-LiPF₆ and PC-EA-LiBOB electrolytes. Arrhenius plots of conductivity for these electrolytes are shown as a baseline, the vertical scale has been adjusted for a clearer comparison.

III.D Understand and Enhance Abuse Tolerance

Objectives

- Determine response of cells to thermal abuse and overcharge.
- Investigate advanced chemistries to overcome abuse tolerance issues.
- Show relationship between abuse tolerance and chemistry, develop physical understanding through advanced diagnostics.

Approach

Thermal Abuse

- Measure shut-down characteristics of alternative separators.
- Establish role of each cell component on the thermal characteristics of the Gen2 cell chemistry.
- Using this information, identify alternative cell components and additives that possess the potential to enhance thermal abuse tolerance and evaluate their impact (mainly via differential scanning calorimetry [DSC]).
- Fabricate 110 mAh sealed prismatic cells and 18650 cells with the most promising cell components and additives to validate and quantify respective enhancements (via accelerated rate calorimetry [ARC] and thermal block studies).

Overcharge Abuse

- Establish overcharge characteristics of Gen2 cells
- Identify methods to enhance overcharge tolerance and evaluate in 18650 cells.

Accomplishments/Findings

- The main reaction at the Gen2 cathode is due to the oxidation of solvent by oxygen released from the cathode at high temperature.
- Anode can be stabilized against thermal decomposition either by additives or by improved carbon particle properties.
- Electrolyte salt effects:
 - LiBOB and LiBETI both result in increased thermal/gas reactions
 - Flame retardant additives can reduce flame intensity but may increase thermal/gas reactions
- Phoslyte flame retardants show promise but low temperature reactions need to be suppressed.
- The onset temperature of thermal decomposition strongly depends on the lithium content in the structure, i.e., it takes place at lower temperature as the degree of Li-ion deintercalation increases.
- The Gen2 cathode is more stable than pure LiNiO₂ cathode but less stable than LiNi_{0.5}Mn_{0.5}O₂.
- Ni ions on the surface of the electrode remain unchanged in the Ni²⁺ oxidation state during charge, in general, the surface of the nickel-based cathodes have a different electronic structure from the bulk.
- Overcharge response is determined by separator shutdown and overpotential:
 - initial heat generation at 125% state-of-charge (SOC), and
 - gas generation at first voltage peak near 145% SOC.
- Extended low-rate charging can result in a highly unstable cell even at low potentials.

Future Studies

- Determine the impact on cell safety of new additive that stabilize the solid electrolyte interface (SEI) layer, of low surface area and spherical carbon, and of a stable cathode material that doesn't generate oxygen during heating.
- Determine the impact on safety of new phoslyte material.
- Model thermal response of full cell using measured cell thermophysical properties.
- Perform in situ X-ray absorption spectroscopy (XAS) and X-ray diffraction (XRD) of pouch cell.
- Use soft X-ray XAS to identify decomposition products from electrolyte salt.
- Investigate the effect of electrolyte on cathode degradation at elevated temperatures and at over charged states.
- Determine effect of additives and alternative electrolytes on overcharge response.
- Measure effect of improved separators on overcharge response.

Selected Publications

1. Proceedings of 204th ECS Meeting, Oct. 12–17, 2003, (Orlando, FL), “Effect of Additives and Anode Carbon on Heat and Gas Generation in Li-Ion Cells,” E. Roth and D. Doughty, K. Amine and G. Henriksen.
2. IMLB 12, June 27–July 2, 2004, (Nara, Japan), “Effects of Additives on Thermal Stability of Li Ion Cells,” D. Doughty, E.P. Roth, C. Crafts, G. Nagasubramanian, G. Henriksen and K. Amine.
3. 44th Battery Symposium, Nov. 4–7, 2003 (Osaka, Japan), “Modeling of Accelerated Power Fade of Li-Ion Cells,” E. Thomas, D. Doughty, R. Jungst, G. Nagasubramanian, and E.P. Roth.
4. 41st Power Sources Meeting, June 15–17, 2004, (Philadelphia, PA), “18650 Li-Ion Cell Building for Electrochemical and Thermal Abuse Testing at Sandia National Laboratories,” G. Nagasubramanian, E.P. Roth, C. Crafts, B. Sanchez, H. Case and D. Doughty.
5. E.P. Roth, D. Doughty, *Journal of Power Sources* 128 (2004) 308–318.

III.D.1 Introduction

This subsection provides highlights and progress on the work that is focused on understanding the factors that limit the abuse tolerance of the Gen2 Baseline cell chemistry and on identifying and developing alternative materials and cell components that enhance the inherent abuse tolerance of high-power Li-ion cells. Early work in this area centered on establishing the thermal abuse and overcharge abuse characteristics of Gen2 cells. During the last year, this work continued and it was supplemented with detailed studies at the cell component level to understand each component's role in the thermal abuse characteristics of the cell chemistry. The information obtained on the Gen2 Baseline cell components were used to identify several new materials that offer promise for enhancing the inherent abuse tolerance of the cell chemistry. Some of the more promising materials were incorporated into sealed 110 mAh prismatic and 18650 cells to verify the component-level improvements at the cell level.

Figure III-23 provides a schematic of how activities in this focus area relate to each other, while Table III-5 provides a summary of how the five Department of Energy (DOE) laboratories contribute to this focus area.

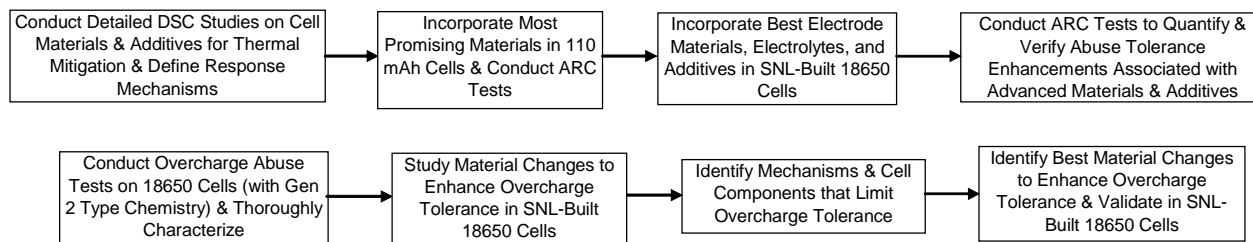


Figure III-23. Diagram of activities conducted under “Understand and Enhance Abuse Tolerance”

Table III-5. Summary of How the Five Department of Energy (DOE) National Laboratories Contribute to this Focus Area

	ANL ^a	BNL ^b	INEEL ^c	LBNL ^d	SNL ^e
Shutdown Tests on Alternative Separators					X
Detailed differential scanning calorimetry (DSC) on Gen2 Cell Materials	X				
Secure Advanced Materials with Enhanced Stability	X				
DSC and accelerated rate calorimetry (ARC) on Advanced Materials	X				
ARC on SNL-Built Cells with Advanced Materials					X
Overcharge on SNL-Built Cells w/Advanced Materials					X
Diagnostics on Abused Cells	X	X		X	X

^a Argonne National Laboratory (ANL)

^b Brookhaven National Laboratory (BNL)

^c Idaho National Engineering and Environmental Laboratory (INEEL)

^d Lawrence Berkeley National Laboratory (LBNL)

^e Sandia National Laboratories (SNL)

III.D.2 Thermal Abuse

III.D.2.1 Component-Level Studies

X-ray Diffraction (XRD) Studies of Thermal Decomposition of Gen2 Cathodes. The structural changes of the cathode material under thermal abuse condition and the interaction between cathode and electrolyte, investigated using time-resolved XRD, are being used to understand thermal abuse response.

Cathode materials electrochemically charged to various states were sealed in quartz capillaries with or without electrolyte. Time-resolved XRD patterns were continuously collected as the capillaries were heated from 25°C to 450°C. Thermal decomposition was not observed at 450°C for the sample at 0% state-of-charge (SOC) without electrolyte. However, for the sample charged to 50% SOC without electrolyte, thermal decomposition is observed at ~280°C, Figure III-24. At higher SOC, the decomposition occurs at still lower temperatures.

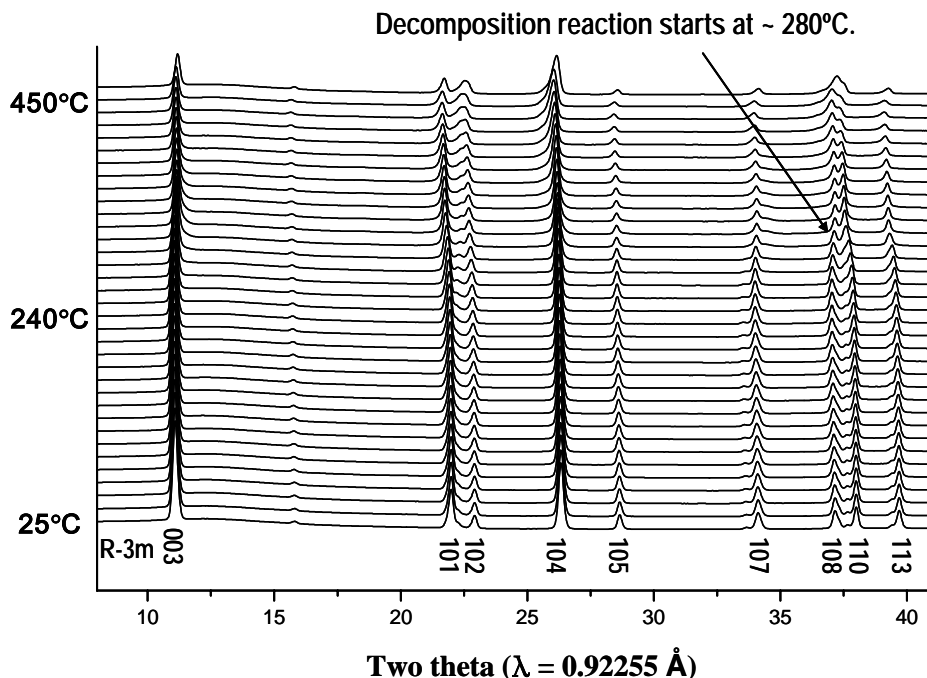


Figure III-24. XRD patterns of $\text{Li}_{0.67}\text{Ni}_{0.8}\text{Co}_{0.15}\text{Al}_{0.05}\text{O}_2$ (50%SOC) with electrolyte

In addition, it has been found that the presence of electrolyte accelerates the thermal decomposition of the charged cathode material. The electrolyte changes the paths of the structural changes and lowers the temperatures for onset of the reactions. In the presence of electrolyte, the solvent acts as a reducing agent and reacts with lithium to form Li_2CO_3 . As shown in Figure III-25, $\text{Li}_{0.27}\text{Ni}_{0.8}\text{Co}_{0.15}\text{Al}_{0.05}\text{O}_2$ (100% SOC) in the presence of electrolyte exhibits decomposition beginning at $\sim 200^\circ\text{C}$. Between 200°C and 250°C the coalescence of the (108) and (110) peaks in the layered structure is observed suggesting the formation of disordered spinel phase. Above 290°C , a rock salt structure is observed, consistent with the formation of NiO-like phase. The disordered spinel phase transforms progressively to the NiO-like phase by a first order phase transition as the temperature increases. During the conversion from a spinel to a rock salt phase, both lithium and nickel ions move randomly to other layers and there is no difference between the cation layers in the resulting structure. The transformation of the spinel phase to NiO-like rock salt phase is completed at the end of heating.

The effects of chemical compositions on the thermal decomposition of layer-structured cathode materials are shown in Figure III-26. For cathode materials charged to the same level, the thermal decomposition temperature for $\text{Li}_{0.33}\text{Ni}_{0.5}\text{Mn}_{0.5}\text{O}_2$ (100% SOC) is the highest (265°C), in comparison with 200°C for $\text{Li}_{0.33}\text{Ni}_{0.8}\text{Co}_{0.15}\text{Al}_{0.05}\text{O}_2$, which is better than 170°C for $\text{Li}_{0.33}\text{NiO}_2$.

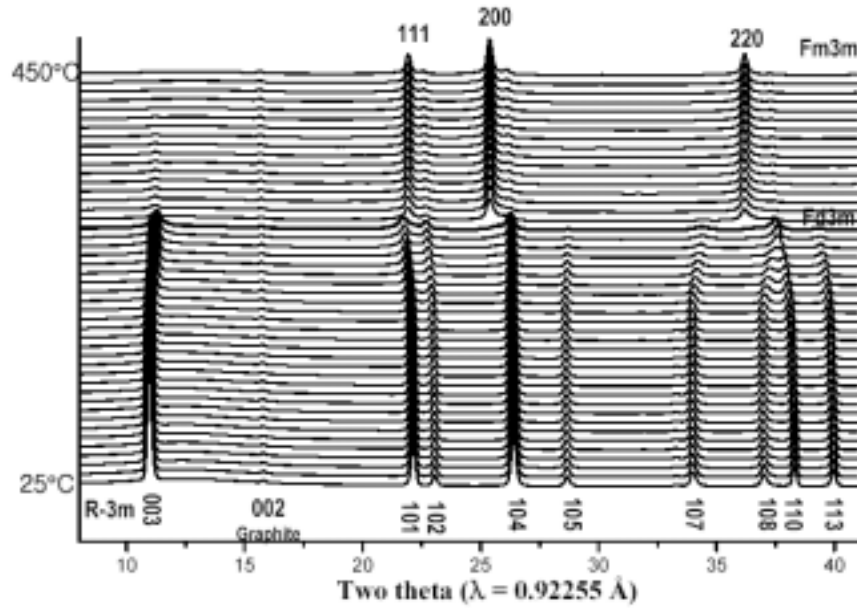


Figure III-25. Time-resolved XRD patterns for $\text{Li}_{0.27}\text{Ni}_{0.8}\text{Co}_{0.15}\text{Al}_{0.05}\text{O}_2$ with electrolyte, when heated from 25°C to 450°C.

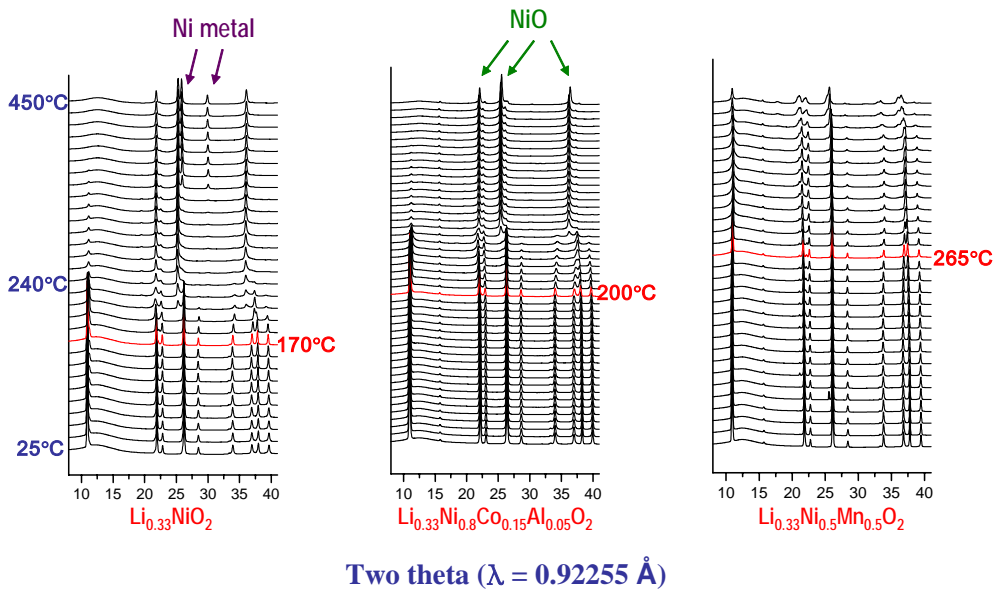


Figure III-26. XRD spectra for cathode material charged to $\text{Li}_{0.33}\text{Ni}_{0.5}\text{Mn}_{0.5}\text{O}_2$ (100% SOC), in comparison with $\text{Li}_{0.33}\text{NiO}_2$ and $\text{Li}_{0.33}\text{Ni}_{0.8}\text{Co}_{0.15}\text{Al}_{0.05}\text{O}_2$, when heated from 25°C to 450°C

Thermal Stability of $\text{LiNi}_{0.8}\text{Co}_{0.15}\text{Al}_{0.05}\text{O}_2$ (Gen2) Charged Powder. To further investigate the thermal stability of the Gen2 cathode, a battery fabricated with Gen2 powder was charged at 4.2 V vs. metallic lithium. The positive electrode consisted of Gen2 powder which was pressed between two layers of an aluminum mesh. This technique allowed the Gen2 powder to be cycled without the use of carbon and binder additives. At the top of the charge, the cell generated a capacity of 120 mAh/g, which was equivalent to 50% lithium uptake. The actual composition of the charged Gen2 powder was determined to be $\text{Li}_{0.53}\text{Ni}_{0.8}\text{Co}_{0.15}\text{Al}_{0.05}\text{O}_2$.

Oxygen release from a charged Gen2 powder was measured using thermo-gravimetry (TG) analysis combined to a gas chromatography (GC) and mass spectrometer (MS) apparatus. The TG/GC/MS in situ setup allowed the quantification of the generated gas from a charged Gen2 powder for the first time. About 10 mg charged Gen2 powder was placed inside the furnace of a TG instrument. After calibration, the sealed furnace was constantly flushed with N_2 gas. The powder was heated at $1^\circ\text{C}/\text{min}$ from room temperature to 700°C .

Figure III-27 shows a TG analysis curve resulting from a thermo-degradation experiment of Gen2 powder between RT and 700°C . Figure III-28 shows the in situ gas analysis during the TG experiment. It is clear that charged Gen2 powder is stable up to 200°C ; thereafter it begins to lose oxygen. The amount of generated O_2 increases following the trend of weight loss and reaches its maximum $\sim 400^\circ\text{C}$. Beyond 400°C , no significant weight loss was observed. By the end of this experiment, only 88 wt% of the starting charged Gen2 powder was left, which was analyzed by XRD. The result shows that the powder adopted an NiO type structure which is consistent with the weight loss observed during the TG experiment. The Ni^{2+} presence was inferred prior to conducting the XRD analysis because of the greenish color of the recovered material.

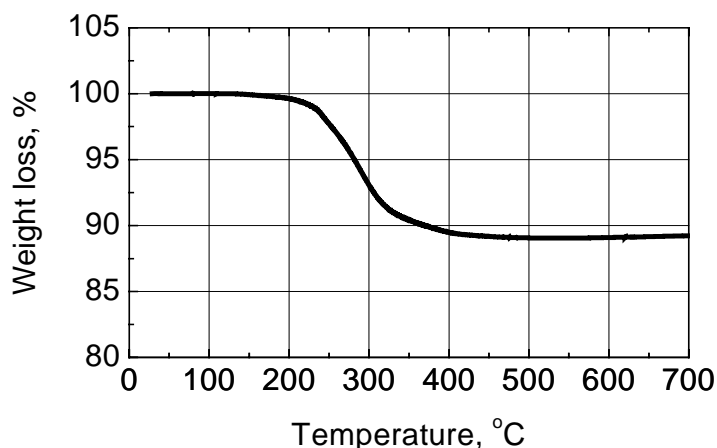


Figure III-27. TG analysis of charged Gen2 powder under N_2 atmosphere

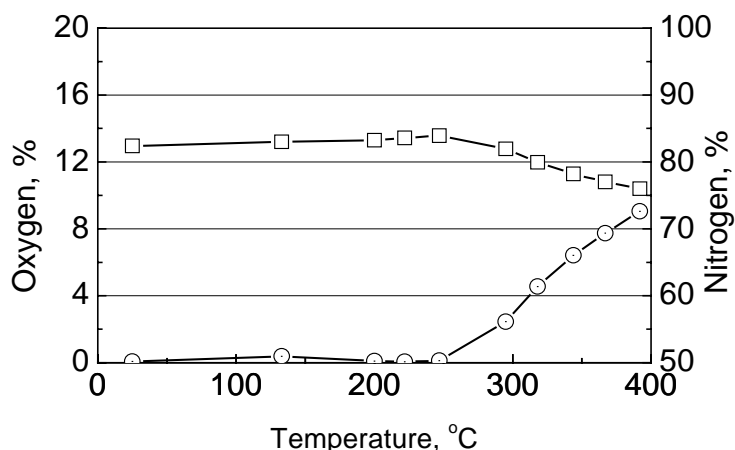


Figure III-28. In situ gas analysis of charged Gen2 powder under N₂ atmosphere

Two more TG experiments were carried under dry air and 4 wt% H₂/N₂ atmospheres. Under oxidizing conditions the TG results shows a similar trend, whereas under the reducing atmosphere, more weight loss (34 wt%) was observed and attributed to a significant bulk O₂ loss. By taking into account the formula Li_{0.53}Ni_{0.8}Co_{0.15}Al_{0.05}O₂, 34 wt% weight loss can only be associated with a complete de-oxygenation of the charged Gen2 powder. XRD analysis clearly confirmed this result because a Ni type material was obtained in the experiment involving reducing conditions (Figure III-29).

Thermal Investigations of Mag-10 Graphite Anode. The mechanisms of thermal runaway reactions for anode materials are useful in understanding the thermal behavior of Li-ion cells; which can lead to the development of new materials with improved safety and stability.

Electrochemical (galvanostatic cycling), thermal (differential scanning calorimetry [DSC]), and structural (XRD) studies were carried out to evaluate the thermal runaway behavior of the natural graphite (Mag-10) anode.

Figure III-30 presents the DSC curves obtained from the lithiated Mag-10 anode samples (every 20% state of charge) at a scan rate of 10°C/min from 50°C to 400°C. It can be seen that only one exothermic peak is detected in the fully de-intercalated sample. This peak is broadened to a wide peak with more intercalated lithium (Li_xC₆, x ≥ 0.18). A peak starting at 269°C and reaching the maximum at 283°C is detected in Li_{0.37}C₆. The trace of Li_{0.57}C₆ is very similar to that of Li_{0.37}C₆. However, a new sharp peak at about 336°C is detected in the curve for Li_{0.71}C₆. This sharp peak shifts to 301°C with more intercalated lithium (Li_{0.91}C₆). Based on these results, it appears that Li_{0.71}C₆ and Li_{0.91}C₆ lose the graphite structure at high temperature. Therefore the sharp peak detected for Li_{0.71}C₆ and Li_{0.91}C₆ samples can be attributed to the collapse of the graphite structure.

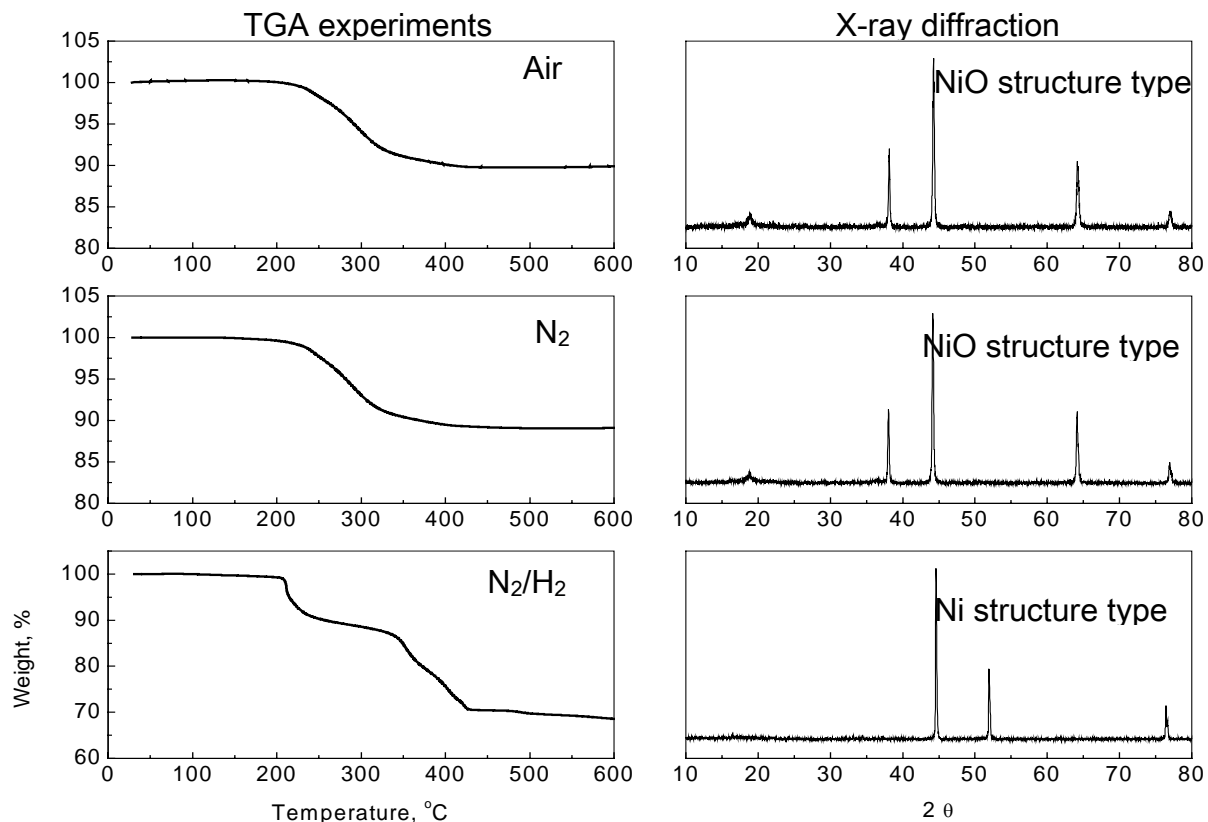


Figure III-29. TG analysis of Gen2 charged powder under different atmospheres. The corresponding XRD patterns were performed by the end of TGA experiments.

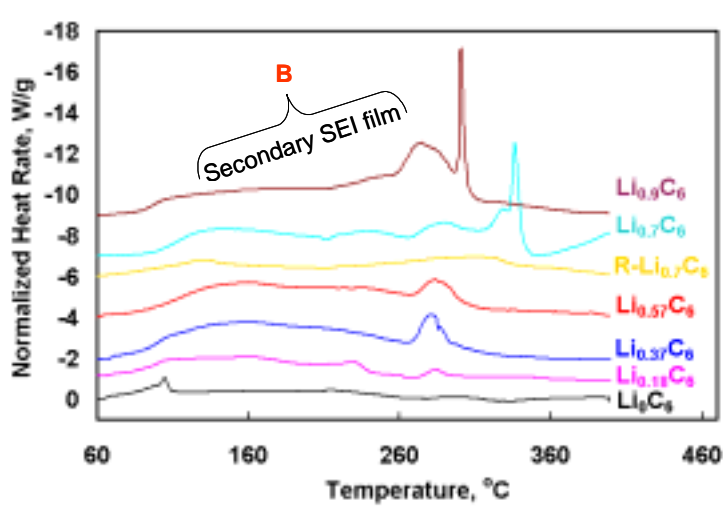


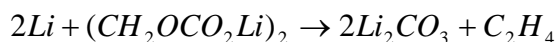
Figure III-30. Curves of Mag-10 samples with different amounts of intercalated lithium. R-Li_{0.71}C₆ represents a graphite anode rinsed with dimethyl carbonate (DMC) and vacuum dried to remove salt and ethylene carbonate (EC).

The Li_0C_6 sample (0% SOC) contains graphite, solid electrolyte interface (SEI) film, and the remaining electrolyte (mainly LiPF_6 and ethylene carbonate [EC]). SEI film comprises stable compounds (LiF , Li_2CO_3 and other inorganics) and meta-stable components (Lithium-alkyl carbonates, lithium semi-carbonate). The meta-stable components are not stable at high temperatures, especially in the presence of Li atoms. The electrolyte employed here does not decompose and produce heat until 250°C . In addition, fresh graphite does not react strongly with electrolyte below 190°C . Therefore, this peak can only be attributed to the SEI breakdown.

One possible reaction mechanism is:



The peak associated with the SEI film decomposition increases with increasing intercalated lithium. There are two possibilities for the peak broadening associated with the SEI breakdown. Firstly, the covered surface that is initially present is exposed due to the melting of poly(vinylidene fluoride) (PVdF) and new SEI film is formed through the reaction between the intercalated Li and electrolyte. Also, the intercalated Li can react with $(\text{CH}_2\text{OCO}_2\text{Li})_2$ compound as:



In the DSC scan of $\text{Li}_{0.18}\text{C}_6$, the heat rate after SEI film decomposition does not drop to zero until 240°C , indicating that there are some new reactions following SEI decomposition. This mild broad peak is enlarged when more lithium ions intercalate, as illustrated in the DSC traces of $\text{Li}_{x>0.37}\text{C}_6$. This reaction disappears in the rinsed $\text{Li}_{0.71}\text{C}_6$ sample (shown in curve R- $\text{Li}_{0.71}\text{C}_6$, which was rinsed with DMC and vacuum dried to remove all the salts and EC). In addition, this peak is absent in the fully deintercalated sample. Therefore, this peak can be attributed to the reaction between the intercalated lithium and the electrolyte.

SEI film compounds contain electronically insulating $(\text{CH}_2\text{OCO}_2\text{Li})_2$ which inhibits further co-intercalation of solvent molecules and/or exfoliation of the graphite surface, hence allowing only Li^+ migration. The $(\text{CH}_2\text{OCO}_2\text{Li})_2$ present on the surface film is removed after the SEI breakdown. Thus, salts and electrolyte can permeate the Li_2CO_3 and LiF film to reach the lithiated graphite surface. It has been reported in the literature that the intercalated Li ions move to the edge of graphite particles at high temperatures. These intercalated lithium ions react with the electrolyte to form a new stable "secondary" SEI film. The formation of secondary SEI film would stop when either the new film is too thick or all the intercalated Li has been consumed. It is likely that only stable compounds such as Li_2CO_3 and LiF are formed at that high temperature.

Assuming that the formation of Li_2CO_3 is the main reaction in the formation of the secondary SEI film, the enthalpy value should be proportional to the amount of consumed Li in this reaction. It is clear from Figure III-31 that the enthalpy is proportional to the lithium content when $x < 0.37$. However, the enthalpy increases rather slowly for $x > 0.37$, indicating that the formation of secondary SEI film stops after 0.37 Li has been consumed.

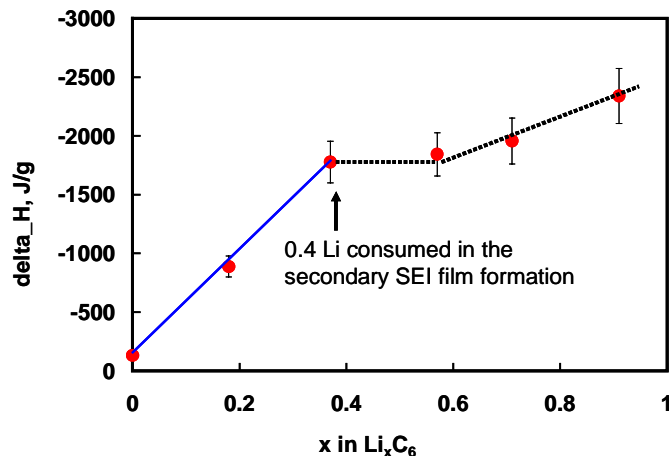


Figure III-31. Overall heat generation of Mag-10 with different amounts of intercalated Li

Based on the primary and secondary SEI film decomposition, one possible explanation for the thermal runaway and structural collapse of the graphite anode is as follows. At first, meta-stable compounds in the SEI film break down at $\sim 80^\circ\text{C}$. Some of the LiPF_6 also decomposes at $\sim 70^\circ\text{C}$ to produce LiF and PF_5 . Due to the SEI film breakdown, EC and LiPF_6 penetrate the SEI film and reach the edge planes of the graphite. The intercalated Li is very active and mobile at high temperatures, and PF_5 accelerates the Li movement by removing electrons from graphite. A secondary SEI film is formed when the electrolyte reacts with the lithium diffusing from the inner structure. This reaction does not stop until either the Li is consumed completely or products such as Li_2CO_3 and LiF block the surface of edge planes.

The formation of the secondary SEI film consumes about 0.37 Li while causing some graphite particles to break into smaller pieces while maintaining the bulk structure. The remaining intercalated Li stays in the graphite structure because all the edge planes are now blocked. However, this new Li_xC_6 structure is very active at high temperature and will collapse and release Li when more than 0.3 Li remains in the C_6 . The more remaining intercalated lithium (≥ 0.34 Li) renders the structure less stable and results in a lower activation energy for the structural collapse reaction which occurs at a lower temperature. The released Li reacts with the PVdF binder to form LiF and hydrogen.

III.D.2.2 Cell-Level Studies

Mitigation Cell Study. Improvements in cell thermal abuse tolerance were demonstrated using improved anode carbon and additives. These cell compositions were specified by Argonne National Laboratory (ANL) and built at Quallion in the form of 110 mAh prismatic cells. The cells use the standard Gen2 positive material but include cells with standard Mag-10 or GDR carbon that has been shown to have more stable thermal properties. The electrolyte included Gen2 electrolyte as well as one with vinyl ethylene carbonate (VEC) and triphenyl phosphate (TPP) additives. Cells with EC:PC:EMC electrolyte were also investigated. Thermal profiles were obtained during accelerated rate calorimetry (ARC) runs to 400°C , gas volumes and species were measured at the end of each run. One sample from each cell composition was cooled prior to cell venting at 140°C

and the gases measured by puncturing the cell directly into a gas chromatography (GC) system for detailed gas analysis. General observations from this study are:

- Anode can be stabilized either by additives or by improved carbon particle properties.
- VEC reduces gas generation prior to vent.
- Gas generation rates after venting is similar for all materials and additives:
 - CO₂ is the dominant decomposition gas species of vented cells, and
 - CO occurs in equal amounts with CO₂ in cells just prior to venting (140°C) due to reduction of CO₂ at the anode.
- Small cells are useful for screening and comparing new materials but variations in cell response and effects of venting require several cell samples for accurate determination of material effects.

18650 Cell Testing. Coated materials from Quallion were used to assemble cells using a commercial Hoshen winder system and a custom cell filling station designed at Sandia National Laboratories (SNL). Baseline materials consisted of 6% GDR graphite anodes and standard Gen2 cathodes and electrolyte. Cells were fabricated with capacities of ~911 mAh and showed stable C/5 capacities up to 220 cycles with an 8.5% loss. ARC runs on these cells showed similar thermal runaway response as seen in cells made at Quallion. The purpose was to investigate alternative salts and electrolyte additives:

- Salts – LiPF₆, LiBOB, LiBET
- Additives –
 - SEI enhancer – vinyl ethylene carbonate (VEC)
 - Flame Retardants – ANL proprietary Phosphazene additives “C,” “B” triphenyl phosphate (TPP) tris(trifluorethyl) phosphate (TFP) from U.S. Army Research Laboratory (ARL)

The thermal abuse response of these cells and the flammability of the vented gases were measured using a thermal block apparatus that allows determination of the onset of cell heat generation and also the flammability of the vented gases in the presence of an external ignition source. Cells were ramped in open air at a rate of 6°C/min until thermal runaway.

Thermal Ramp Response/Flammability Study. The baseline cells without additives showed self heating beginning at 150°C with thermal runaway occurring at 195°C. The vent gases ignited and burned for several seconds after runaway. The temperature difference between the cell and thermal block was differentiated to obtain a heat generation rate similar to the data for the accelerated rate calorimetry (ARC) runs (Figure III-32). This calculation showed that the cell thermal response during forced thermal ramp was clearly divisible into three regions:

- low-rate onset region up to 150°C,
- acceleration region from 150°C–190°C, and
- final runaway region above 190°C.

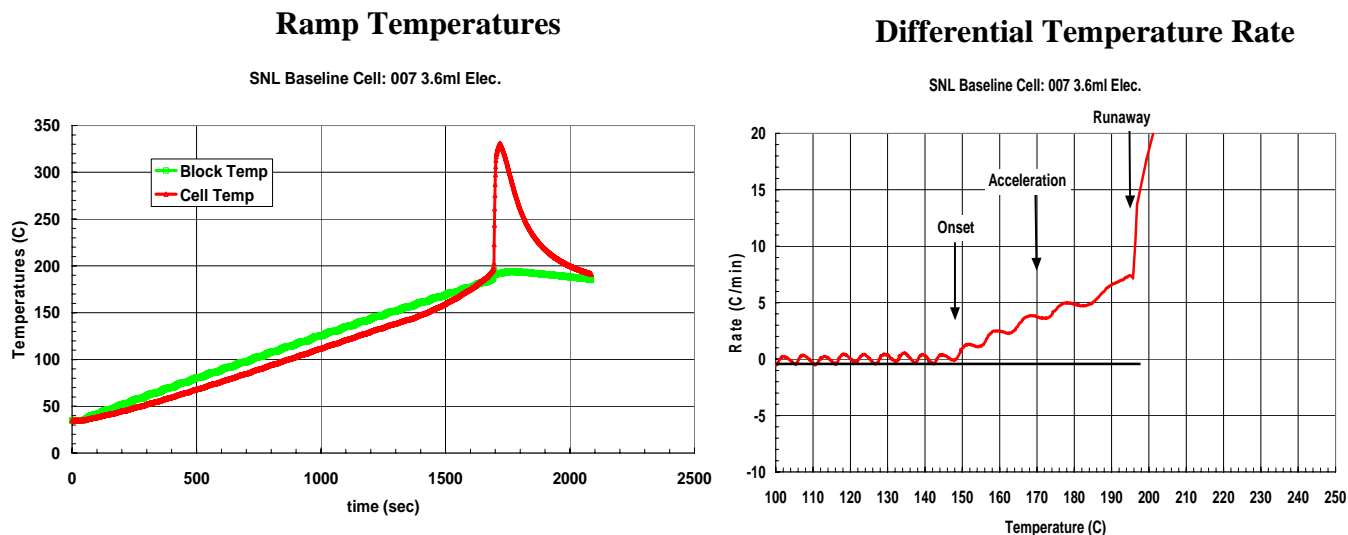


Figure III-32. Temperatures and heating rates for baseline cell during ramp to thermal runaway

The results of the various tests for the different materials and additives are summarized below:

- Cells with ANL flame retardant additive C showed an abrupt reaction at 140°C at the 5 and 10wt% level for fresh cells with only 5 cycles, indicating instability of the additive with this chemistry.
- Cycling reduced reactivity of additives in the cells:
 - Cells with 95 cycles showed thermal runaway response at 192°C, similar to baseline cells, but with no sustained flames, even with spark source.
 - Cells with 220 cycles also showed thermal runaway at 190°C but lost any visible indication of flame suppression suggesting that the additive was effectively consumed with cycling.
 - Gas chromatography/mass spectroscopy (GC/MS) analysis of electrolyte from fresh and cycled cells (30 cycles) showed a 20% reduction in additive C confirming this result.
- Cells with 15% and 20% ANL flame retardant additive B showed:
 - abrupt reactions at 140°C for cells with 20 cycles or less improved response with runaway at 192°C with more cycling (35 cycles), and
 - reduced flame intensity and duration compared to baseline cells but not complete flame suppression.
- Cells with 5% ARL TFP additive showed runaway response at 188°C with continuous flame.
- Cells with 2% VEC and 5% TPP (30 cycles) behaved much like the Gen2 Baseline cells with thermal runaway around 192°C but still showed sustained flames.
- Cells with alternative salts showed poorer runaway response compared to LiPF₆ (Figure III-33).
 - Cells with 0.5M LiBOB salt showed:
 - similar onset temperature as seen for baseline cells (145°C),
 - lower acceleration rates, possibly due to increased gas evolution,
 - smokeless flame at relatively low intensity during acceleration region, and
 - runaway temperature (192°C), slightly lower than seen for Baseline cells.

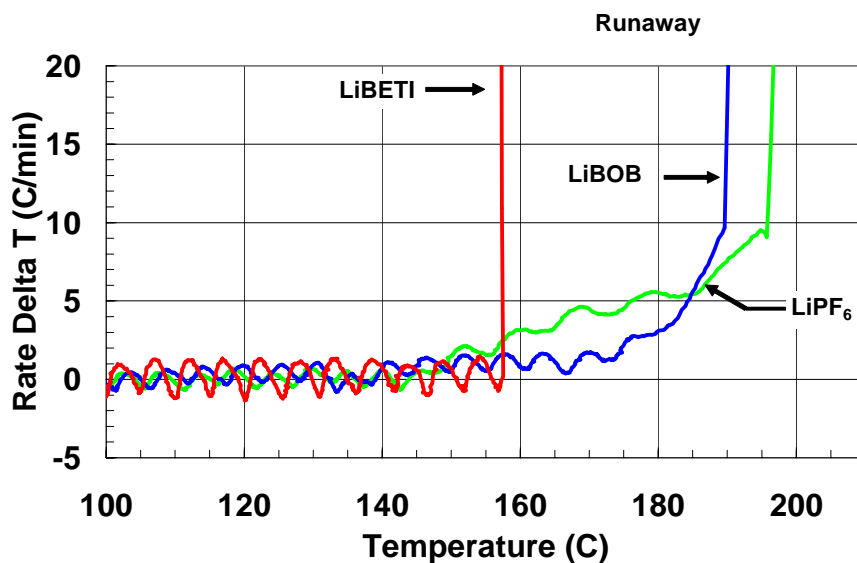


Figure III-33. Thermal ramp runs for 18650 cells with different electrolyte salts

- Cells with 1M LiBETI salt showed abrupt runaway at 158°C after 35 cycles.

ARC Results. ARC runs were performed on fully charged cells in a closed 18650 cell holder up to 400°C. Gas volume evolution was calculated based on measured pressures and system parameters. ARC data confirmed cell responses seen during thermal ramp experiments. The ARC results are summarized below:

- Equivalency of Sandia and Quallion cells was demonstrated under equal ARC conditions.
- ANL additive C cells showed increased thermal runaway temperatures with cycling.
- Cells with VEC and TPP additives showed reduced heating rates.
- TFP additive (ARL) had no effect on heat rate.
- LiBOB cells had increased thermal reactivity starting at 125°C in agreement with literature reports (greater reactivity with cathode), peak reaction temperatures about 20°C lower than Baseline cells, and increased gas generation starting at 110°C.
- Equal gas volumes evolved for all additives after complete reaction to high temperatures (see Figure III-34).
- No material, salt or additive showed better thermal response than the Baseline GDR/Gen2 cells. Similar reaction profiles and peak rates during thermal runaway for all cells.

In short, there is no “magic bullet” for producing completely stable Li-ion cells. Thermal abuse tolerance will result from informed choices of improved cell materials, additives and cell design.

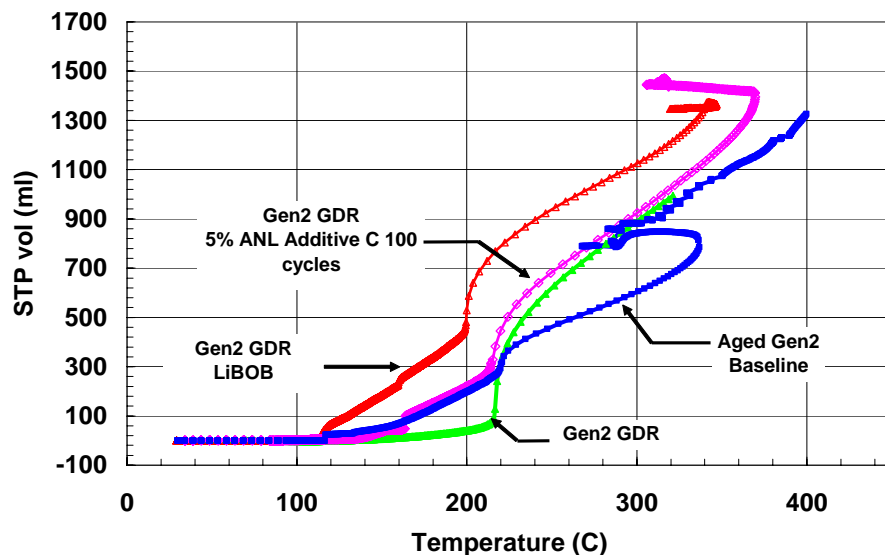


Figure III-34. Volume of gas generated during ARC runs with different additives and salts

III.D.3 Overcharge Abuse

The goal of this work is to determine the effects of overcharge and thermal decomposition leading to cell thermal runaway. Overcharge studies have continued using a custom apparatus at Sandia National Laboratories (SNL) which allows quantitative measurements of the cell heat generation during overcharge and real-time gas monitoring. It has previously been demonstrated that high-rate overcharge can lead to thermal runaway. Similar investigations have been made at low rates to show that thermal runaway does not automatically occur for Gen2 cells even for extended overcharges as long as the cell temperature remains below the separator melt temperature (135°C). Figure III-35 shows a cell charged at a 1.1C rate with stable cell temperatures for extended overcharge. The heat generation increased sharply at 125% state-of-charge (SOC), peaked at 225% SOC and eventually acted as a passive resistive load where the heat out equaled the power in. Gas generation occurred at the first voltage peak at 145% SOC and consisted primarily of H_2 , CO , and CO_2 followed by a second gas release at 225% SOC. These cells were shown to be very unstable and could go into runaway with a thermal impulse driving the cell temperature above the separator melt.

Electrode materials from overcharged (150% SOC) 18650 cells were removed to study the structure and properties of these materials. The major research efforts were to determine the electrode crystal structures at high state of overcharge; compare full cell electrodes with T-cell electrodes, and determine the reactivity of overcharged electrode materials.

Both full 18650 cells and T-cells were overcharged to the peak in cell voltage around 150% SOC. Additional T-cells were overcharged up to 250% SOC. Cell materials were removed in an Argon glove box and sealed in plastic bags for X-ray diffraction (XRD) analysis. Differential scanning calorimetry (DSC) samples were also prepared and measured. The results of these tests are summarized below.

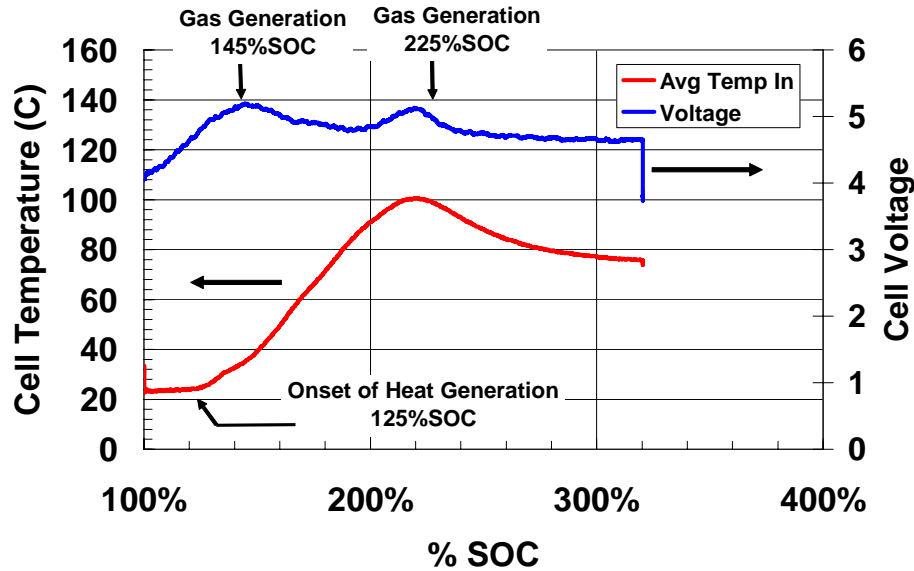


Figure III-35. Low rate (1.1C) overcharge of Li-ion cell below separator melt temperature

Disassembled 18650 cells:

- Anodes: Evidence of Li staging and incomplete lithiation of anode due to cathode limited cell design and reduced Li in fully charged $\text{Li}_x\text{Ni}_{0.8}\text{Co}_{0.15}\text{Al}_{0.05}\text{O}_2$.
- Cathodes: Maintain layer structure but show strain-broadening of c-axis peaks.

T-Cells:

- Anodes appear:
 - metallic after cycling against Li metal to 150% SOC, and
 - bronze after cycling against cell cathode nominally to 150% SOC and 250% SOC indicating incomplete lithiation.
- Cathodes:
 - cathode layered structure maintained even up to “nominal” 250% SOC,
 - similar full cell and T-cell cathode crystal structures, and
 - no difference in structure measured for cathodes charged to 250% SOC either against Li metal or GDR graphite anode indicating that the anode does not limit cathode charging.

DSC analysis:

- Anodes:
 - Overcharge increases high-temperature peak reaction rate.
 - Li metal plating not observed for cathode limited Gen2-based cells.
 - Extended charging of anode vs. cathode to 250% SOC resulted in reduction of anode reactivity indicating that side reactions at high potentials were either consuming Li from the anode or creating a more passivating layer (Figure III-36).
 - Extended charging of anode vs. Li to 250% SOC resulted in deposition of Li metal on surface indicated by a Li melt endotherm at 180°C and significantly increased reactivity (Figure III-36).

- Cathodes: Extended charging of cathode vs. anode lowered peak reaction temperature eventually resulting in a sharp reaction peak at 260% SOC (Figure III-37).

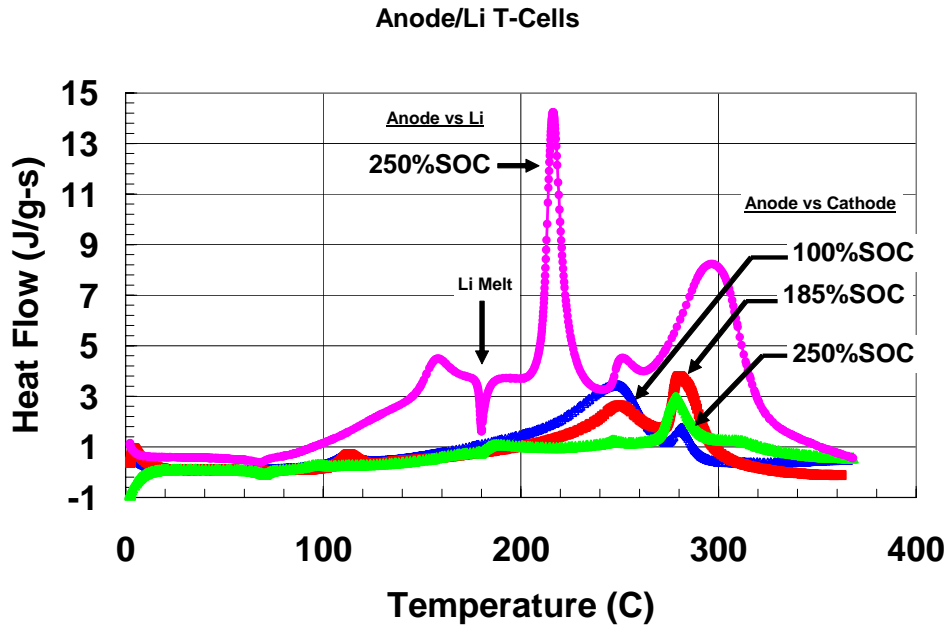


Figure III-36. DSC runs of overcharged anodes vs. Li and vs. cathodes

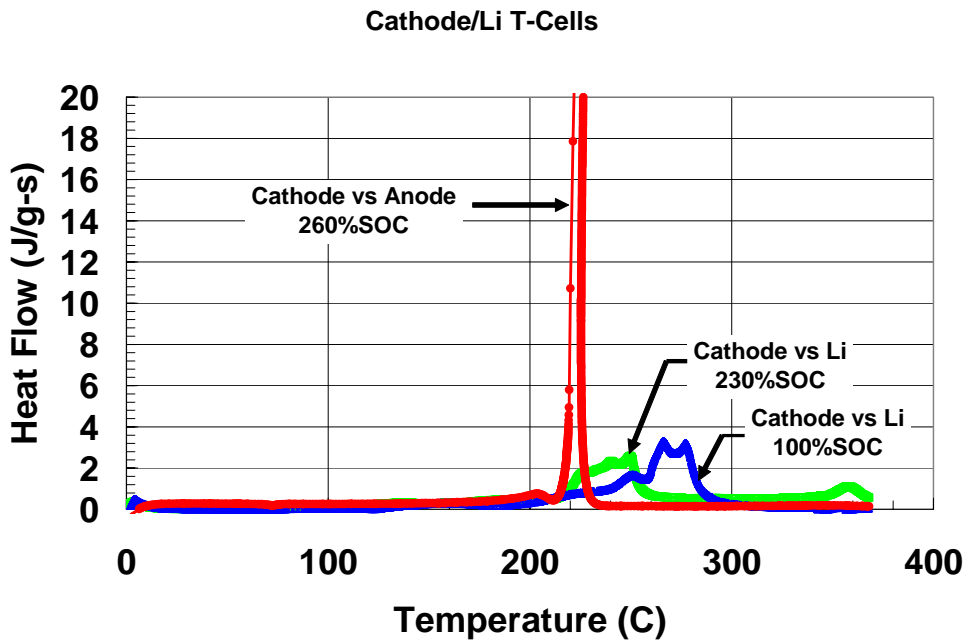


Figure III-37. DSC runs of overcharged cathodes vs. Li and vs. anodes

III.E. Cell Level Cost Reduction

Objectives

- Identify and secure advanced low-cost cell materials from international material suppliers and evaluate samples for high-power hybrid electric vehicle (HEV) applications. Provide feedback to material suppliers on the capabilities and limitations of their materials.
- Develop lower-cost high-power cell chemistries — using the most promising materials — and conduct preliminary performance, life, and safety evaluations to establish their viability.
- Conduct post test analyses of gel electrolyte cells to understand performance decay mechanisms and delamination problems.
- Explore novel approaches for reducing the cost of cell packaging.

Approach

- Secure samples of the most advanced materials from material suppliers.
- Refine rapid screening test protocols to assess the suitability of novel materials. Employ protocols to evaluate material capabilities, provide feedback to the material suppliers.
- Produce cells from the most promising low-cost materials and conduct preliminary evaluations on their performance, life, and safety characteristics, using sealed prismatic cells.
- Thoroughly examine aged/tested cells for adhesion, wetting, and gassing problems.
- Develop a new flexible pouch design that limits permeation of electrolyte and moisture.
- Develop a new class of organoclay nanocomposite materials that improve the barrier properties of the sealant layer and the adhesion of the sealant layer to the aluminum foil layer.

Accomplishments/Findings

- Established and maintained contacts with material suppliers in Japan, Korea, and Europe.
- Obtained samples of advanced natural and synthetic graphite materials, advanced layered and 3D spinel cathode materials, electrolyte salts, separators, and binder materials for evaluation.
- Conducted screening tests on advanced materials and provided feedback to suppliers. One notable accomplishment was the development of a Li-rich version of the 123 cathode material that appears to provide improved cost, abuse tolerance, and similar power compared to the Gen2 material.
- Further evaluated the power and aging of cells employing Daiso and Damus-Kaye-Stansel (DKS) gel electrolytes.
- Showed that gel electrolytes can slow the capacity fade of Mn-spinel cathode materials.
- Collaborated with Sumitomo Electric Industries (SEI) to improve HEV-sized flexible battery packaging.
- Improved an organoclay nanocomposite material which resulted in a large improvement in water vapor barrier properties.

Future Studies

- Solicit samples of separator materials from industrial firms that are developing low-cost separators under the FreedomCAR and Fuel Partnership.

- Continue conducting screening tests of new materials and providing feedback to the suppliers.
- Continue working with Showa Denko and Quallion to evaluate the Showa Denko technology.
- Continue development of materials for use with gel electrolytes (lithium salts, electrodes, etc.)
- Continue collaboration with SEI to evaluate their HEV-sized flexible battery packaging under abuse conditions, perform a cost analysis on the packaging and submit this and other cell designs to vibration tests.

III.E.1 Introduction

This subsection provides highlights and progress on the work that is focused on cell-level cost reductions. Since the Applied Battery Research program began, it has been searching for lower-cost cell materials and components that possess enhanced stability. These materials include: electrode active materials, conductive additives, binders, electrolyte salts and solvents, as well as separators. Some internal research and development (R&D) has been conducted in collaboration with U.S. Army Research Laboratory (ARL) to develop lower-cost electrolyte systems. The program has also been studying the use of flexible cell packaging as a low-cost alternative to metal cans, and working to improve the barrier properties of this type of cell packaging to achieve the 15-year life goal. In this connection, some internal R&D has been conducted on the development of a suitable organoclay nanocomposite technology that shows promise for significantly enhancing the barrier properties of the conventional polymer films used for flexible packaging.

Figure III-38 provides a schematic of how activities in this focus area relate to each other, while Table III-6 provides a summary of how the five Department of Energy (DOE) laboratories, together with ARL, contribute to this focus area.

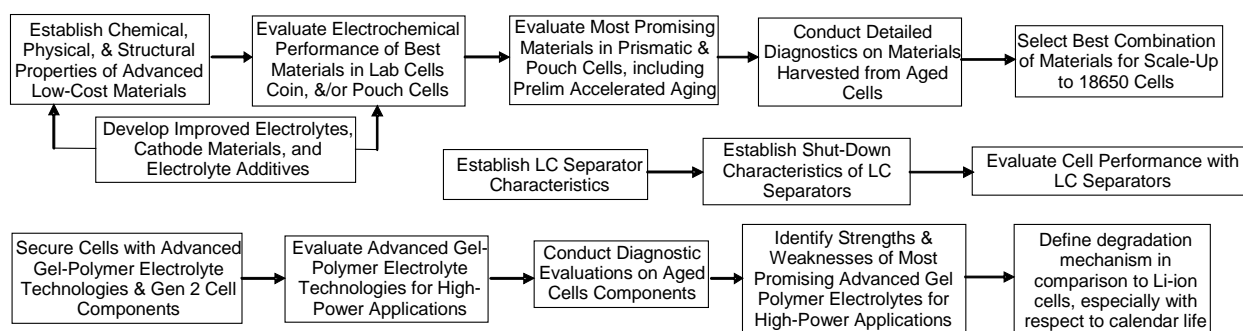


Figure III-38. Diagram of related activities conducted under this “Cell-Level Cost Reduction” focus area

Table III-6. Summary of How Five DOE National Laboratories, Together with ARL, Contribute to this Focus Area

	ANL ^a	ARL ^b	BNL ^c	INEEL ^d	LBNL ^e	SNL ^f
Secure and Evaluate Materials	X					
Develop Electrolytes and Materials	X	X		X		
Preliminary Accelerated Aging Tests	X					
Cell Component Diagnostics	X		X		X	
Gel-Polymer Electrolyte Evaluations	X					
Low-Cost Flexible Packaging	X					

^a Argonne National Laboratory (ANL)

^b U.S. Army Research Laboratory (ARL)

^c Brookhaven National Laboratory (BNL)

^d Idaho National Engineering and Environmental Laboratory (INEEL)

^e Lawrence Berkeley National Laboratory (LBNL)

^f Sandia National Laboratories (SNL)

III.E.2 Material Screening and Development

A major effort associated with securing and evaluating the newest advanced low-cost cell materials, from international suppliers, has always been a major part of this program. Many of these advanced materials are being developed for high-energy applications, e.g., consumer electronics. The evaluations focus on the applicability of these materials for the high-power hybrid electric vehicle (HEV) application and frequently result in providing feedback to the industrial material suppliers, including recommendations as to how their materials could be modified to make them more optimal for high-power applications. This approach has resulted in the development of better materials for use in HEV batteries. Also, some internal research and development (R&D) is performed in the areas of more optimal cathode active materials and electrolytes for high-power HEV batteries.

There was a major focus on more optimal cathode materials this year, due to several factors. The Gen2 $\text{LiNi}_{0.8}\text{Co}_{0.15}\text{Al}_{0.05}\text{O}_2$ cathode material is fairly expensive and contributes to both the life and abuse tolerance limitations of the cell. For the last 2–3 years, this program has been focusing on two types of advanced cathode materials: the layered $\text{LiNi}_{1/3}\text{Co}_{1/3}\text{Mn}_{1/3}\text{O}_2$ (or 123) and the 3-dimensional $\text{Li}_2\text{Mn}_2\text{O}_4$ spinel material. This year these efforts received a significant boost due to the cost of cobalt rising dramatically (almost a 5-fold increase). This caused commercial Li-ion battery manufacturers to consider alternative cathodes to the conventional LiCoO_2 cathode material. Some are switching to the 123 material, while others are blending $\text{Li}_2\text{Mn}_2\text{O}_4$ spinel with the LiCoO_2 cathode material. Therefore, industrial material suppliers are working to improve these new cathode materials and scale up their production capabilities to meet the rising demand for these materials.

From a cost perspective, the $\text{Li}_2\text{Mn}_2\text{O}_4$ spinel cathode is the most attractive. It possesses a relatively low cost relative to other materials, but even more important is its extremely high rate capability relative to other materials. This latter characteristic allows use of cells with much lower capacity, which reduces the quantity (and associated costs) of all the other cell components. Thus, R&D efforts have been underway to stabilize this material against dissolution of Mn^{2+} which leads to a fairly rapid capacity fade, especially during elevated temperature operation. The stabilization efforts include the use of various dopants and surface coatings (at the particle level). To date, these approaches have reduced the rate of capacity fade, but they have not solved the problem.

Work on this program has clearly showed that the problem is further complicated for high-power applications by a fairly rapid impedance rise, which is associated with an interfacial impedance growth at the anode. Reduction of Mn^{2+} to Mn^0 at the surface of the anode was confirmed. Apparently, a very low level of Mn^0 can act as a catalyst in the formation of a resistive film on the surface of the anode. Therefore, we have focused our efforts on combining the partially stabilized $\text{Li}_2\text{Mn}_2\text{O}_4$ spinel cathodes with electrolytes that are more compatible with these cathodes. LiPF_6 salt reacts readily with traces of H_2O to form HF which will attack the Mn^{2+} at the surface of the cathode. Therefore, electrolyte systems that employ less reactive salts are being studied, as are electrolyte additives that can either protect the cathode from Mn^{2+} dissolution or protect the anode from the catalytic effects of Mn^0 .

One of the more promising partially stabilized $\text{Li}_2\text{Mn}_2\text{O}_4$ spinel materials studied this year was supplied to the program by Nippon Denko. Their spinel materials are surface coated with WO_3 , which is then available to react with HF and thereby help protect against Mn^{2+} dissolution. Figure III-39 illustrates the improvement in reducing the rate of impedance rise associated with using this type of cathode material. These cells incorporate a GDR graphite anode and 1.2M LiPF_6 in EC:PC:DMC (1:1:3) electrolyte. They were aged at 55°C and 60% state-of-charge (SOC). Materials with higher levels of WO_3 have been obtained from Nippon Denko for evaluation.

Use of LiBOB salt in place of LiPF_6 salt is another way to reduce the dissolution of Mn^{2+} and the corresponding rate of impedance rise. Figure III-40 demonstrates this improvement in cells that employ a different spinel cathode material from Toda and a GDR graphite anode. In both cases the electrolyte solvent system is the same [EC:PC:DMC (1:1:3)]. When LiPF_6 is the salt, it is present at the 1.2M level and when LiBOB is the salt, it is present at the 0.7M level. Again, the accelerated aging tests were performed at 55°C and 60% state of charge (SOC).

A third approach that has demonstrated improvements is the use of electrolyte additives. Figure III-41 shows capacity fade data on two cells that employ the same electrodes and electrolyte, except one of them incorporates an electrolyte additive (4-vinyl pyridine) that provides a polymeric film on both the anode and the cathode, thereby suppressing the dissolution of Mn^{2+} at the cathode and/or the catalytic effects of the Mn^0 at the anode. Both cells were tested at 55°C to accelerate the capacity loss process.

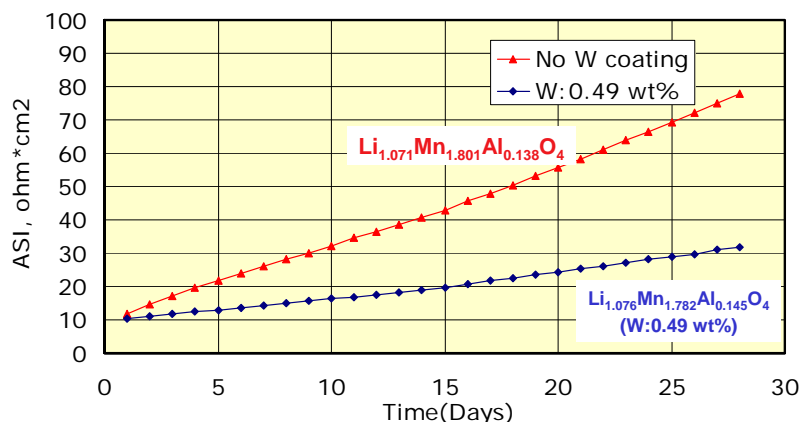


Figure III-39. Impedance vs. time during accelerated calendar life aging at 55°C and 60% SOC

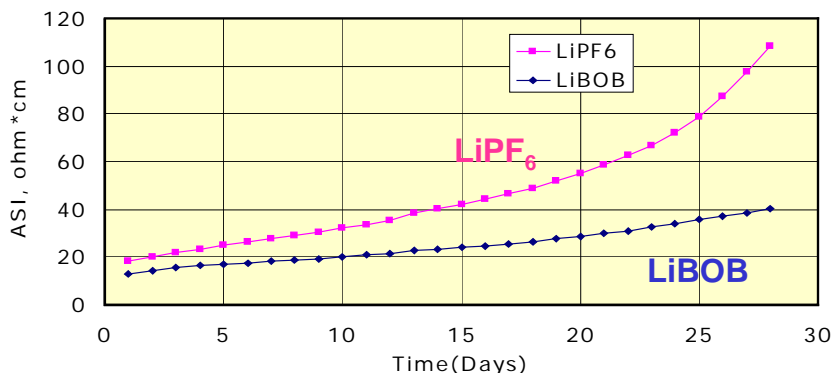


Figure III-40. Impedance vs. time during accelerated calendar life aging at 55°C and 60% SOC

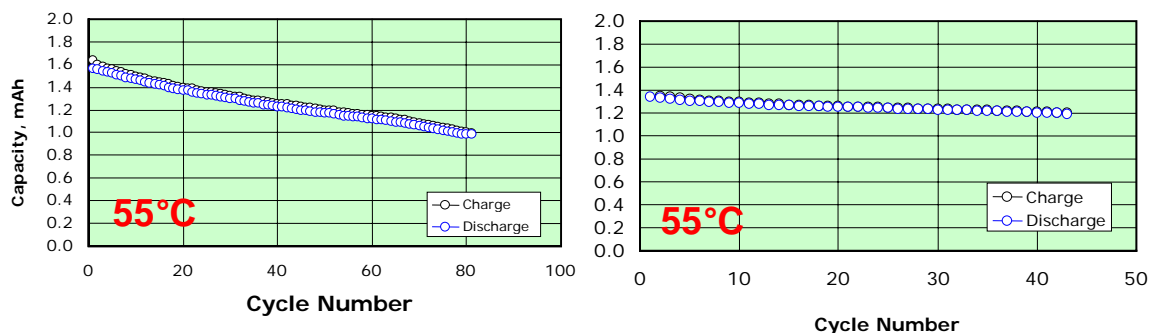


Figure III-41. Capacity vs. cycle number for cells incorporating GDR graphite anodes, spinel cathodes, and 0.7M LiBOB in EC:PC:DMC (1:1:3) electrolyte, when tested at 55°C.

For the layered 123 cathode materials, samples were obtained from several material suppliers and evaluated. The stoichiometric materials are not good high-power materials, however when doped with excess lithium these materials perform as well or better than the Gen2 cathode material, as shown in Figure III-42. The cells employ GDR graphite anodes and a 1.2M LiPF₆ in EC:PC:DMC (1:1:3) electrolyte. The Li_{1+x}Ni_{1/3}Co_{1/3}Mn_{1/3}O₂ cathodes were made on the lab-scale by Argonne National Laboratory (ANL) and on a larger scale by Mitsui Mining & Smelting. Both materials have ~10% excess lithium. The area-specific impedance (ASI) values were obtained using hybrid pulse power characterization (HPPC) tests from 10-90% depth-of-discharge (DOD). Scanning electron microscopy (SEM) photomicrographs of the materials are provided in Figure III-43. Both materials possess a spherical shape but differ in their particle size and surface roughness.

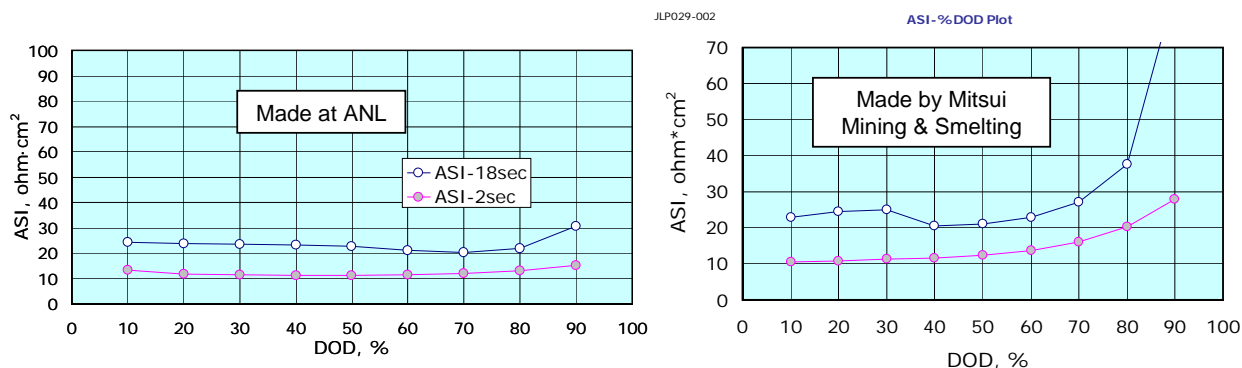


Figure III-42. Area-specific impedance (ASI) vs. DOD as measured during HPPC tests. Cells employing both materials exhibit acceptable power characteristics for use in HEV applications.



Figure III-43. Scanning electron microscopy (SEM) photomicrographs of $\text{Li}_{1+x}\text{Ni}_{1/3}\text{Co}_{1/3}\text{Mn}_{1/3}\text{O}_2$ powders with spherical shapes

Other data were collected on both the $\text{Li}_2\text{Mn}_2\text{O}_4$ spinel and $\text{Li}_{1+x}\text{Ni}_{1/3}\text{Co}_{1/3}\text{Mn}_{1/3}\text{O}_2$ cathode materials that demonstrate their more optimal thermal abuse characteristics relative to the Gen2 cathode material. Reactions of these delithiated materials with conventional electrolytes occur at higher temperatures and possess significantly lower heats of reaction than those associated with the delithiated $\text{LiNi}_{0.8}\text{Co}_{0.15}\text{Al}_{0.05}\text{O}_2$ material.

As part of these material screening studies, many other cell components (including carbon and graphite anode materials, electrode binders and conductive additives, as well as other advanced electrolyte salts, solvents, and additives) were evaluated for use in high-power Li-ion cells. Results of these studies are being published elsewhere.

Novel Electrolytes. The Applied Battery Research activity has also continued to investigate a relatively new class of LiBOB based electrolytes; see Figure III-44. The advantages of these materials are that they:

- contain no fluorine,
- appear to passivate the Al current collector,
- stabilize graphite in propylene carbonate (PC)-based electrolytes, and
- can cycle Gr/ $\text{Li}_x\text{Ni}_{1-y-z}\text{Co}_y\text{Al}_z\text{O}_2$ cells at 70°C with low capacity fading.

However, their low-temperature performance is less than ideal and they exhibit solubility limits.

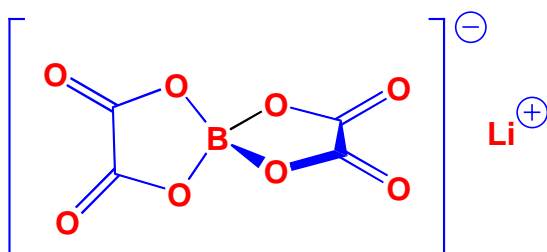


Figure III-44. Structure of the LiBOB electrolyte

Work in the past year has focused on viscosity and conductivity studies of a number of salts, including LiBF_4 , LiPF_6 , LiBOB, and Et_4NBF_4 in several solvents, with results shown in Figure III-45.

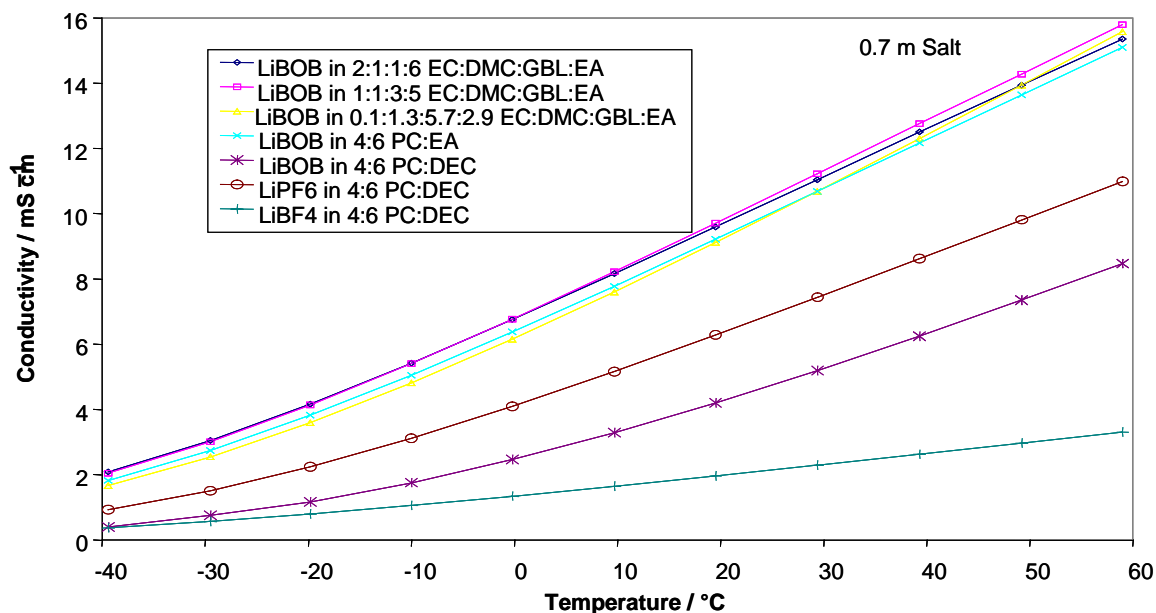


Figure III-45. Conductivity of various salt-solvent combinations as a function of temperature

The effect of various solvents on the usefulness at low temperature was also investigated. The results show that (liquidus temperature is decreased $\sim 10\text{--}20^\circ\text{C}$ when 1M of salt is added)

- EC-EMC (3:7): liquidus temp. $\sim 3^\circ\text{C}$
- EC-PC-DMC (1:1:3): liquidus temp. -13°C
- EC-DMC- γ BL-EA (2:1:1:6): liquidus temp. $< -20^\circ\text{C}$
- γ BL: $T_m = -45^\circ\text{C}$

Which indicates that γ BL is an attractive solvent for LiBOB use at low temperature.

Finally, X-ray photoelectron spectroscopy (XPS) analyses were conducted to determine the role of LiBOB on the performance of cells, with the result that LiBOB is deeply involved in forming the unique solid electrolyte interface (SEI) on the anode and the main reduction of BOB anion completes at $\sim 0.55\text{ V}$, forming a protective layer.

The results of these studies on the LiBOB material are that:

- Highly purified LiBOB salt is now available commercially. The program will next attempt to determine how pure the salt must be to perform adequately.
- Most compatible solvents with LiBOB are carbonates. Esters such as γ BL, EA, and MB are not compatible with LiBOB at elevated temperatures.
- The fact that BOB^- is larger than PF_6^- and BF_4^- suggests that Li^+ is more severely solvated in LiBOB solutions than in LiPF_6 or LiBF_4 solutions. This hampers the conductivity and also the low temperature performance.
- Surface analysis indicates that ethylene carbonate (EC) is a key component for achieving thin, stable and less resistive SEI in LiBOB-based electrolyte.

III.E.3 Gel-Polymer Electrolyte Technologies

The objective of this work is to evaluate advanced gel-polymer electrolytes and establish their capabilities and limitations for use in high-power Li-ion batteries. The evaluations include both physical and chemical gel technologies. In most cases, these evaluations involve some level of collaboration with the industrial firms developing these technologies or battery developers that have secured rights to them. In order to obtain data that are somewhat comparable, the Gen2 baseline anode and cathode materials are employed, when appropriate and feasible.

There exists the possibility that gelled electrolytes could improve the stability of cell chemistries that employ lithium manganese spinel cathodes — by suppressing Mn^{2+} dissolution and/or transport to the negative electrode — and thereby extend the life of cells that use these cathode materials. Therefore, some cells were fabricated using spinel cathodes to test this hypothesis. The typical evaluation process involves: (a) Establish impedance and power characteristics, (b) study area-specific impedance (ASI) during accelerated aging at 60% state-of-charge (SOC) and 55°C, and (c) study capacity fade during C/1 full-capacity charge/discharge cycling at 55°C (with cells that employ spinel cathodes). Table III-7 provides a summary of the main gel-polymer electrolyte technologies that were evaluated during the last year.

Table III-7. Gel-Polymer Electrolyte Systems Evaluated for High-Power Hybrid Electric Vehicle (HEV) Application

Gel-Polymer Technology	Anode	Cathode	Electrolyte
LG Chemical	Graphite	Spinel	1.2M EC-based
Damus-Kaye-Stansel (DKS) (poly[ethylene oxide] [PEO] macromonomer)	GDR Graphite	Gen2	1.2M LiPF ₆ in EC/PC/DMC 0.7M LiBoB in EC/PC/DMC
DAISO (branched PEO)	GDR Graphite	Gen2	1.5 M LiBF ₄ in EC/PC/EMC
Argonne National Laboratory (ANL) poly(vinylidene fluoride) (PVdF)	Mesocarbon microbead (MCMB)	Gen2 Spinel	1.2M LiPF ₆ in EC/PC/DMC 0.7M LiBoB in EC/PC/DMC

1.2 Ah Gel-Polymer Electrolyte Cells (with spinel positive). LG Chemical supplied 1.2 Ah commercial grade gel-polymer pouch cells for evaluation. The initial power characterization tests indicated that these cells provide the power necessary for hybrid electric vehicle (HEV) applications. The effect of incorporating the gel-polymer electrolyte on stabilizing the capacity of cells that employ spinel cathodes is illustrated in Figure III-46. The rate of capacity fade is reduced in the cell with the gel-polymer electrolyte operated at 55°C.

The impedance — measured by hybrid pulse power characterization (HPPC) tests — increases for these gel-polymer electrolyte cells during 16 weeks of accelerated aging, as reported in Figure III-47. Electrochemical impedance spectroscopy (EIS) measurements give clues as to the cause of the impedance rise. The EIS data, also seen in Figure III-47, show that the interfacial impedance stabilized after the initial two-week period of accelerated calendar life testing, but the ohmic component continued to increase. The potential causes for the ohmic impedance rise are being investigated.

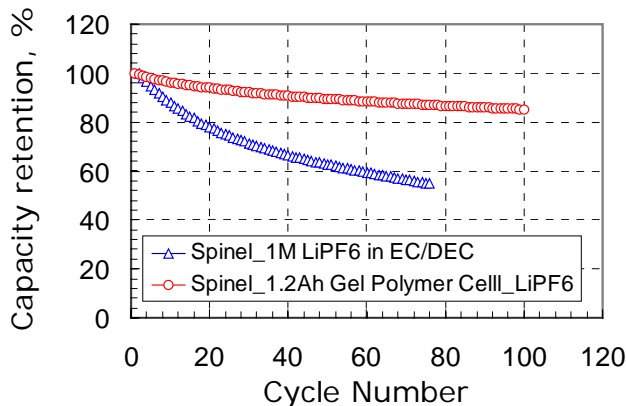


Figure III-46. C1/1 capacity fade for cells with spinel cathodes (aged at 60% SOC and 55°C) show reduced fade rates in the cells employing the gel-polymer electrolyte.

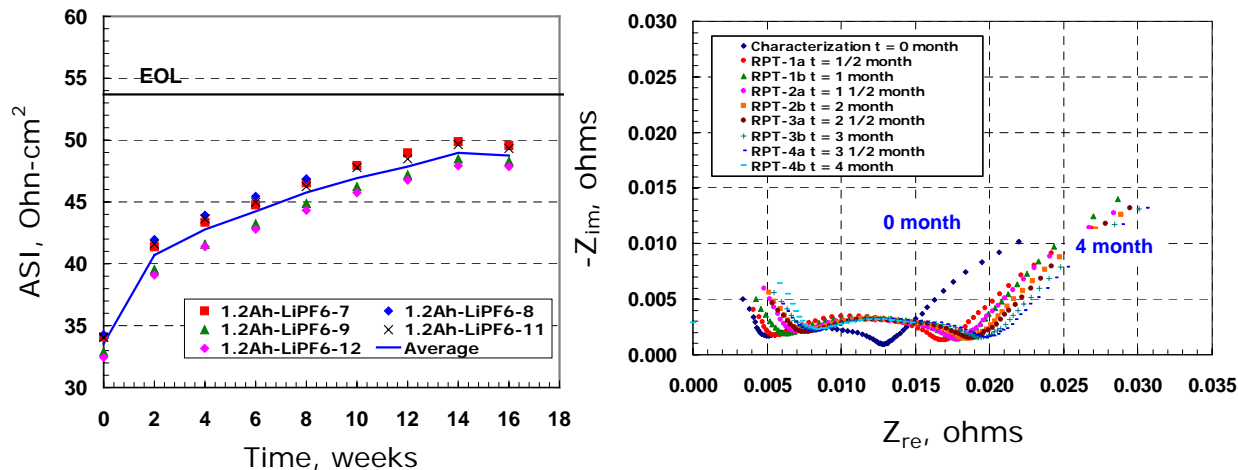


Figure III-47. ASI data obtained from: L-HPPC tests (left) and EIS measurements (right) on cells aged at 60% SOC and 55°C

Poly(ethylene oxide) (PEO) Type Gel Polymer Cells. Evaluations continued on two types of advanced PEO gel polymer electrolyte technologies, using cells with the Gen2 cathode material and GDR graphite anodes. In the Damus-Kaye-Stansel (DKS) cells — with a PEO macromonomer gel — LiPF₆ and LiBOB salts were studied in EC/PC/DMC (1/1/3) electrolytes. In the DAISO cells — with a branched PEO gel — LiPF₆ in EC/PC/DMC (1/1/3) was used. The impedance of the DKS cells was somewhat higher with the LiBOB electrolyte, but good capacities were achieved with both the LiPF₆ and LiBOB electrolytes (see Figure III-48). DKS cells using both types of electrolytes exhibited low rates of impedance rise during accelerated aging at 60 % SOC and 55°C.

In earlier evaluations of the DAISO branched PEO gel-polymer system, long cure times and a significant loss of electrolyte conductivity after curing was observed. DAISO has developed a new low molecular weight PEO with similar chemical structure. The new system is easy to cure and produces a mechanically stable gel (see Figure III-49). This system is currently being evaluated to establish its power and early-life aging characteristics.

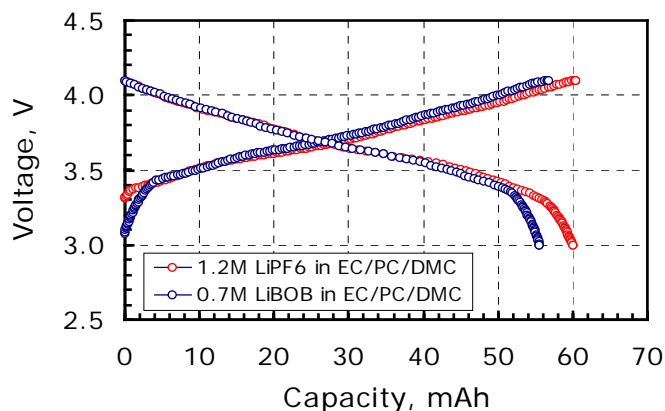


Figure III-48. C/1 charge/discharge profiles for DKS cells with different electrolytes

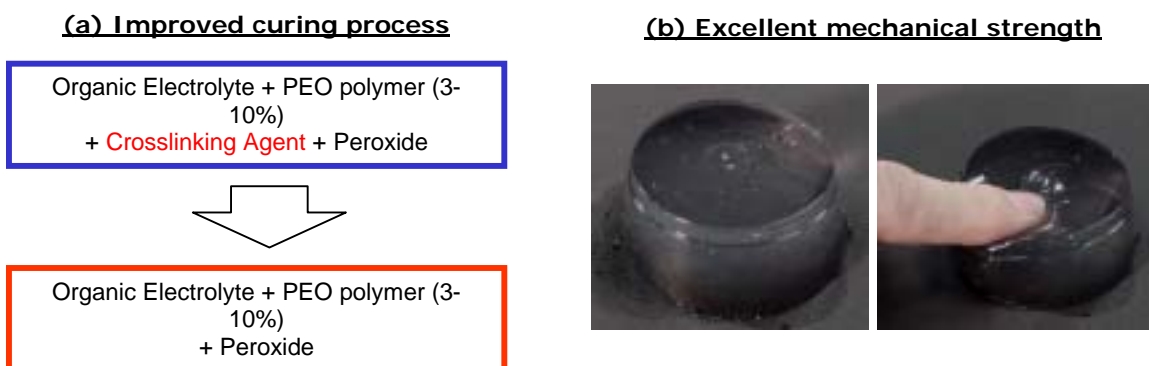


Figure III-49. Improved curing and mechanical properties of DAISO gel-polymer electrolyte

New Poly(vinylidene fluoride) (PVdF) Gel-Polymer Electrolyte. A new PVdF gel-polymer electrolyte system was developed in which a gellable microporous polymer layer is formed by laminating a plasticized gellable polymer film directly onto one or both electrodes. The formed microporous polymer layer on electrode can be used as the separator as well as the Li-ion conductor. The included plasticizer helps to soften PVdF-HFP film at $\sim 100\text{--}120^\circ\text{C}$ and combine physically with electrode. The microporous structure is formed by extracting the plasticizer from the laminated film with the ethyl ether. Early results on cells with this technology are encouraging in terms of power and early-life aging characteristics.

III.E.4 Low-Cost Flexible Cell Packaging

Packaging Test Protocols. New test protocols for flexible packaging were developed to aid battery and packaging developers in meeting the challenges posed by a hybrid electric vehicle (HEV) battery. These protocols are described in a recently published report, ANL-04/09, “Low-Cost Flexible Packaging for High-Power Li-Ion HEV Batteries,” available on-line at www.osti.gov/servlets/purl/828774-HvIkJi/native/. Flexible laminates show potential to be a replacement for the traditional rigid container that is used in present batteries. However, it is very important that the complete flexible packaging system be subjected to accelerated testing. Key areas to monitor are signs of excessive electrolyte permeation, delamination of the sealant layer from the metal foil, seam splitting, electrolyte creep at the feed-throughs, and reactions between the laminate

and the cell components. The best indicator of the packaging performance is the quality of the electrolyte upon completion of the test protocols. Table III-8 lists the criteria that must be met by the complete packaging system if it is to be acceptable for an HEV battery. This battery is required to have a calendar life of 15 years and operate between -30°C and 52°C . More information on the battery criteria can be found in the “FreedomCAR Battery Test Manual for Power Assist Hybrid Electric Vehicles,” DOE/ID-11069, October, 2003.

Table III-8. Flexible Packaging Survival Goals

Criteria ¹⁸	Units	Minimum	Desired	Protocol
Electrolyte Loss Rate at 55°C and Dry	g/cm/year	0.007	0.003	2.1
Survival at 55°C and 83% RH	days	300	600	2.2
Survival of Thermal Cycling between 60°C and -40°C at Ambient Humidity	cycles	2500 (1 year) ¹⁹	5000 (2 years)	2.3
Electrolyte Property after Testing				
Moisture	ppm	<100	<100	2.4
Acid	ppm (HF)	<400	<200	
Controlled Pressure Release	atm	1	2	2.5
Cross-Sectional Area of Feed-Throughs: (for 25-kW battery)				
Copper	cm^2	0.15	TBD	2.6
Aluminum		0.24		
Vibration Survival	cycles	TBD	TBD	2.7

Results of HEV-sized Pouch Testing. Accelerated aging tests of HEV-sized pouches from Sumitomo Electric Flat Components, Inc. (now a subsidiary of Sumitomo Electric Industries, Ltd., or SEI) were completed. Thirteen of these HEV-sized pouches were stored at 55°C and ~83% relative humidity (RH) and another ten pouches underwent rapid thermal cycling between -40°C and 60°C . Three of the pouches undergoing rapid thermal cycling have reached more than 2400 thermal cycles without signs of rupturing, delamination, or seam splitting. The electrolyte loss rate was estimated to be $1.4\mu\text{g}$ per thermal cycle per centimeter of perimeter. As a worst-case scenario, if this HEV-sized pouch (59-cm perimeter) was thermally cycled once a day between -40°C and 60°C , it would lose only 0.5 grams of electrolyte over the 15-year life. This analysis ignores the influence of moisture uptake on the true electrolyte weight loss. Five of the pouches stored at 55°C and 83% RH reached over 370 days without signs of rupturing, delamination, or seam splitting. A slight weight loss was observed for these pouches and estimated to be 8 mg per year per centimeter of perimeter. This implies that 7 grams of electrolyte would be lost for this HEV-sized pouch (59-cm perimeter) over the 15-year life if it was stored continuously at 55°C (ignoring moisture uptake).

Several of the 30 pouches were removed because they showed signs of corrosion at the bottom corner where the pocket was formed. This defect was due to the sharp radius of curvature at the pocket corners combined with a dimpling (creasing) at the pocket corner. Even for these pouches, no

¹⁸ Package must be complete, i.e., fully formed to shape (if used) with electrode feed-throughs, pressure relief mechanism, and ~50g of electrolyte (for a 25-kW battery). Cell components (negative and positive electrodes and separator) are optional for evaluation of packaging material, but must be included for final validation testing. Approximate dimensions of a cell in a 25-kW battery are $100 \times 110 \times 20$ mm.

¹⁹ Estimated duration of test to achieve targeted number of thermal cycles.

signs of delamination or seam splitting were observed. SEI is in the process of changing the thickness of some of the layers in the laminate and retooling the die used to form the pouch pockets to ameliorate pocket corner cracking. When these improvements have been completed, this new generation of pouches will be tested. The effects of non-carbonate solvents, additives, and other lithium salts will be studied with this new laminate. A cost analysis will also be done.

Electrolyte was extracted from all of the removed pouches and the pouches were cut open for visual inspection. No sign of attack of the sealant layer or the seal around the electrode feed-throughs was evident. Samples of the electrolyte and of the inner (sealant) film were analyzed with Fourier transform infrared (FTIR) spectroscopy. No changes in the infrared (IR) spectra were observed for the film or for the electrolyte samples. The electrolyte samples were also analyzed for moisture, acidity, and color. These values are shown in Table III-9 and Table III-10. From these data it is apparent that storage at 55°C and 83% relative humidity (RH) is the most aggressive test protocol. Further analysis of the data indicated that the moisture adsorbent that is incorporated into the sealant layer limits the level of moisture and acid in the electrolyte. However, the darkening of the electrolyte correlated well with the degree of thermal abuse despite nearly constant levels of moisture and acid for each test scheme. This suggests that the moisture adsorbent does not completely prevent decomposition of the electrolyte, but may limit its extent.

Organoclay Technology. During FY 2004, the focus of the organoclay effort was to continue improving the compatibility of the clays with polyolefins such as low-density polyethylene (LDPE). Additional high melting surfactants were synthesized and new methods developed to permit exchange of water-insoluble surfactants onto hydrophilic clays dispersed in water. The target of this effort was to achieve a reduction of $\geq 50\%$ in water vapor transport relative to the base polymer.

Significant reductions in oxygen transport were achieved by dispersing modest amounts of organoclay into LDPE, however, no measurable reduction in water vapor transmission was observed. The mechanism for permeation of water vapor through polyolefins is considered to be much more complex than that of oxygen or nitrogen. The diffusivity of water molecules is significantly higher because of its smaller kinetic diameter (2.7\AA) compared to those of nitrogen and oxygen (3.6 and 3.5\AA).

This approach differs from others in the field by attempting to increase clay/polymer interaction energies by synthesizing new surfactants which (a) are high molecular weight and (b) have melt/freeze thermal transitions that match those of the polymer. To date, surfactants were produced that displayed thermal transitions that match those of LDPE. Using this approach, the gas barrier, including water vapor barrier, were increased using only small amounts of clay (i.e., 0.7 wt%) dispersed in LDPE. Water vapor transmission across LDPE is shown in Figure III-50 and compared with that of an unfilled film. The data for the nanocomposite film show a lag time of ~ 2500 s as opposed to 33 s for the reference film, suggesting that the organoclay scavenges water vapor. Scavenging ability, however, does not affect steady-state permeability, which shows a 74% reduction in water vapor permeability compared to pure LDPE.

Table III-9. Analysis of Electrolyte from SEI's Pouches that Underwent Rapid Thermal Cycling

Pouch	Moisture (ppm)	Acid % (HF)	Color
SEI-0 Un-cycled pouch	28	0.049 (490 ppm)	
SEI-1 600 Rapid Thermal Cycles (109 days)	49	0.070	
SEI-2 1350 Rapid Thermal Cycles (250 days)	35	0.030	
SEI-6 2100 Rapid Thermal Cycles (400 days)	42	0.054	

Table III-10. Analysis of Electrolyte from SEI's Pouches that Underwent Storage at 55°C and 83% RH

Pouch	Moisture (ppm)	Acid % (HF)	Color
SEI-0 Un-cycled pouch	28	0.049 (490 ppm)	
SEI-11 Stored at 55°C and 83% RH for 103 days	22	0.092	
SEI-13 Stored at 55°C and 83% RH for 172 days	31	0.078	
SEI-15 Stored at 55°C and 83% RH for 246 days	34	0.084	

Organoclays prepared with straight-chain aliphatic surfactants, while compatible with LDPE, do not afford like performance in all hydrophobic polymers. For example, initial transport data for an LDPE nanocomposite containing 0.7 wt% clay were compared with a poly-1-butene nanocomposite containing 10 wt% clay. While the poly-1-butene nanocomposite showed a 74% reduction in oxygen permeability, the clay had no effect on water vapor transmission in this polymer, nor was there any evidence of water scavenging behavior. Thus, it appears that enhanced gas barrier performance will require the design of organoclay surfactants tailored to each polymer type.

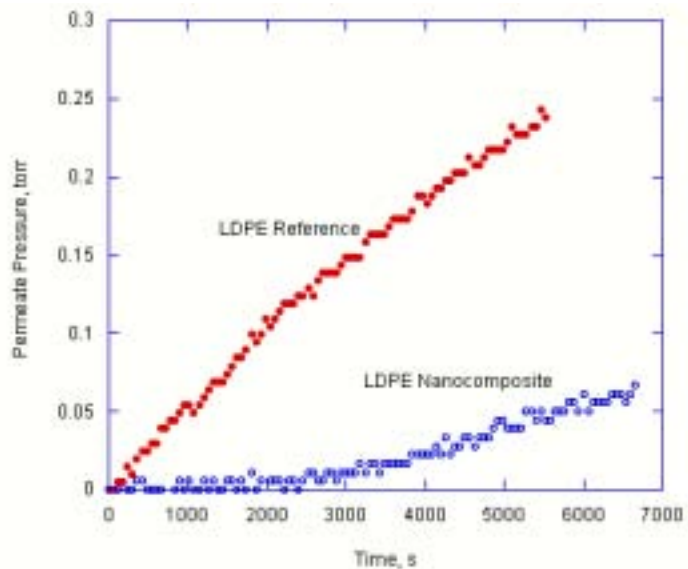


Figure III-50. Water vapor permeation across LDPE films at 30°C. The nanocomposite contains 0.7 wt% clay.

IV. LONG-TERM RESEARCH

The Long-Term Research activity is supported by the Department of Energy's (DOE's) FreedomCAR and Vehicle Technologies (FCVT) Program to research and analyze new materials for high-performance, next generation, rechargeable batteries for use in electric vehicles (EVs) and hybrid electric vehicles (HEVs).

Background and Program Context

The development of an advanced battery for automotive applications is difficult, although companies are making more progress each year. Current batteries are nearly all NiMH, but Li-ion continues to show promise due to the possibility of improved performance, reduced weight and volume, and potentially lower price. Thus, there remains a need to identify and understand performance and lifetime limitations to help guide the search for new battery materials. The Long-Term Research program addresses fundamental issues of chemistries and materials that face all lithium battery candidates for vehicular applications. The program emphasizes the identification and mitigation of failure modes, coupled with materials synthesis and evaluation, advanced diagnostics, and improved electrochemical models. Battery chemistries are monitored continuously with periodic substitution of more-promising components. This is done with advice from within this program, from outside experts, and from assessments of world-wide battery research and development (R&D).

The work is carried out by the Lawrence Berkeley National Laboratory (LBNL) and several other organizations. In 2004, the Long-Term Research program redefined its baseline systems (Figure IV-1) and carried out investigations into:

- The $\text{LiNi}_{1/3}\text{Mn}_{1/3}\text{Co}_{1/3}\text{O}_2$ (called 123 or one third) cathode material in a high-energy cell with a $\text{LiPF}_6/\text{PC-EC-DMC}$ electrolyte and a carbon-coated graphite anode. The cathode is less expensive and can provide higher energy than the Gen2 cathode, plus the lower-cost polypropylene carbonate (PC)-containing electrolyte is possible due to the amorphous carbon coating that prevents anode exfoliation.
- The low cost and safe LiFePO_4 system, using a propylene carbonate-ethylene carbonate-dimethyl carbonate (PC-EC-DMC)-based electrolyte. The program is working to develop significantly improved materials through the use of a liquid electrolyte, without the complications of a gel. This is regarded as a moderate-energy, low-voltage system that is inherently stable and low-cost.
- A high-rate spinel system with a liquid-electrolyte, aiding work in the applied research program to develop a low-cost high-power battery.

Also in 2004, the program has been re-organized into chemistry specific research areas:

- (1) LiNiCoMnO₂ and Spinel Systems: Performance and Limitations
- (2) Electrolyte Limitations
- (3) New, High Energy Materials
- (4) LiFePO₄ System: Performance and Limitations
- (5) Li/Polymer: Component Limitations

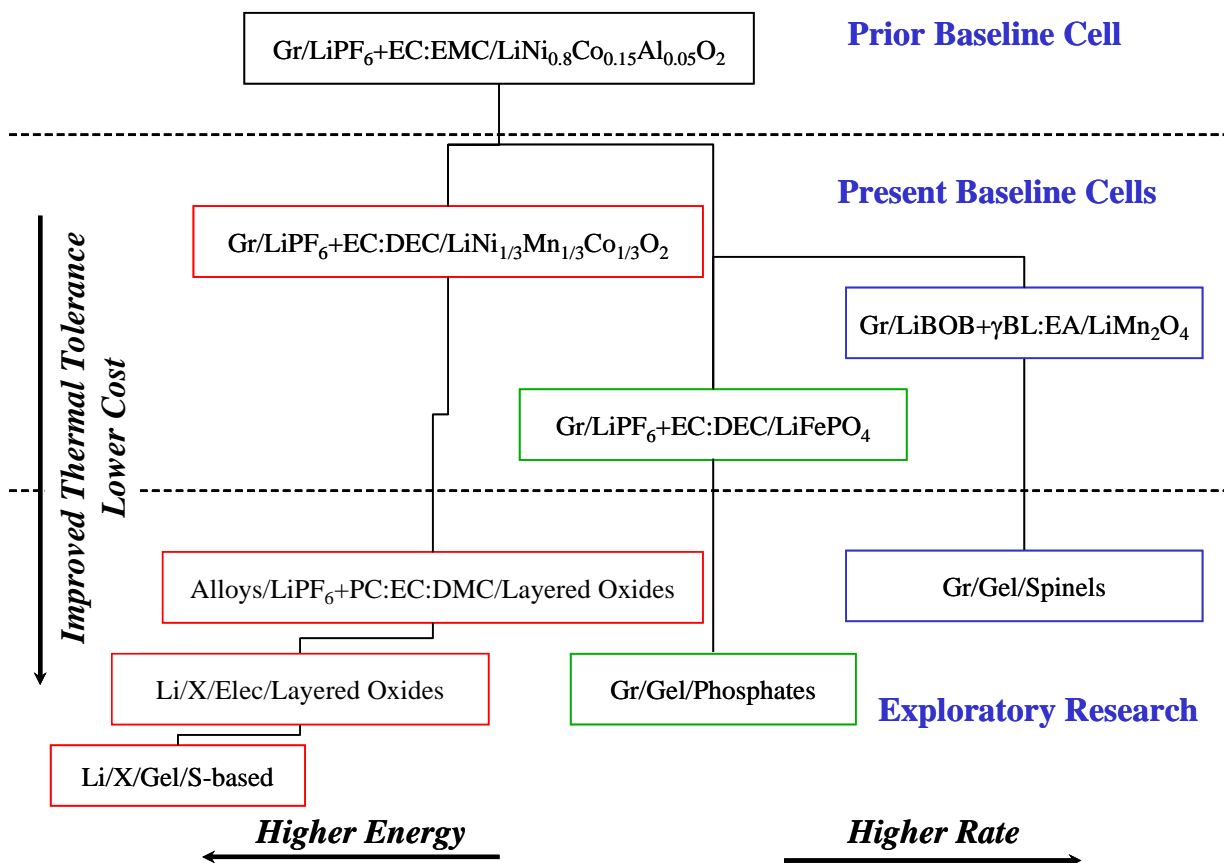


Figure IV-1. Overview of long-term research chemistries

These new task areas provide the program with additional focus on the issues and possible solutions associated with some of the most promising chemistries in the Li-ion battery field while also permitting the researchers to collaboratively address the barriers common to all of these chemistries. Brief descriptions of each research area follow.

1. The **LiNiCoMnO₂ and Spinel Systems: Performance and Limitations** task aims to understand the failure and degradation modes in the 123 system and the Mn spinel systems using cell builds, cell cycling, empirical and first principals calculations, and advanced diagnostics. Researchers are also evaluating electrode materials from multiple suppliers and developing self-actuating overcharge protection mechanisms.

2. The **Electrolyte Limitations** task involves investigating interfacial properties of advanced high power batteries by studying the solid electrolyte interface (SEI) formation and its change with cycling using Fourier transform infrared (FTIR) spectroscopy. It also involves studying the changes in electrode structure at high temperatures using X-ray absorption fine-structure (XAFS), and applying modeling to understand the contribution of electrolyte properties to cell performance.
3. The **New, High Energy Materials** task aims to find improved transition metal oxide cathode materials. This task also includes investigations into composite negative electrodes containing one (or more) metal components within a graphite matrix, for example, C/Sn and C/Sb systems, and high-capacity and high-rate $x\text{Li}_2\text{M}'\text{O}_3 \bullet (1-x)\text{LiMO}_2$ “composite” electrodes (M'=Ti, Mn, Zr; M=Mn, Ni).
4. The **LiFePO₄ System: Performance and Limitations** task includes studies of capacity and power fade in the iron phosphate system, including the performance of iron phosphate in gel polymer electrolytes. This cathode material promises safe performance at a relatively low cost. Researchers are investigating the impact of processing steps on performance, and theoretical investigations were performed on various carbon coatings and their impact on performance.
5. The **Li/Polymer Component Limitations** tasks investigate the limitations of Li polymer cells that offer tremendous promise for low cost and safe batteries. Post-test analyses and spectroscopic and microscopic techniques are used to investigate morphology, structure, and compositional changes of electrode materials, and molecular dynamics simulations are used to study Li transport through the polymers.

This chapter summarizes the research activities of this program in FY 2004. The website for the Long-Term Research Program is located at <http://berc.lbl.gov/BATT/BATT.html>.

IV.A. LiNiCoMnO₂ and Spinel Systems: Performance and Limitations

Objectives

This task addresses a number of issues important to the development of safe, cost-effective, Li-ion batteries with adequate energy and power densities and extended lifetimes. These include overcharge protection, general issues of component structure and stability, and exploratory work on the fundamental life and safety issues associated with the one-third and the Mn spinel materials.

The primary objectives of this task are to:

- Support cell development through structural characterization of active electrode components before, during, and after cycling.
- Investigate inexpensive, self-actuating overcharge protection mechanisms.
- Model baseline systems to optimize performance, identify limiting factors, and understand failure mechanisms. Measure the thermodynamic, kinetic, and transport parameters for use in models.
- Establish direct correlations between electrode surface chemistry, interfacial phenomena, and cell capacity or power decline.
- Develop high-capacity, stable cathode materials by working with redox-active metal ions that can exchange multiple electrons in a narrow voltage range, focusing initially on the Ni²⁺/Ni⁴⁺ couple.

Approach

One approach used in this task is to correlate capacity and power fade in advanced systems with changes in the composition and structure of electrode active materials. Techniques employed include X-ray diffraction (XRD), vibrational spectroscopy, and electroanalytical testing. Researchers also use in situ and ex situ Raman microscopy, scanning probe microscopy (SPM), ellipsometry, and standard electrochemical methods to characterize cell components taken from baseline cells, fresh electrode materials, and thin-film model electrodes. Data collected include electrode surface morphology and chemistry, structure, electronic conductivity, and solid electrolyte interface (SEI) thickness and composition, all of which may change during cell cycle-life tests.

In addition, solid-state nuclear magnetic resonance (NMR) and X-ray absorption spectroscopy (XAS) are used to characterize local structure and oxidation states of cations as a function of state-of-charge (SOC) and number of cycles. First-principles calculations (density functional theory) are used to identify redox-active metals, the relative stability of different structures, the effect of structure on cell voltages, and to identify promising cathode materials. Finally, possible instabilities in materials are investigated by using calculations and NMR to identify low-activation-energy pathways for cation migration.

Finally, as the response of lithium cells to overcharge may present a significant danger, an overcharge protection mechanism based on a conductive polymer that will provide a reversible, low-resistance internal shunt that will allow overcharge currents to pass harmlessly through a cell while maintaining its discharge capacity is being developed and analyzed.

Accomplishments

LiNi_{1/3}Mn_{1/3}Co_{1/3}O₂/Natural Graphite (NG) Cell Characterization. Benchmarking of the LiNi_{1/3}Mn_{1/3}Co_{1/3}O₂/NG cells is underway. Cathode films were prepared from four sources of the 123 cathode material: Mitsui, Tanaka and Seimi, and a Li-doped spinel from Toda. Half-cell studies have been carried out with the result that the L333 (Seimi) cathode showed the best high-rate performance and was selected for initial baseline studies. The material had a discharge capacity of 230 mAh/g when charged to 4.7 V vs. Li/Li⁺ without severe degradation.

The baseline 123 cell has thus been defined as one containing cathode-active material from Seimi Chemical (L333) and the LA-2-2 (GDR) carbon-coated graphite from Mitsui Mining. Anodes prepared with the GDR graphite were purchased from Quallion Corp. and used as received with dual-side coating of the current-collector. The capacity of this cell as a function of C-rate is shown in Figure IV-2.

Cathodes were made in several coating thicknesses in order to match the capacity of the anode and cells were prepared with PC-containing electrolyte (1.0M LiPF₆ EC/PC/DMC, 1:1:3). At room temperature, the best performing cells show a fade rate of 0.55%/cycle during C/2 cycling and an area-specific impedance (ASI) at 50% SOC of about 136Ωcm². At 45°C, this fade rate increases to 0.9%/cycle. Single electrode ASI tests suggest that a major portion of this impedance arises from the cathode and the increase in this impedance is responsible for the capacity fade. Further studies on the capacity retention of this cathode at voltages higher than 4.3 V are underway with the L333 material and some experimental material received from Seimi.

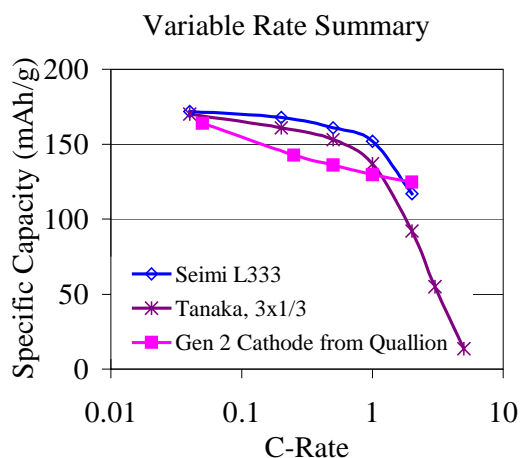


Figure IV-2. Specific capacities of 123 and Gen2 cathode materials

Nickel-rich cathodes become contaminated with Li₂CoO₃ when exposed to air. Cells made with these electrodes have low capacity and poor power characteristics. It has been shown that the formation of a thick carbonate coating on the active particle surfaces causes electronic isolation of a significant portion of the active material. Since this phenomenon is especially noticeable in Ni-containing cathodes, LiNi_{1/3}Mn_{1/3}Co_{1/3}O₂ was studied to evaluate its resistance to degradation in air. Based on XRD data (Figure IV-3), the tendency to form Li₂CoO₃ is considerably diminished in the new composition.

LiNi_{1/3}Mn_{1/3}Co_{1/3}O₂ Models. Comparison of new model results to experimental data for the 123 material shows that the main potential drops are caused by kinetic and transport losses in the solid particles. This suggests that decreasing the particle size, whereby both the diffusion length is decreased and the surface area for reaction is increased, would be very helpful in improving the cell performance. Subsequently, optimization studies (wherein the specific energy was maximized by changing the thickness and porosity) were conducted for two charging voltages, 4.3 and 4.5 V. The model results show that this baseline exhibits as much as 20% higher specific energy and power when charged to 4.3 V compared to the FePO₄ baseline system. An additional 10% increase in performance was seen when charged to 4.5 V owing to the higher capacity at higher charging voltages. Thus, the 123 material appears competitive, on a capacity and rate basis, with other advanced chemistries, (Figure IV-4).

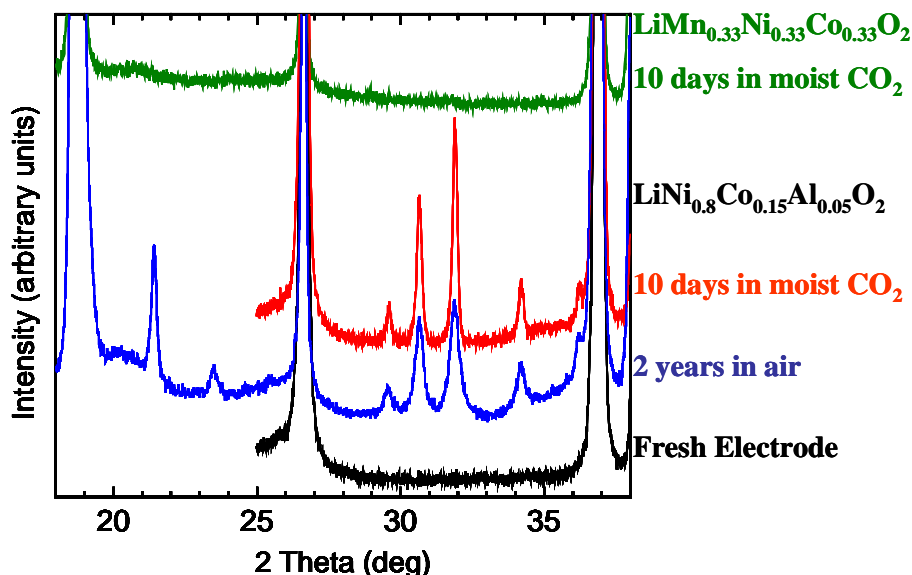


Figure IV-3. XRD showing Lithium Carbonate growth

Interpretation of Power Fade. The mechanism of carbon retreat/re-arrangement in composite cathodes has been further investigated. Thin film carbon black electrodes were prepared on an Al current collector then characterized and stored or cycled vs. Li-metal in 1.2M LiPF₆ EC/EMC (3:7) electrolyte at 57°C. The voltammetric scans show large anodic and cathodic currents above 3.8 V and below 2.9 V, respectively. Interestingly, the electrochemical response of the carbon electrodes changes during cycling. The intensity of anodic and cathodic peaks increases during initial cycles. However, the peak current starts to decrease gradually after ~20 cycles and vanishes completely after 130 cycles.

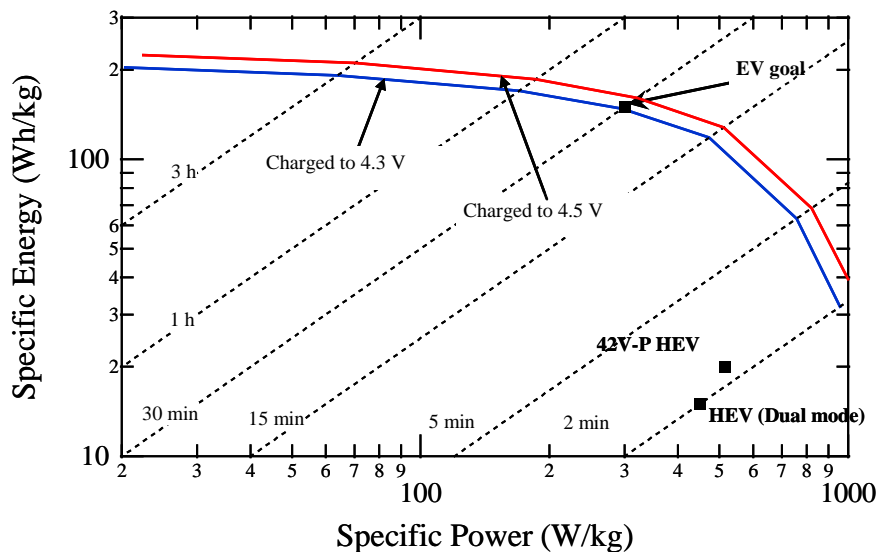


Figure IV-4. Optimized Ragone Plot for the 123 Material

These tests indicate that carbon black is electrochemically active at elevated temperatures (57°C) and at potentials above 3.8 V. Reversible processes such as PF_6^{-1} anion intercalation-deintercalation into carbon and carbon surface oxidation-reduction possibly contribute to the observed current. Raman analysis shows that the structure and electronic properties of the carbon additive undergoes significant changes upon cycling in LiPF_6 containing electrolytes.

Substantial surface morphology changes in the electrodes cycled between 2.5 and 4.4 V (Figure IV-5) were also observed. The particles of carbon black appear larger and the carbon film seems less densely packed compared to the fresh carbon electrode or the electrode that was stored in electrolyte at 57°C . Deconvolution of Raman spectra of the cycled carbon electrode showed that the structure and electronic properties of carbon black undergoes degradation upon cycling in LiPF_6 containing electrolytes. Carbon displacement was observed in the cycled cells and carbon particles were detected in the Celgard[®] separator and on the surface of the lithium anode.

The potential role of carbon retreat/redistribution on cathode impedance rise and capacity loss was demonstrated in diagnostic studies of $\text{LiNi}_{0.8}\text{Co}_{0.15}\text{Al}_{0.05}\text{O}_2$, LiFePO_4 and 123 material cathodes from tested cells. Surprisingly, they display similar symptoms of degradation, (a) loss of surface electronic conductivity, (b) surface composition changes, and (c) a non-uniform state of charge of active material at the end of testing. The loss of a direct electronic path through the carbon matrix leads to an increased resistance within the electrode and, eventually, total isolation of some particles.

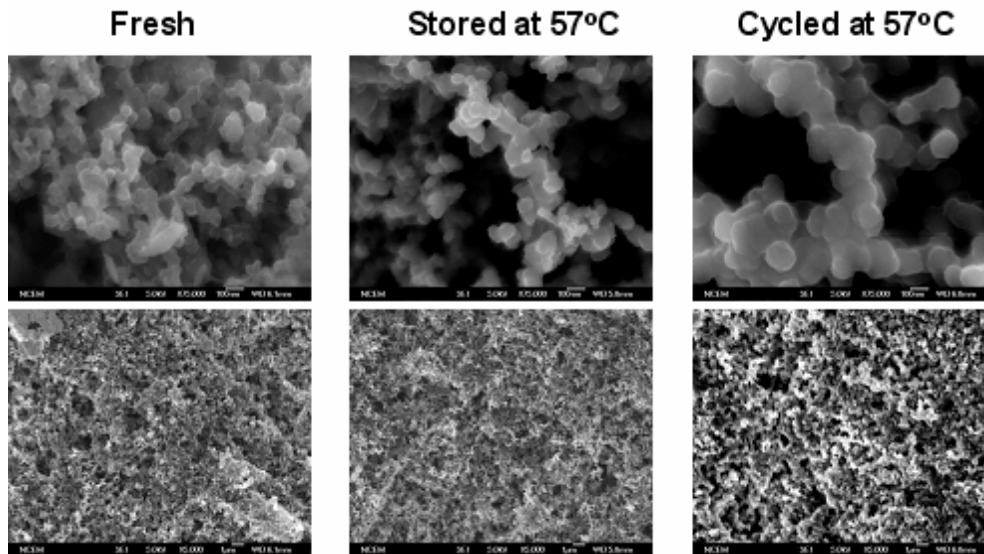


Figure IV-5. Scanning electron microscopy (SEM) images of carbon black electrodes tested in 1.2 M LiPF₆, EC:EMC electrolyte at 57°C

Diagnostics on Li[Ni_xMn_{(2-x)/3}Li_{(1-2x)/3}]O₂. This work is focused on the development and characterization of materials that access the Ni²⁺/Ni⁴⁺ redox couple. Results from first-principles computations, NMR, transmission electron microscopy (TEM), XRD, and neutron diffraction now explain many of the structural and electrochemical observations in this material. Specifically, the cations in the transition metal (TM) layer are long-range ordered, even in the Li(Ni_{1/2}Mn_{1/2})O₂ material, previously suspected to have no cation ordering. Ordering occurs in supercells and contains Li in specific sites in the TM layer. Hence, the substantial Li-Ni disorder, previously attributed to processing, is an integral component of the stable structure of this material and it is unlikely that it can be reduced. The Li-Ni-Mn ordering in the TM layer, shown in Figure IV-6, explains the strong dependence of electrochemical behavior on processing in these materials. When the ordering is well formed, Li from the TM layer can be electrochemically extracted or may migrate to tetrahedral sites.

Using NMR to probe the local structure of these materials, two different areas that impact utility and performance have been investigated. NMR spectra and XRD patterns have been obtained for the $x = 1/2$ and $1/3$ materials as a function of cycle number which demonstrate that the local structure surrounding Li slowly becomes more disordered. After 5 cycles, Li is still present in the transition metal layers surrounded predominantly by Mn. In contrast, the long range order decreases rapidly on cycling. The “superstructure” peaks in the $x = 1/3$ material, which are indicative of ordering in the transition metal layers, disappear after 5 cycles. After 20 cycles, the concentration of Li in the layers (as seen by NMR) has dropped by more than 75%. Similar results are seen for $x = 1/3$; see Figure IV-7. The results suggest that Li vacancies in the transition layers, formed on charge, may provide a mechanism for Mn/Ni disordering following multiple cycles, leading to a reduction of sites for Li in these layers.

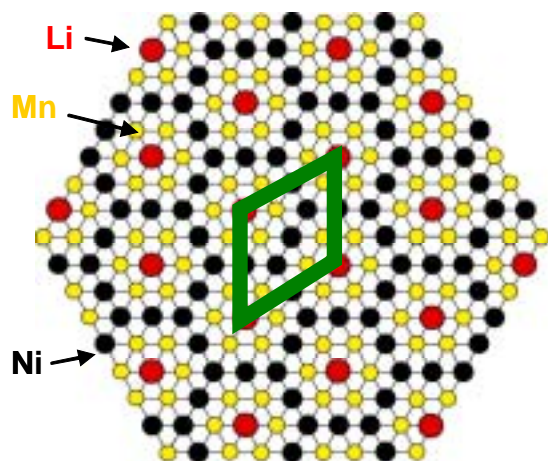


Figure IV-6. Li, Ni, Mn order

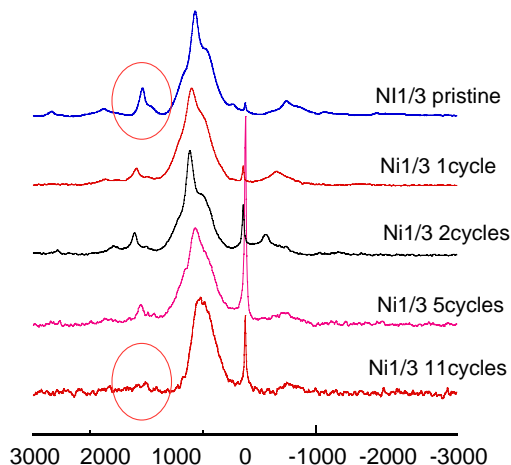


Figure IV-7. ${}^6\text{Li}$ spectra of $x = 1/3$ as a function of cycling, showing the intensity decrease of the Li resonance in the transition metal (TM) layers (circled).

In order to understand how structure affects the electrochemistry of these systems, electron spin resonance (ESR) was used to follow oxidation state change. It was found that the amount of Ni^{3+} formed as a stable intermediate upon charging is less than expected based on two simple one-electron reactions $\text{Ni}^{2+} \rightarrow \text{Ni}^{3+} \rightarrow \text{Ni}^{4+}$, and for $x > 1/3$, the oxidation process does not involve Ni^{3+} as a stable intermediate.

In confirmation, first principles computations on the 123 material showed that, upon charge, Ni^{2+} oxidizes to Ni^{4+} before the Co redox couple is activated. The $\text{Co}^{3+}/\text{Co}^{4+}$ capacity sits at quite high potential making it unlikely to be completely used in practical battery applications, thereby limiting the capacity enhancements that can be achieved.

Finally, in a parallel investigation, the oxidation states of transition metals in different charged states were studied using synchrotron-based X-ray absorption techniques. For the $\text{Li}_{1-x}\text{Ni}_{1/2}\text{Mn}_{1/2}\text{O}_2$ cathodes, it was found that charge compensation was obtained through oxidizing the Ni^{2+} to Ni^{4+} , while the Mn cations remaining at the Mn^{4+} state during charge.

NiMnCo System. The layered nickel/manganese system $\text{LiNi}_y\text{Mn}_y\text{Co}_{1-2y}\text{O}_2$ has been systematically studied for $0.33 \leq y \leq 0.5$ to determine the optimum composition, the nature of the electrochemically active species, and the role of cobalt. Physical and electrochemical characterization of these materials shows that they may best be described as stabilized nickel oxides. The composition $\text{LiNi}_{0.4}\text{Mn}_{0.4}\text{Co}_{0.2}\text{O}_2$ gave the best capacity, exceeding 180 mAh/g for 20 cycles, (Figure IV-8). Their chemical and thermal stability have been determined, and coatings will be studied to enhance the chemical stability in fluoride-based electrolytes. There is minimal volume change during cycling.

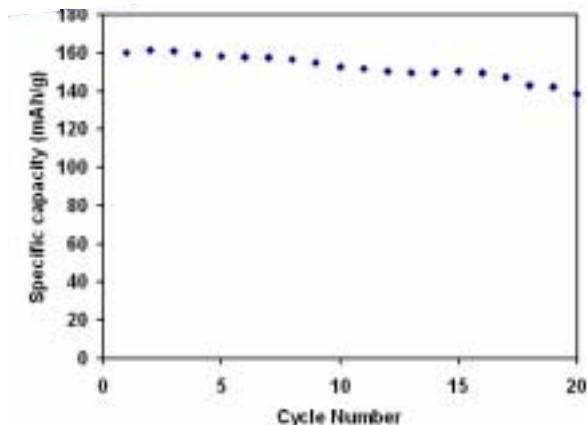


Figure IV-8. Capacity vs. cycle number for $\text{LiMn}_{0.4}\text{Ni}_{0.4}\text{Co}_{0.2}\text{O}_2$

Finally, a systematic study of several singly and doubly substituted spinel manganese oxide compositions reveals a correlation between the capacity fade and a number of characteristics such as initial lattice parameter, initial manganese valence, degree of manganese dissolution, and lattice parameter difference, Δa , between the two cubic phases formed during cycling. Moreover, other electrochemical performance parameters such as rate capability, storage performance, and irreversible capacity (IRC) loss during the first cycle also bear a relationship to the sample characteristics. The samples exhibiting good capacity retention are characterized by a high initial Mn valence of >3.58 , and low initial lattice parameter a , IRC, and Δa . The low Δa minimizes the microstrain and leads to a maintenance of good crystallinity with sharp diffraction peaks upon cycling. For example, the doubly substituted $\text{LiMn}_{2-y-z}\text{Ni}_y\text{Li}_z\text{O}_4$ samples satisfy these criteria and exhibit a combination of superior capacity retention, rate capability, and storage characteristics with low IRC compared to LiMn_2O_4 despite a similar amount of Mn dissolution, Figure IV-9.

However, the doubly substituted composition $\text{LiMn}_{1.85}\text{Ni}_{0.075}\text{Li}_{0.075}\text{O}_4$ exhibits a lower capacity of about 95 mAh/g. Preliminary experiments show that the capacity values can be increased further by optimizing the microstructure and incorporating additional cations such as Cu^{2+} . Researchers are currently in the process of evaluating the rate capability and storage characteristics of the $\text{LiMn}_{2-y-z-\eta}\text{Ni}_y\text{Li}_z\text{Cu}_\eta\text{O}_4$ compositions. In parallel, work is focusing on eliminating the $\text{Li}_x\text{Ni}_{1-x}\text{O}$ impurity phase in the 5 V spinel cathode system $\text{LiMn}_{1.5}\text{Ni}_{0.5}\text{O}_4$ via suitable cationic substitutions and an evaluation of their cycle life and rate capability.

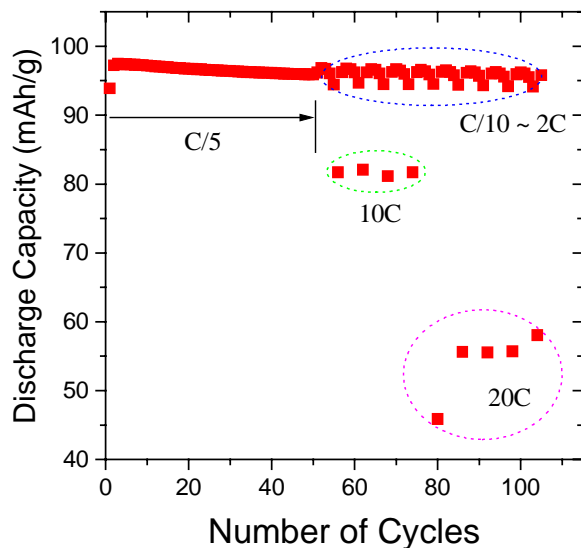


Figure IV-9. Rate Capability of $\text{LiMn}_{1.85}\text{Ni}_{0.075}\text{Li}_{0.075}\text{O}_4$

O_2/O_3 Intergrowths. Work on layered manganese oxide intergrowths was changed from Ni and Co substituents to Al, which is expected to provide cost and safety advantages. The O_3 component is associated with higher capacity but is unstable with respect to formation of spinel. In contrast, O_2 is stable, but exhibits lower capacity. Intergrowths are intermediate in behavior and represent a possible route to high energy, stable, layered manganese oxide electrodes, if properly designed. This year, numerous Al-substituted compositions were synthesized; of these, 29 were phase-pure O_2 or O_3 , or intergrowths of O_2/O_3 . As Al content increases, the resistance to spinel conversion increases in O_3 compounds but capacity also decreases. $\text{O}_2/\text{O}_3\text{-Li}_x\text{Al}_{0.15}\text{Mn}_{0.85}\text{O}_2$, in contrast, delivers more than 150 mAh/g and cycles with little capacity fading. After 100 cycles, there is some evidence of spinel formation, but full phase conversion is inhibited by the presence of the O_2 component. Evaluation of the $\text{Li}_x\text{Mn}_{1-y}\text{Al}_y\text{O}_2$ system is nearly complete. Figure IV-10 shows cycling data for Li cells containing O_3 phases. Substitution levels of 12–18% Al give the highest capacity electrodes.

The layered LiMO_2 compounds, with $\text{M} = \text{Co}$ or $\text{Ni}_{1-x}\text{Co}_x$, are used commercially; but cobalt is expensive, and operation on the $\text{Co}^{4+}/\text{Co}^{3+}$ and/or the $\text{Ni}^{4+}/\text{Ni}^{3+}$ couples results in oxygen evolution when more than half of the Li is removed. The $\text{LiNi}^{2+}_{1-x}\text{M}^{4+}_x\text{O}_2$ compounds, with $\text{M} = \text{Ti}$ or Mn , do not contain cobalt and should allow operation on the $\text{Ni}^{3+}/\text{Ni}^{2+}$ redox couple without loss of voltage. However, the performance with Ti was poor whereas that with Mn was fair. Because the layered LiMO_2 structure offers the best chance for high Li^+ -ion mobility together with a capacity in excess of 150 mAh/g, work focused on resolving the issues with $\text{LiNi}^{2+}_{1-x}\text{M}^{4+}_x\text{O}_2$ compounds.

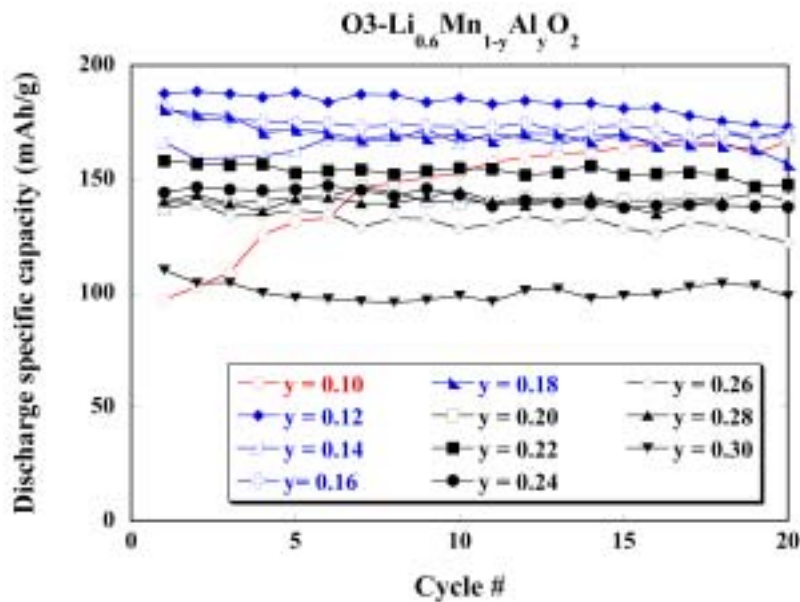


Figure IV-10. Cycling data for Li/O₃-Li_{0.6}Mn_{1-y}Al_yO₂ cells

First, a criterion was used for monitoring the degree of ordering (from XRD data) of the Li ions into alternate (111) layers of the rock-salt structure. It was then noted that the critical parameter driving the ordering was the ratio of the ionic radii of the alkali ion and the mean radius of the transition-metal ions. A smaller ratio corresponds to ordering yielding a larger reduction in elastic strain energy, which thus favors an ordering of the structure. For example, well-ordered NaFeO₂ has the ionic radius ratio (IRR) of 0.63 whereas disordered LiFeO₂ has an IRR = 0.87 (Figure IV-11). Because LiNi²⁺_{0.5}Ti⁴⁺_{0.5}O₂ has an IRR = 0.88, it appears that LiNi_{0.5}Ti_{0.5}O₂ cannot be well ordered. However, LiNi²⁺_{0.5}Mn⁴⁺_{0.5}O₂ has an IRR = 0.83, which makes it easier to obtain cation order.

Placement of an “M” atom in the Li layer blocks Li-ion motion and reduces the free volume for ion movement by clamping the separation of the oxide-ion sheets bordering the Li layers. In order to further lower the IRR while retaining a large fraction of Ni²⁺ ions, LiNi_{0.6}Mn_{0.4}O₂ was studied. Another task was to develop a synthetic procedure that would yield molecular-level mixing of the Mn and Ni atoms prior to calcination. It is now possible to produce cathodes which contain no cobalt but have a performance equal to or superior to that of the LiCoO₂ reference. At a C/23 rate, the cathode has an average voltage vs. Li of 4 V and a capacity of 170 mAh/g if operated over the range 4.3-2.75 V, and there was no capacity fade within experimental error after 50 cycles.

Conductive Polymer Overcharge Protection. Given the susceptibility of lithium-based batteries to energetic venting and even explosion following overcharging, a reliable overcharge-protection mechanism is an indispensable requirement for large cell assemblies. Ideally, this would be achieved with a minimum of added weight, volume, and cost. This program has previously shown that electroactive polymers whose conductivity depends upon their state of charge can provide overcharge protection by means of a reversible, self-actuating, low-resistance internal shunt that allows overcharge currents to pass harmlessly through a cell while maintaining its discharge capacity and allowing the rest of the cell stack to operate normally.

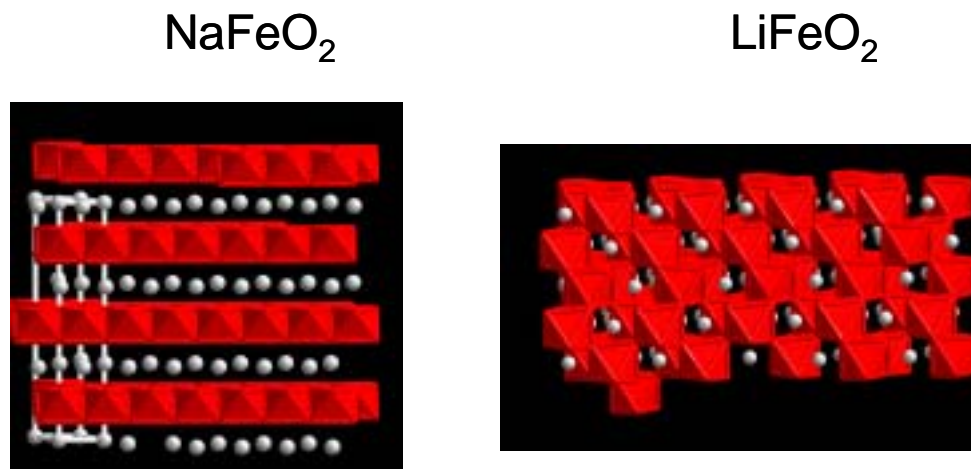


Figure IV-11. Layered (NaFeO_2) and disordered (LiFeO_2) materials

The feasibility of this approach was first demonstrated in low-voltage cells. In FY 2004, higher-voltage cells containing LiFePO_4 (3.5 V) and 123 (>4 V) cathodes exposed to moderate-rate overcharge were protected. In addition, the mechanism works as well with carbon anodes as with lithium, the temporary internal short does not cause significant self discharge at the end of charging, the presence of the polymer does not compromise the conductivity of the electrolyte, and the polymer can be used either external or internal to the cell. A sample of overcharge protection in a 4V cell is shown in Figure IV-12, which also shows overcharge protection with the electroactive polymer either external or internal to the cell.

The morphology and distribution of the conducting polymer within the separator strongly influences the overcharge current density that can be maintained. When cast onto a fibrous, non-woven separator with large pores, a stable current density of more than 1 mA/cm^2 can be achieved, while the same polymer on Celgard[®] 2500 may pass only 0.1 mA/cm^2 .

Cells are currently being fabricated in which the overcharge protection portion of the separator is in direct contact with one or both current collectors. This is expected to improve the long-term stability of the electroactive polymers.

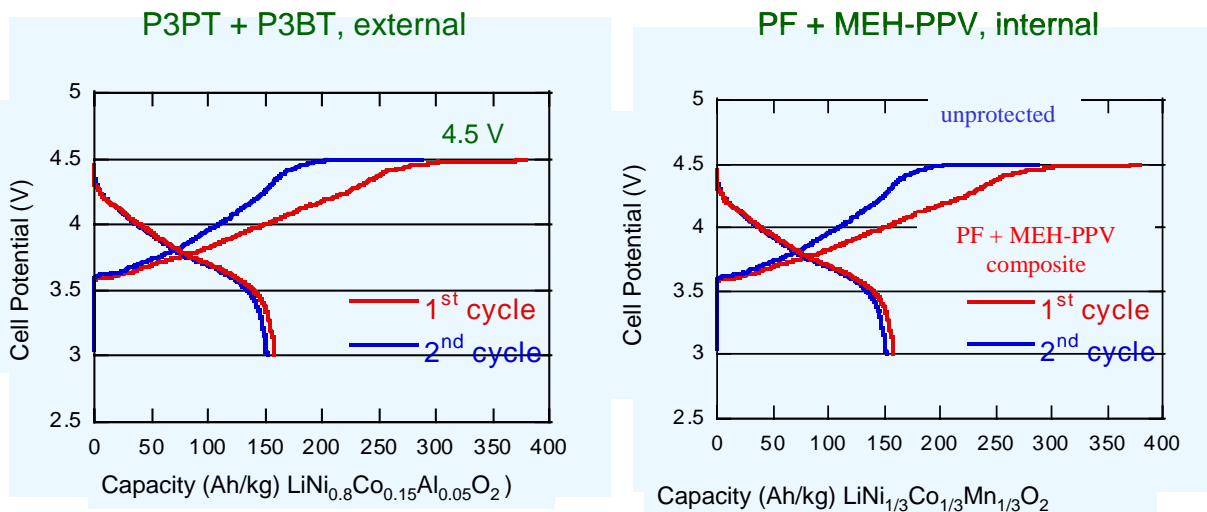


Figure IV-12. Overcharge Protection in Gen2 and 123 Cells

Future Plans

Nickelate Systems including 123 Material

- Investigate optimal processing conditions and ordering schemes for the $\text{Li}(\text{Ni},\text{Mn},\text{Li})\text{O}_2$ system.
- Establish large-scale search (computational) for novel cathode systems.
- Investigate electronic conductivity in oxides. Continue development and testing of predictive method for electron activation barrier.
- Complete baseline characterization with GDR graphite electrodes from Quallion
- Expand baseline testing to high energy and variable temperature
- Determine cell cycle life with hybrid electric vehicle (HEV) protocol, and evaluate storage life at high temperature.
- Determine:
 - The voltage that should be used for charging the 123 battery.
 - If there is a side reaction occurring at higher voltages.
 - If side reactions, if present, have any impact on cycle life.
 - If so, the reactions' thermodynamics and kinetics.
 - The optimal particle size.
- A series of electrochemical calendar life/cycle life tests of cells with ^{13}C -enriched cathodes will be carried out to further investigate carbon migration or rearrangement.
- Evaluate other Batteries for Advanced Transportation Technologies (BATT) baseline cathodes (LiMn_2O_4 , $\text{LiNi}_{1/3}\text{Mn}_{1/3}\text{Co}_{1/3}\text{O}_2$) with water-soluble binder (WSB) and compare the results with LiCoO_2 as a reference.

Layered Manganese Oxides

- Determine optimum substitution levels and O_2/O_3 ratios for $\text{Li}_x\text{Al}_y\text{Mn}_{1-y}\text{O}_2$ system.
- Determine how the distribution of O_2 and O_3 affects material properties.
- Exploit and optimize 3.0-3.5 V spinel-spinel couples for high-rate cells ($\text{Li}_4\text{Ti}_5\text{O}_{12}$ anode).
- Evaluate performance of high potential (>4.5 V) spinel and layered composite electrodes with metal oxide protective layers (ZrO_2 , Li_2ZrO_3) and/or with pre-conditioned surfaces.

IV.B. Electrolyte Limitations

Objectives

- Develop experimental methods for measuring transport, kinetic, and thermodynamic properties of electrolytes and electrodes.
- Model electrochemical systems to optimize performance, identify limiting factors, and mitigate failure mechanisms.
- Determine the contributions of electrode materials changes, interfacial phenomena, and electrolyte decomposition to cell capacity and power decline.

Approach

A model of dendrite formation on lithium metal has been developed to determine material requirements needed to inhibit dendrite growth. Simulations are being used to improve understanding of the solid electrolyte interface (SEI) layer.

In situ Fourier transform infrared (FTIR) spectroscopy is used to study the interfacial chemistry in model systems. The spectrometer optics and spectro-electrochemical cell have a design that enables any electrode material to be studied. FTIR spectroscopy is accompanied by classical electroanalytical methods such as cyclic voltammetry and the rotating ring-disk electrode.

A combination of in situ and ex situ synchrotron techniques are used to characterize electrode materials and electrodes taken from baseline cells. Techniques that are sensitive to both bulk and surface processes, including K and L-edge X-ray absorption spectroscopy (XAS), are applied. Exploratory work is continuing on other techniques such as non-resonant inelastic X-ray scattering (NRIXS).

Finally, researchers are developing improved experimental methods for measuring transference numbers in liquid and polymer electrolytes.

Accomplishments

SEI Investigations

Modeling Dendrite Initiation and Propagation. This modeling effort has helped to determine the bulk properties that are necessary for a polymer to inhibit interfacial roughening, and subsequent Li dendrite growth, by mechanical action. The goal of the work was to determine if a pure lithium anode was feasible in polymer-electrolyte systems, or if failure by dendritic deposits was an insurmountable obstacle. The results show that polymers must have shear moduli in the gigapascal range in order to inhibit interfacial roughening, providing a useful target for scientists in materials development. In contrast, present polymer research has focused on materials with moduli in the megapascal range. The general kinetic model developed has broad utility, and can be employed to treat interfacial roughening in many systems.

The Solid Electrolyte Interphase. A mathematical model of the SEI on the negative electrode has been developed. Results indicate that film growth and impedance rise are greater at lower electrode potentials, indicating that failure may be accelerated for systems in which the cell is fully charged, in agreement with many experimental observations. The potential of the negative electrode with

respect to a lithium reference electrode drops to zero before the electrode is fully charged, indicating that the electrode capacity is not fully utilized. This effect is enhanced at higher rates of charge, confirming that the SEI has a detrimental impact on rate capability. Parameter estimation will allow a comparison of simulations with experimental results.

In addition, the behavior of the SEI and the associated impedance was investigated in both electric vehicle (EV) and hybrid electric vehicle (HEV) usages, indicating that impedance rise at the negative electrode might be more of an issue in EV applications (Figure IV-13).

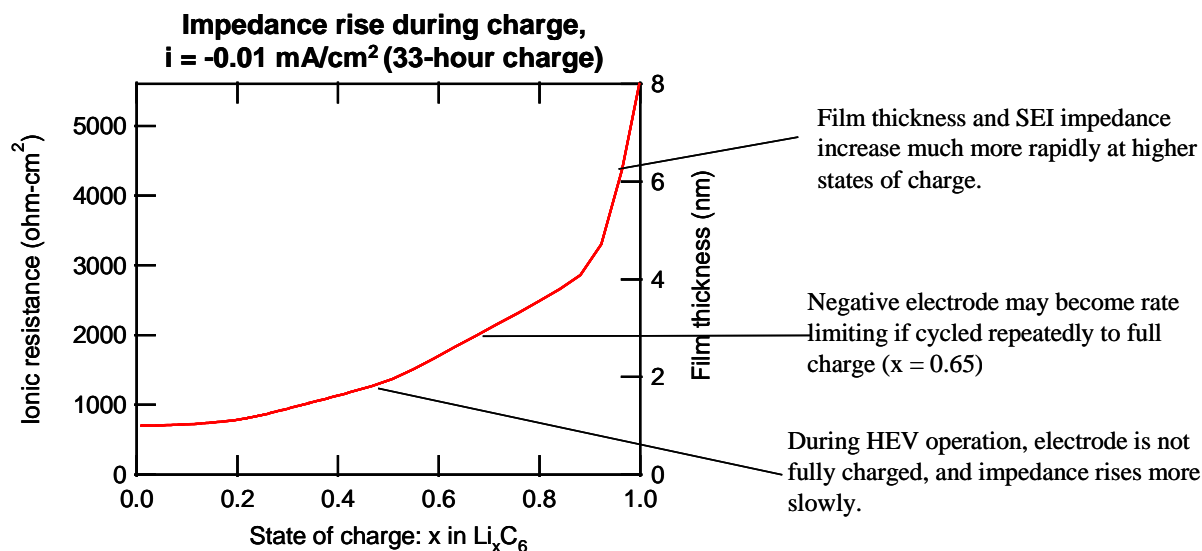


Figure IV-13. Impedance rise and film thickness

LiBOB Electrolyte Experimental Diagnostics. The chemistry of the SEI layer formed on graphite anodes cycled in a PC/LiBOB electrolyte was studied by ex situ FTIR analysis in the attenuated total reflection (ATR) mode (Figure IV-14). The vibrational spectra clearly show that electrochemical reduction of the BOB anion is a part of the SEI layer formation chemistry, in agreement with recent results in the applied battery research area. The reduction reaction changes the oxygen coordination around the B atom from tetrahedral BO_4 to trigonal BO_3 , e.g., esters of boric acid. BOB anion reduction appears to prevent propylene carbonate (PC) co-intercalation into graphite and allows for cycling of graphite anodes without exfoliation.

LiNiCoAlO Surface and Thermal Analyses. The surface films formed on commercial Gen2 cathodes charged from 3.75V to 4.2V vs. Li/Li^+ in EC:DEC/1M LiPF_6 were analyzed using the ex situ FTIR-ATR technique. A surface layer of lithium carbonate (Li_2CO_3) is present on the fresh cathode, probably from reaction of the active material with air during the cathode preparation procedure.

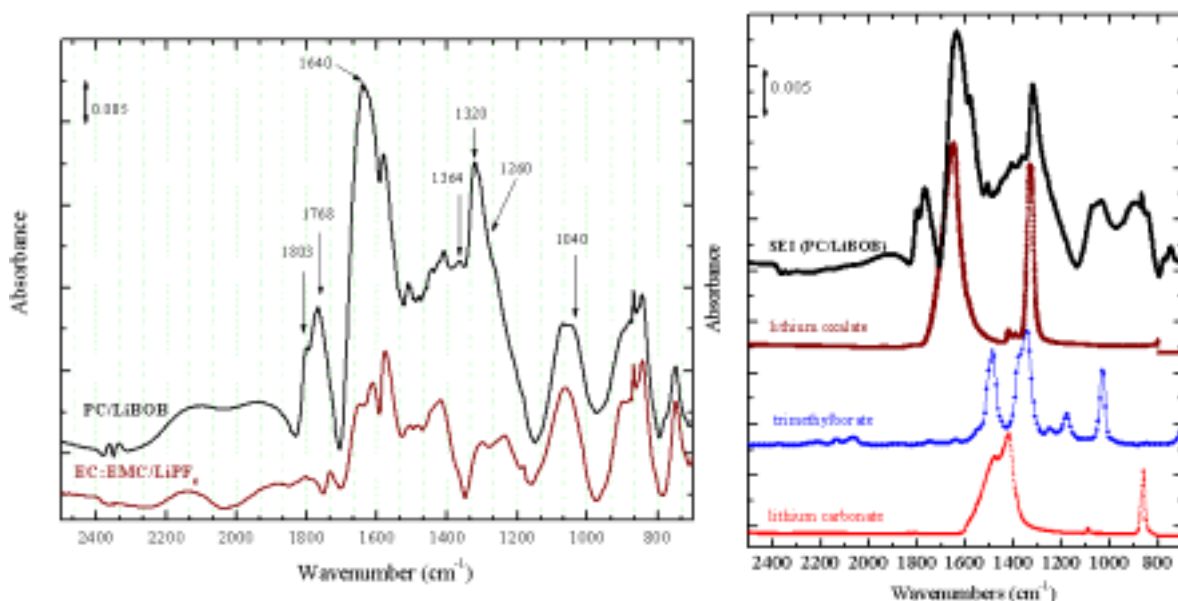


Figure IV-14. FTIR of LiBOB and Gen2 Electrolyte

The Li_2CO_3 layer disappears after soaking in the electrolyte (Figure IV-15), indicating that the layer dissolved into the electrolyte possibly even before cycling. Infrared (IR) features arising only from the binder poly(vinylidene fluoride) (PVdF) and a trace of polyamide from the Al current collector, likely from the PVdF binder, were observed on the surfaces of cathodes charged to below 4.2 V, i.e., no surface species from electrolyte oxidation. Some new IR features were, however, found on the cathode charged to 4.2 V and higher. An electrolyte oxidation product was observed, and it appeared to contain dicarbonyl anhydride and (poly)ester functionalities. The reaction appears to be an indirect electrochemical oxidation with overcharging (removal of > 0.6 Li ions) destabilizing oxygen in the oxide lattice, resulting in oxygen transfer to the solvent molecules. This finding is in also close agreement with a similar one reported in the applied research program.

Researchers have also completed in situ X-ray diffraction (XRD) and a combination of in situ and ex situ X-ray absorption spectroscopy (XAS) studies of the initial charging processes in $\text{LiNi}_x\text{Mn}_{1-x}\text{O}_2$ and $\text{LiNi}_{1/3}\text{Mn}_{1/3}\text{Co}_{1/3}\text{O}_2$. They have developed and applied a new technique, using time-resolved XRD to study the thermal decomposition of Gen2 cathode materials, $\text{Li}_{1-x}\text{Ni}_{1/2}\text{Mn}_{1/2}\text{O}_2$, and $\text{Li}_{1-x}\text{Ni}_{1/3}\text{Mn}_{1/3}\text{Co}_{1/3}\text{O}_2$ at different states of charge. XRD studies were carried out during heating from 25°C to 450°C . For a Gen2 cathode charged to 50% state of charge (SOC), decomposition occurs at about 280°C . This temperature decreases with increasing SOC (see Figure IV-16). The presence of electrolyte can decrease the decomposition temperature even further.

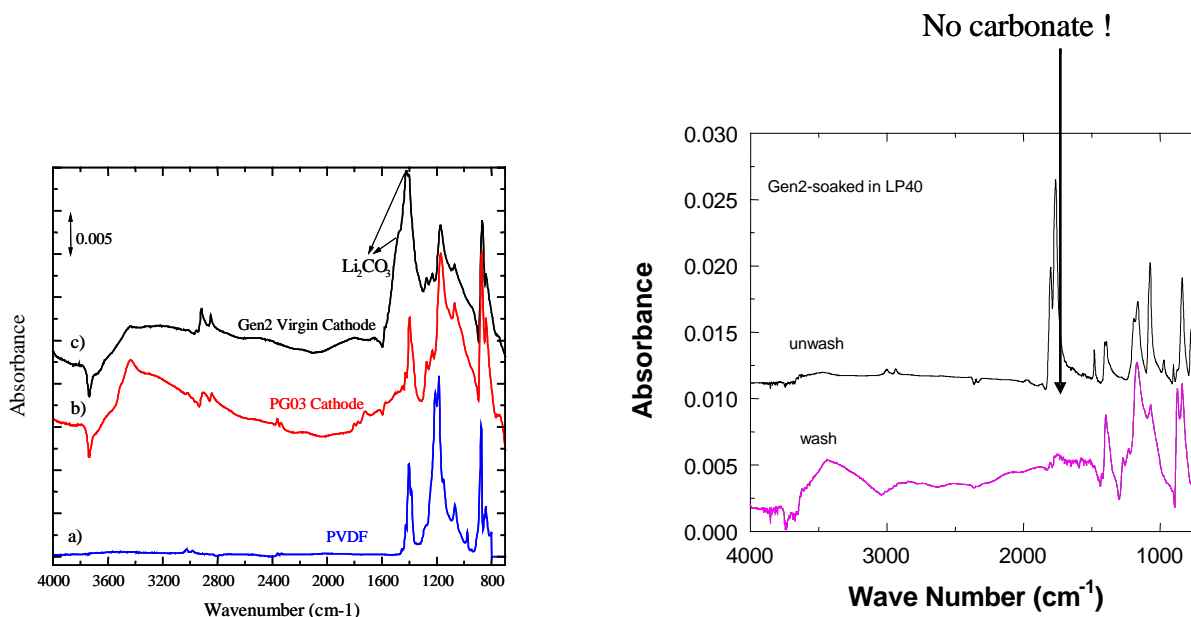


Figure IV-15. Pre-existing lithium carbonate “removed” by soaking in LP40

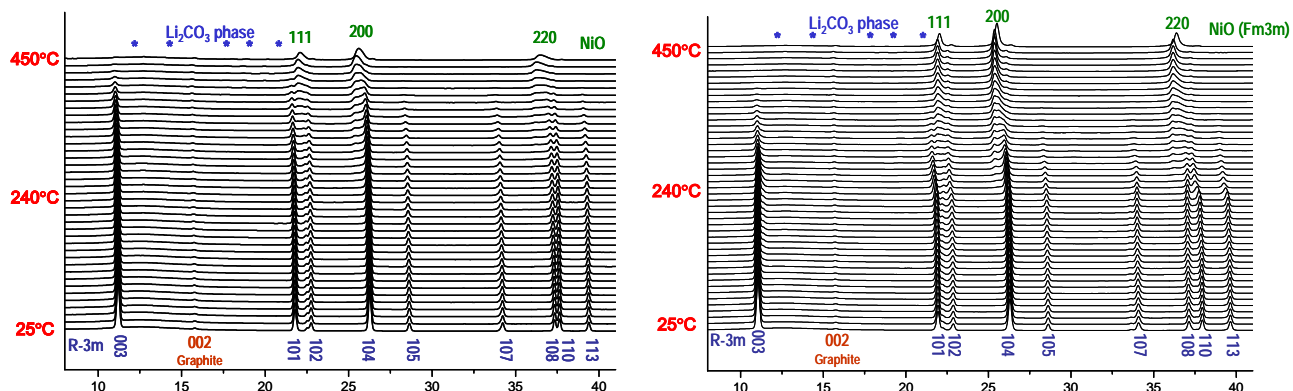


Figure IV-16. (left) Thermal response of Gen2 cathode 0% SOC, and (right) 50% SOC

As the degree of Li-ion deintercalation increases, the thermal decomposition takes place at lower temperatures. Time-resolved XRD studies were performed on $\text{Li}_{0.0}\text{Ni}_{1/2}\text{Mn}_{1/2}\text{O}_2$ in the presence of electrolyte. When the cell was overcharged to 4.8 V, the cathode did not show the (002) graphite (used as conducting additive) peak at ambient temperature. This might be the result of the disorder caused by the intercalation of PF_6 into the graphite layer structure. At $\sim 95^\circ\text{C}$, the intercalated PF_6 apparently migrates out of the graphite and the graphite (002) peak reappears.

Finally, comparative studies between the Gen2 and LiMn_2O_4 spinel cathode were made using the in situ XRD technique. Both cathodes were cycled at room temperature and 55°C . The kinetics of the structural changes at different temperatures for Gen2 and spinels are quite different. For Gen2, more structural changes were observed at room temperature, showing that the controlling factor is the lithium ion diffusion rate, which is higher at higher temperatures. On the other hand, for spinel materials, more phase separation was observed after cycling at high temperatures, indicated that the

damaged surface structure restricted the lithium ion insertion. This surface damage is caused by high-temperature (high-voltage) cycling for spinels.

Future Plans

- Use soft X-ray XAS to identify decomposition products from electrolyte salts, study the LiBOB salt electrolyte.
- Investigate the effects of electrolyte on the degradation at elevated temperatures and at over charged states for spinel and stabilized spinel cathode materials by Al doping.
- Perform time-resolved XRD studies of thermal decomposition of cell components, including new cell chemistries.

IV.C. New, High-Energy Materials

Objectives

- To replace carbon with an inexpensive anode material that will be compatible, in particular, with low-cost manganese oxide cathodes. The project also addresses the need for improved safety of Li-ion cells.
- To develop low-cost cathodes based on benign materials having electrochemical characteristics (e.g., cycle life, energy and power densities) consistent with the goals of the United States Advanced Battery Consortium (USABC). Specifically, evaluate alternative layered oxides as cathode materials for a Li-ion battery.

Approach

The approach being used to search for new anode materials is to explore, synthesize, characterize, and develop inexpensive materials that have a potential ~500 mV above that of pure Li (to minimize the risk of Li plating and thus enhance safety) and have higher volumetric energy densities than carbon. Emphasis is being placed on simple metal alloys/composites. All materials are evaluated electrochemically in a variety of cell configurations, and for thermal and kinetic stability.

Novel cathode materials are synthesized using both conventional solid-state techniques and solution methods (e.g., sol-gel, glycine-nitrate combustion). The microstructures and atomic structures of the materials are determined, and electrochemical analysis is carried out in a variety of cell configurations.

Accomplishments

Anodes

During FY 2004, the emphasis of some anode investigations changed from intermetallic electrodes that operate by topotactic reactions, such as Cu_6Sn_5 and Cu_2Sb , to composite electrodes containing one or more metal components within a graphite matrix, for example C/Sn and C/Sb. When the metal component is restricted to approximately 10 atomic percent, capacities of approximately 400mAh/g have been achieved for 100 cycles (Figure IV-17). Metal oxide electrodes such as Li_2MoO_3 and LiVO_2 have also been explored in an attempt to find an alternative electrode to $\text{Li}_4\text{Ti}_5\text{O}_{12}$ that (a) operates at lower potential (0–1 V vs. Li) than $\text{Li}_4\text{Ti}_5\text{O}_{12}$ (1.5 V vs. Li) and (b) provides a practical capacity of ~150 mAh/g or more.

Work has also continued on electrochemical evaluations of oxide-based anode systems and on metal-graphite composite anodes. Theoretical first-principles calculations have shown, and experimental results have confirmed, that $\text{LiMO}_2 - \text{Li}_2\text{MO}_2$ lithium insertion reactions occur between 2.0 and 1.0 V vs. Li and are favored only for $M=\text{Mn}$ and Ni ; and displacement reactions are favored for $M=\text{V}$, Co , and Cr . Although Li_2MoO_3 could deliver 200 mAh/g for more than 50 cycles, the electrode exhibited (like many other metal oxides) an unacceptably high irreversible capacity loss (ICL). Cathode research, however, has shown that composite electrodes with a Li_2MnO_3 component may compensate for such initial capacity losses.

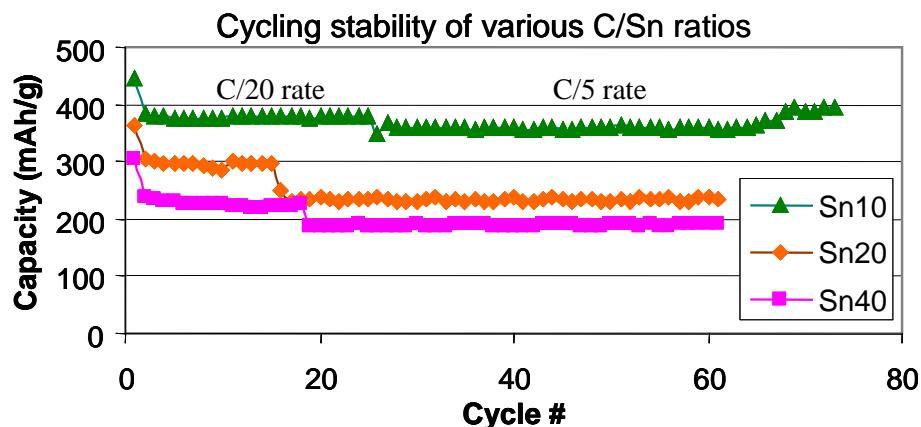


Figure IV-17. Capacity of C/Sn anodes

For LiCoO_2 , a high electrode capacity in the voltage window 3.0 to 0 V was observed. Although a large ICL exists, part of which is attributed to the formation of a Li-rich solid electrolyte interface (SEI) phase, continued cycling gave a reversible capacity of 550 mAh/g, corresponding to the reaction of 2.0 Li per LiCoO_2 unit (Figure IV-18). Most of this capacity is discharged below 500 mV vs. Li^0 (Figure IV-18a). In situ X-ray diffraction (XRD) analysis of a LiCoO_2 electrode during electrochemical discharge showed that the electrode was reduced first to CoO and thereafter to Co with the concomitant formation of Li_2O in both stages, in agreement with theoretical predictions. On subsequent charge, the Co is oxidized only as far as CoO . LiNiO_2 electrodes behave in a similar manner, yielding a reversible capacity of ~ 500 mAh/g, which corresponds to the reaction of ~ 1.8 Li per initial LiNiO_2 unit (Figure IV-18b).

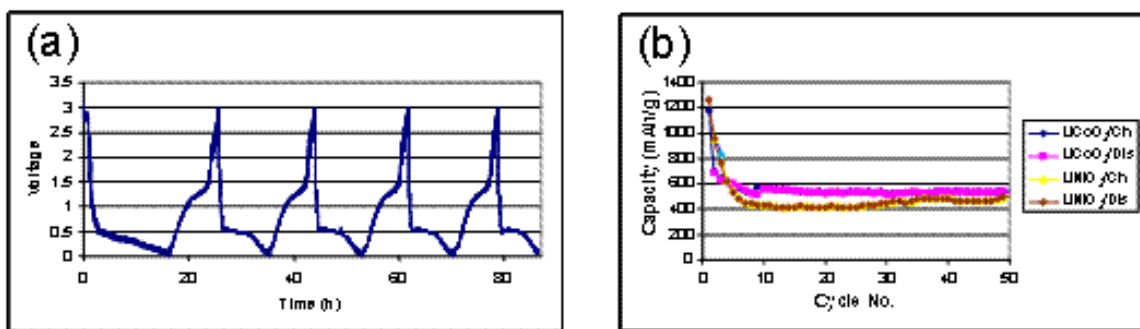


Figure IV-18. (a) Discharge and charge profiles of a Li/LiCoO_2 cell (3.0 to 0.0 V) and (b) Capacity vs. cycle no. plots for Li/LiCoO_2 and Li/LiNiO_2 cells

Metal-Based Anodes. The graphitic carbon anode presently used in lithium cells can pose safety problems under high charge rates. As a result, a number of alloy-forming metals have been studied. Part of this task involves studying the behavior of bulk metal foil, wherein there is no need for conductive diluent or binder, and therefore minimum likelihood of side reactions. This allows a better understanding of what causes capacity fade in metal anodes.

The electrochemical cycling of metal foils is being compared with expanded metal grids (supplied by Hydro-Québec [HQ]) where the expansion upon reaction can be better accommodated. Tin foil,

even at cycling rates of 3 mA/cm^2 , is comparable to alloys such as Cu_6Sn_5 formed in situ by heating a tin film electrodeposited on copper.

Recently expanded tin and aluminum grids have been obtained from HQ to determine if their open structure will mitigate the capacity fade. They show a cycling behavior similar to tin foil, with a slightly higher initial discharge capacity. After the first discharge, three plateaus corresponding to $\text{Li}_{0.4}\text{Sn}$, LiSn , $\text{Li}_{2.33}\text{Sn}$ respectively appear. Compared with tin foil, the grid has a slightly better electrochemical performance beyond 10 cycles but still shows unacceptable capacity fade.

HQ also provided three aluminum grids whose behavior is shown in Figure IV-19. All show the formation of LiAl during cycling, and an initial high capacity of $\sim 1000 \text{ mAh/g}$, followed by a fast decrease to $\sim 400 \text{ mAh/g}$, which is still higher than graphite. Although this behavior is significantly better than aluminum foil, it shows that aluminum cannot be cycled extensively in carbonate electrolytes.

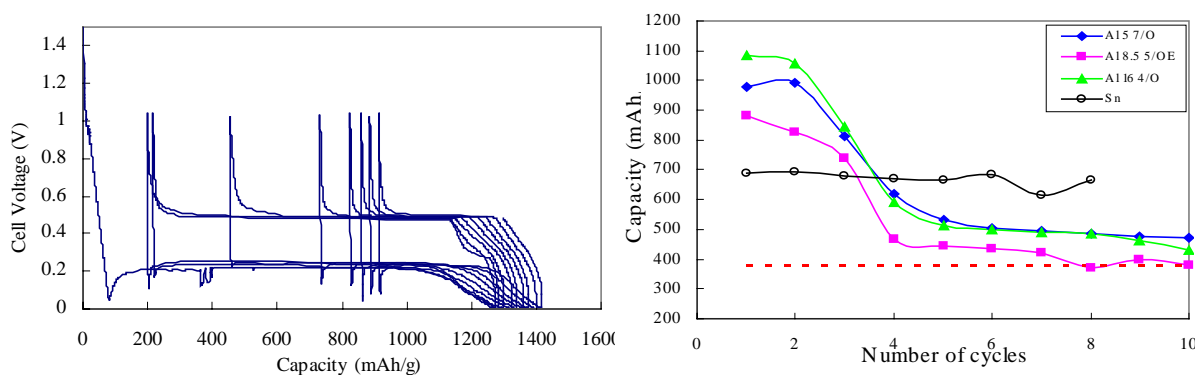


Figure IV-19. (left) Cycling of expanded aluminum grid; (right) Discharge capacity comparison of aluminum and tin grid

Cathodes

Layered $\text{Li}_{1-x}\text{Ni}_{1-y}\text{Co}_y\text{O}_2$ oxides have been shown to exhibit a high Li mobility. On the other hand, these oxides are metastable and decompose on removal of a large fraction of lithium from between the host MO_2 layers. Moreover, transition-metal ions, M, that do not have a strong octahedral-site preference migrate to vacancies in the Li layer, which limits the choice of transition-metal atom. Ohsuku and Mikimura reported nearly 150 mAh/g over the range 2.5 to 4.3 V vs. Li for 30 charge/discharge cycles with $\text{Li}_{2-x}\text{Ni}^{(\text{II})}\text{Mn}^{(\text{IV})}\text{O}_4$, but only with a low current density. This system is being investigated to determine (a) whether the capacity could be increased at higher current densities by coating the particle with carbon and (b) the role of the $\text{Mn}^{(\text{IV})}$ ions since $\text{LiNi}^{(\text{II})}\text{Ti}^{(\text{IV})}\text{O}_4$ did not appear to be a good cathode material.

Work has continued on high-capacity and high-rate $x\text{Li}_2\text{M}'\text{O}_3 \cdot (1-x)\text{LiMO}_2$ “composite” electrodes ($\text{M}' = \text{Ti, Mn, Zr}$; $\text{M} = \text{Mn, Ni}$). The inactive $\text{Li}_2\text{M}'\text{O}_3$ component is a ‘structural dopant’ which stabilizes the layered LiMO_2 electrodes and reduces the oxygen activity at the surface of charged electrode particles. Researchers have recently obtained 180 mAh/g at 50°C from $0.03\text{Li}_2\text{ZrO}_3 \cdot 0.97\text{LiMn}_{0.5}\text{Ni}_{0.5}\text{O}_2$ electrodes for 100 cycles nearly meeting the targeted capacity (Figure IV-20). Despite the strong structural compatibility between the $\text{Li}_2\text{M}'\text{O}_3$ and LiMO_2 components, XRD data, in combination with nuclear magnetic resonance (NMR) data and

high-resolution transmission electron microscopy (HRTEM) data, showed that the structures are not simple solid solutions but consist of complex atomic and compositional arrangements, yielding domains with short-range order. Acid treatment of electrodes containing a Li_2MnO_3 component significantly reduced the ICL of the initial charge-discharge cycle when cells were charged to 4.6 V without compromising the overall capacity (200 mAh/g).

Synthesis and electrochemical testing of the pseudobinary cathode $x\text{LiCoO}_2 - (1-x)\text{Li}(\text{Ni}_{2/3}\text{Nb}_{1/3})\text{O}_2$ have been performed. Diffraction results indicate that even for compositions comprising 50% LiCoO_2 , the $\text{Li}(\text{Ni}_{2/3}\text{Nb}_{1/3})\text{O}_2$ structure is maintained and no evidence for a layered structure is seen. This result is mirrored in the electrochemistry, where LiCoO_2 doping actually decreases the electrochemical performance. This is consistent with the ordering in the rock-salt derived material, $\text{Li}(\text{Ni}_{2/3}\text{Nb}_{1/3})\text{O}_2$, which in contrast to LiCoO_2 , contains transition metals (Nb^{5+} and Ni^{2+}) in all the metal layers. A cubic rock salt structure is seen for $x = 0.7$, which also suffers from poor electrochemical performance.

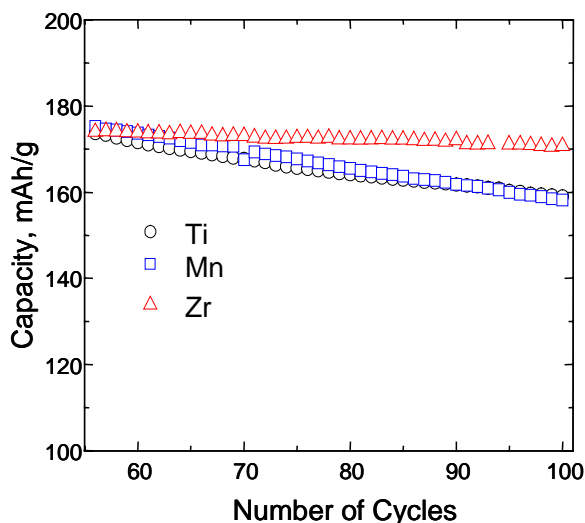


Figure IV-20. Cycling stability of $\text{Li}/0.03\text{Li}_2\text{M}'\text{O}_3 \cdot 0.97\text{LiMn}_{0.5}\text{Ni}_{0.5}\text{O}_2$ cells

Future Plans

Anodes

- Understand what drives intercalation versus exchange reactions.
- Compensate for initial ICL of negative electrodes (metal oxides and intermetallics) using FMC Corporation's "SLMP" technology or coupling with Li_2MnO_3 -based composite electrodes.
- Compare SEI layer on intermetallic and oxide negative electrodes: >0.7 V and <0.7 V.
- Investigate low temperature behavior of carbon/metal intermetallic composite (powder) electrodes — capacity and power capability.

Cathodes

- Study the role of carbon additives in composite cathodes and its implications for battery performance.
- Focus efforts on composite Al-, Si-, Sn-, and Sb-based composite electrodes.
- Manufacture and test enriched composite cathodes.
- Continue studies of composite $x\text{Li}_2\text{M}'\text{O}_3 \cdot (1-x)\text{LiMO}_2$ electrodes, $\text{M}=\text{Co}, \text{Ni}, \text{Mn}$ to improve rate capability.
- Investigate low-temperature behavior of carbon/metal (intermetallic) composite (powder) electrodes — capacity and power capability.

IV.D. LiFePO₄ System: Performance and Limitations

Objectives

- Synthesize low-cost graphite anodes and LiFePO₄ cathode materials for Li-ion/polymer cells.
- Model iron phosphate systems to determine performance and limiting factors, and understand failure mechanisms. Measure relevant thermodynamic, kinetic, and transport parameters for use in the models.
- Predict the long-term corrosion performance of Al current collectors in Gen2 cells based on statistical analyses of corrosion of Al current collectors in batteries.
- Determine the cause(s) of Al corrosion. Determine the mechanism of passivation and identify the passive film responsible for the corrosion resistance of Al current collectors. Determine the influence of the level of purity of Al on its corrosion resistance in Gen2 and in multicomponent, noncorrosive electrolytes.

Approach

One approach used in these investigations is to synthesize and coat electrodes (both anode and cathode) with low-cost materials, and use these materials to assemble prismatic cells. Additional work is focused on gel polymers, as well as studies of pressure effects and interfacial phenomena at the polymer/electrode interfaces.

In addition, simulations have been used to design combinations of conductive additives to improve battery performance, and specifically reduce the irreversible capacity loss (ICL). This involves performing electrode conduction studies with cell testing to confirm the materials' effect on battery performance.

Also, mechanistic models have been developed for specific chemistries and are used with controlled half-cell experiments to understand limiting mechanisms. This understanding is then used to suggest changes to the materials and quantify the improvements. In addition, full cell models with a natural graphite negative electrode are used to perform cell design and optimization studies to evaluate the maximum possible performance of these chemistries.

The current corrosion research project consists of three tasks. In the first, Al current collectors taken from life tested batteries are inspected for corrosion damage. The results of the failure analyses are analyzed to predict 10- and 15-year performance of Al current collectors in Li-ion batteries. In the second task, the passive films that are responsible for the corrosion resistance of Al, which has been rendered free of its air-formed film, are identified in Gen2 and multicomponent non-corrosive electrolytes. In the third task, virgin coin cells are charged and overcharged and the type and extent of corrosion of Al current collectors are identified.

Accomplishments

LiFePO₄ Cells. A model was developed for LiFePO₄ in the prior fiscal year, and it was concluded that both transport limitations in the solid phase and conductivity in the matrix phase limited its high-power capability. The model allows for the differences in loading and thickness to be normalized, whereby the intrinsic differences between each of the materials were exposed. The performance of six different sources of LiFePO₄ with varying amounts and types of in situ carbon

was compared with the help of the above mentioned model. The study revealed that both the carbon coating and extra added carbon are critical to performance and that small and uniform particle sizes are preferable. Subsequently, the model was used to perform optimization studies wherein the specific energy was maximized by changing the thickness and porosity. The optimization was performed for discharge-times ranging from 10 h to 2 min, thereby spanning both the electric vehicle (EV) and hybrid electric vehicle (HEV) goals. This approach showed that the LiFePO_4 cathode does show promise in high-power applications (Figure IV-21).

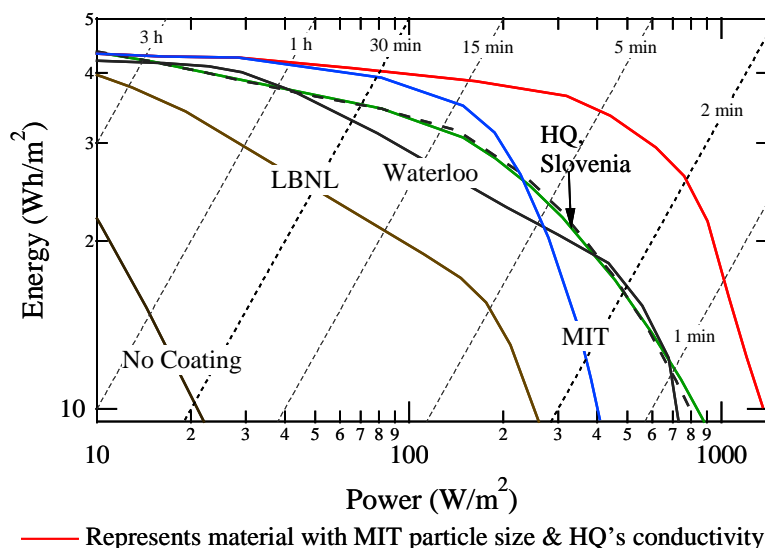


Figure IV-21. Comparative iron phosphate performance

Carbon Structure/Type and Cell Performance. Recent studies showed a clear correlation between carbon structure and cell capacity, Figure IV-22. This research has determined the key elements necessary for high-rate performance of LiFePO_4 cathodes. Utilization of solid-state or sol-gel prepared LiFePO_4 samples as cathodes in lithium cells depends primarily upon the structure of the residual carbon (0.5–2%) co-produced from either inorganic or organic precursors during the synthesis process. Strategies to overcome low rate capability in LiFePO_4 (e.g., carbon coating) often result in unacceptably low energy density. Recent work is directed toward optimizing the structure of in situ carbon produced during LiFePO_4 synthesis. Carbons with low D/G ratios (disordered/graphene) have higher electronic conductivities and improved electrochemical performance, even when present in small amounts (≤ 1 wt%). In FY 2004, ways to promote formation of low D/G ratio carbon were explored, including using additives during synthesis. One finding resulting from this investigation is that iron nitrate improves carbon structure (Figure IV-23).

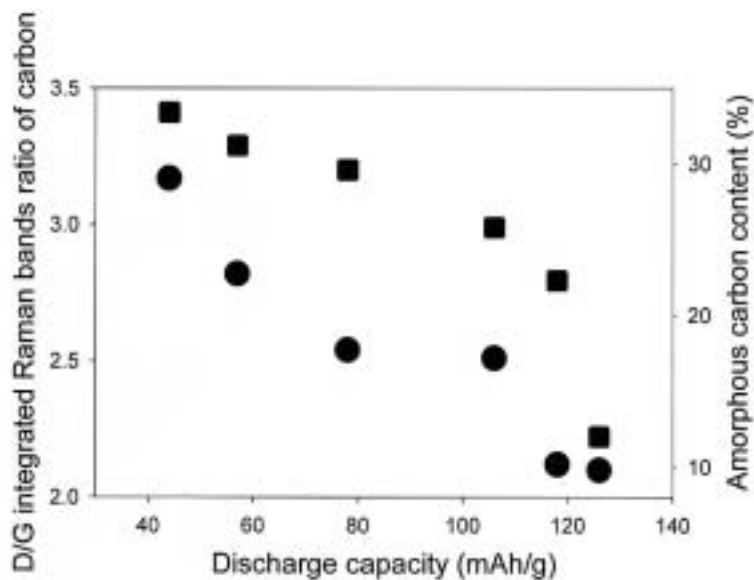
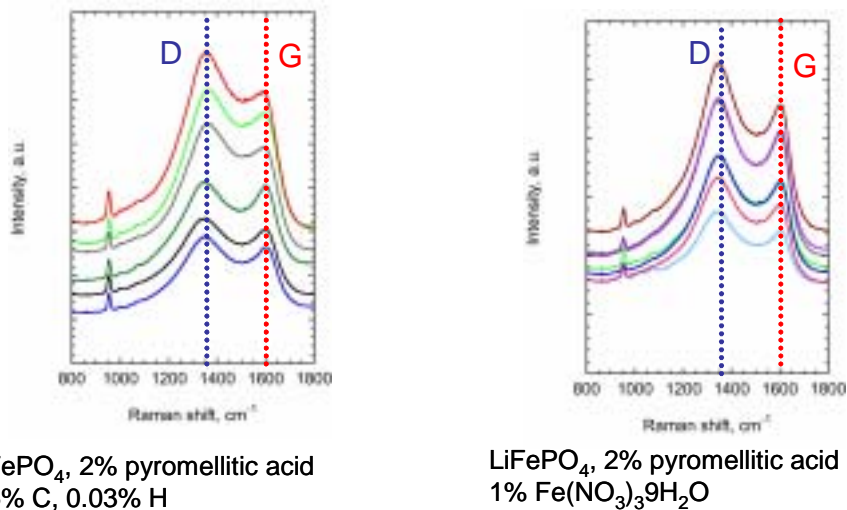


Figure IV-22. Cell capacity vs. carbon structure



LiFePO₄, 2% pyromellitic acid
0.5% C, 0.03% H

LiFePO₄, 2% pyromellitic acid
1% Fe(NO₃)₃·9H₂O

Figure IV-23. Addition of iron nitrate improves D/G carbon ratio

Figure IV-24 shows cycling data for several samples containing pyromellitic acid (PA). Although utilization is lower than theoretical at low current densities, the rate capability is good. Decreasing the particle size and using carbon-coated current collectors should improve the low rate utilization.

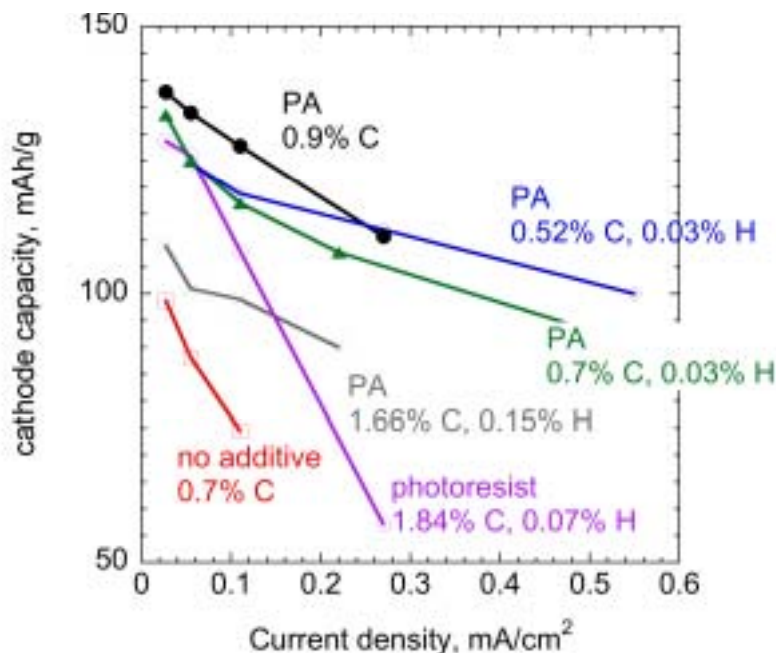


Figure IV-24. Rate data for a Li/LiFePO₄ cell

Doping and LiFePO₄ Performance. To characterize the effect of doping on LiFePO₄ performance, samples of highly conductive Nb-doped LiFePO₄ material from Prof. Yet-Ming Chiang (MIT) were examined. A current-sensing atomic force microscopy (AFM) (current-sensing atomic force microscopy [CSAFM]) and Raman microscopy diagnostic study of surface electronic conductivity, composition, and structure was carried out at nanometer-scale lateral resolution (Figure IV-25). Surface analysis of 1% Nb-doped and pristine LiFePO₄ samples indicated:

- significantly higher carbon content in the Nb-doped LiFePO₄ than in the pristine sample;
- a non-uniform distribution of carbon at the sample surface;
- no electronic conductance in the pristine LiFePO₄ sample; and
- non-uniform conductivity of the Nb-doped LiFePO₄. The carbon distribution at the cathode surface corresponds to the conductivity pattern.

Thus, the doping effect (if any) is masked by the residual carbon from organic precursors. The higher carbon content in the 1% Nb-doped LiFePO₄ is thus most likely responsible for improved conductivity and electrochemical performance.

Advanced Diagnostic Techniques. A technique for nondestructive determination of the electronic conductivity and contact resistance of each sublayer in composite LiFePO₄ cathodes has been developed and used to measure the electronic conductivity of the cathodes with carbon additives. Cathodes with varying amounts (3 to 12 wt%) and types of conductive carbon additives were pressed onto carbon-coated current collectors patented by Hydro-Québec (HQ). Compression was carried out to reduce the contact resistance between active materials and current collectors. Sample cathodes were tested and the data obtained were compared with electrochemical conduction performance.

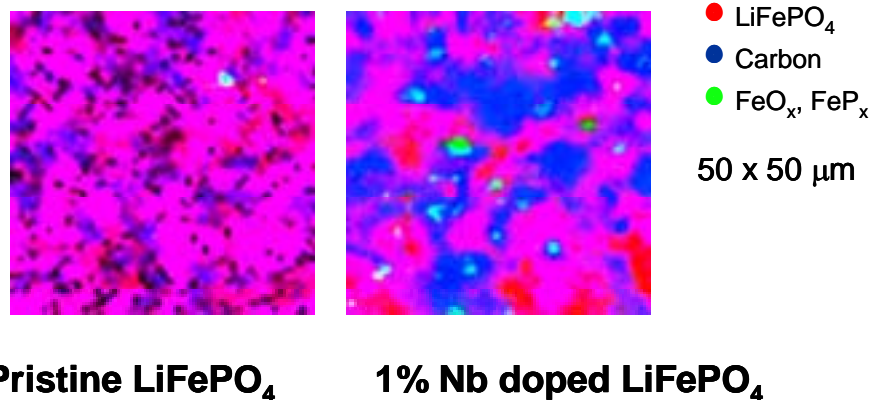


Figure IV-25. Raman spectra of pure and doped iron phosphate

Four-point probe conduction experiments were analyzed using a numerical approach to solve for the conductivity of each layer and contact resistances between layers. Conductivity data confirm that carbon additives significantly improve overall LiFePO₄ electrical conductivity. For example, measured resistivity dropped from 176 to 67 Ωcm as carbon black increased from 3 to 10 wt%. For concentrations of conductive additives above 6 wt%, homogeneous electronic resistivity was observed. Contact resistances at interfaces between the LiFePO₄ matrix and carbon coating of current collector, and between carbon coating and current collector were similar in all cases, indicating manufacturing consistency. It has been found that the addition of ~3 wt% carbon black significantly improves the electronic conductivity of LiFePO₄ composite cathodes.

LiFePO₄ Cells with LiBOB Salt. In addition, sixteen LiFePO₄/graphite cells were assembled from anodes and cathodes received from HQ. Cells were filled with either LiPF₆ or LiBOB salts in carbonate solvents. Twelve of the cells were tested at room temperature with 100% depth-of-discharge (DOD) cycling at a rate of C/2, and four were tested at 45°C. Post-test diagnostics were carried out on components from several of the cells, including electrochemical diagnostics, Raman spectroscopy, and transmission electron microscopy (TEM). The cells with the LiBOB electrolyte show somewhat better capacity retention when compared with the LiPF₆ electrolyte cells, especially at elevated temperature.

The lowest room temperature capacity fade rates were 0.1%/cycle and 0.05%/cycle for the LiPF₆ and LiBOB-electrolytes, respectively. This low fade rate was maintained for at least 80 cycles before cell disassembly for diagnostics. Electrochemical analysis of the electrodes removed from these cells showed that capacity fade is primarily due to the loss of cycleable lithium from the cell. The cathode active material was essentially unchanged when cycled against a source of lithium (Li foil in the half-cell).

Electrodes from the cycled cells showed no electrochemical deterioration of the active materials. However, Raman spectroscopy of the cycled anodes revealed the presence of iron species (Figure IV-26), as well as an increase in the relative disorder of the graphite. The presence of iron was confirmed with TEM/energy-dispersive X-ray (EDX) analysis. The location and morphology of the iron-containing species appears similar to that observed for Mn deposition on the anode of the LiMn₂O₂/graphite cell cycled in LiPF₆-containing electrolytes.

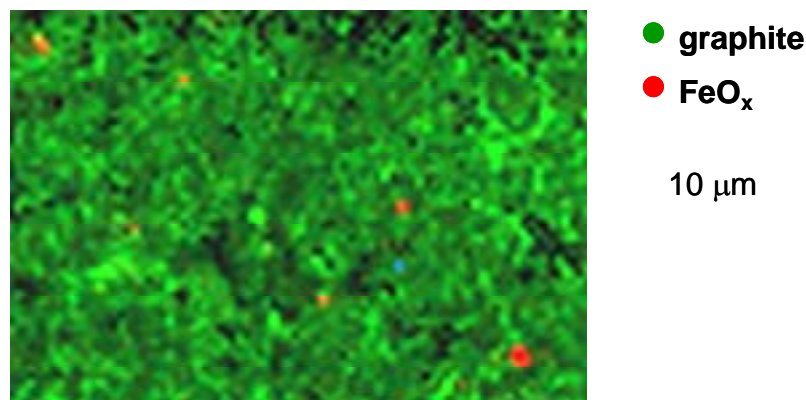


Figure IV-26. Raman analysis showing presence of FeO on anode of cycled cell

Polymer Gel Electrolyte. Studies on the effect of the polymer on the gel electrolyte system of composition $x\%$ polymer- $(1-x)\%$ EC- γ BL-1.5M LiTFSI were completed. Two significant findings from this study are:

1. the vapor pressure decreases with a decrease in the amount of γ BL, and
2. at high temperature (100–125°C), the vapor pressure decreases when the polymer content increases.

This effect helps improve the battery safety characteristics. Thermogravimetric (TGA) analysis was used to investigate the influence of the polymer content (100%, 30%, 20% and 10% by weight) in the gel on the weight loss of the electrolyte at higher temperatures. The results show an increase in the polymer content produced a decrease in the weight loss of the gel. In addition, a comparison of the thermal stability with different salt species was completed, with the result that imide salts were found to be more thermally stable than LiPF₆ or LiBF₄ (Figure IV-27).

Optimization studies showed that a 10/90 polymer/liquid weight ratio yielded good mechanical properties, and with only 20% swelling. The ionic conductivity decreased linearly from 10.1 to 3.50×10^{-3} S/cm with increasing polymer content in the gel with pure liquid electrolyte and a 35/65 wt% polymer/liquid ratio.

Current Collector Corrosion. Previously, a small incidence of aluminum current collector corrosion was reported in life tested Li-ion batteries. To determine why corrosion sometimes occurs, this work has concentrated on the factors that are responsible for the good corrosion resistance of aluminum in battery electrolytes.

It has been found that Al is susceptible to severe corrosion in ethylene carbonate (EC)+dimethyl carbonate (DMC) that is free of LiPF₆ and that contains a small amount of water as a contaminant. Decreasing the water concentration decreases the amount of corrosion. Varying the relative amounts of EC and DMC does not prevent corrosion, but adding a minimum of 0.02 M LiPF₆ prevents significant corrosion. Second, LiPF₆ causes the formation of a protective film of AlF₃. The thinner the air-formed film of Al₂O₃, the more readily AlF₃ forms. Third, when the air-formed film of Al₂O₃ is completely removed, the film of AlF₃ forms at the very low potential of 1.0 V vs. Li/Li⁺. Since

AlF_3 can form at 1.0 V vs. Li/Li^+ , its formation does not depend on (a) oxidation of the solvent, which is stable to potentials above 4.0 V, or (b) voltage breakdown of PF_6^- , which is stable to potentials as high as 5.0 V. Either very little water contamination, or possible no water at all, is needed to provide F for forming the film of AlF_3 . The results to date indicate that water contamination is not harmful to corrosion resistance of Al provided a small concentration (i.e., 0.02 M) of LiPF_6 is present.

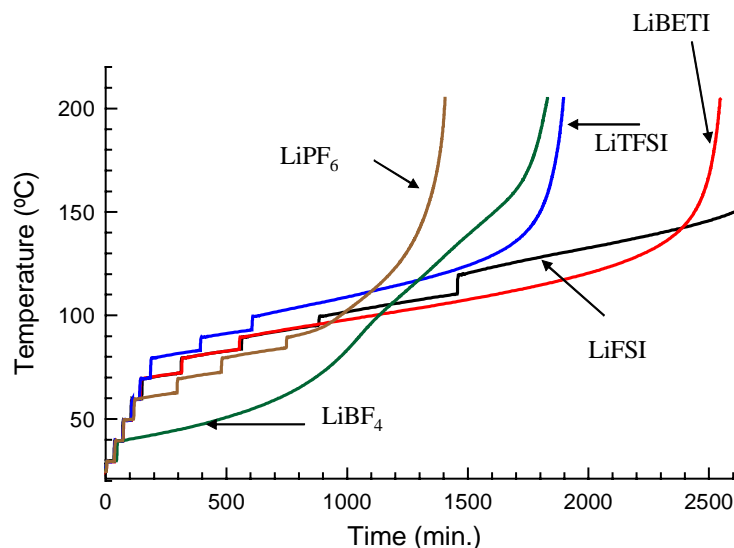


Figure IV-27. Thermal stability of various salts

Recently, the role of aluminum oxides on the corrosion behavior of aluminum was studied in several electrolytes. In particular, the influence of three different surface conditions on aluminum's corrosion was investigated: (a) aluminum covered with an air-formed oxide, (b) aluminum covered with a thick oxide, prepared by anodization in sulfuric acid, and (c) bare aluminum, which was stripped of its air-formed film by in situ abrasion in the electrolyte.

The electrochemical behavior of aluminum covered by surface films of Al_2O_3 of different thickness was characterized by cyclic current-voltage (C-V) curves in LiPF_6 containing electrolytes. The voltage spanned the range between the corrosion potential and 5V vs. Li. The corrosion potential increased with the thickness of Al_2O_3 and was approximately 2.5 V for aluminum with an air-formed film of Al_2O_3 . There were two main effects of oxide thickness on the C-V curve. As the oxide thickness increased, (1) the current during the first cycle decreased, and (2) the voltage at which the oxidation rate during the first cycle abruptly increased, was raised. Electrochemical quartz crystal microbalance (EQCM) experiments indicated that the abrupt increase in current was caused by the formation of another surface film, which was most likely AlF_3 . The AlF_3 -type film appeared to form on top of the Al_2O_3 , as opposed to replacing the Al_2O_3 . The AlF_3 -type film provided additional protection against corrosion and its thickness increased with the applied voltage.

The additional protection against corrosion provided by the thicker Al_2O_3 was investigated by potentiodynamic and potentiostatic anodic polarization experiments in 1.0M LiTFSI/EC+DMC . A 48 μm thick anodized film of Al_2O_3 significantly increased the corrosion resistance of aluminum during these tests (Figure IV-28). However, considerable corrosion of aluminum occurred when potentials of 5 V and 6 V were applied for 20 hours. Inspection by scanning electron microscopy

(SEM) of the anodized samples polarized at 6.0 V for 20 hours indicated that the thick, anodized Al_2O_3 film itself was not corroded. Rather, aluminum was corroded beneath the anodized film. This result suggests that current collectors covered by thin, air-formed films of Al_2O_3 corrode in a similar way. That is, corrosion initiates at defects in the air-formed film and then attacks the aluminum beneath the air-formed film.

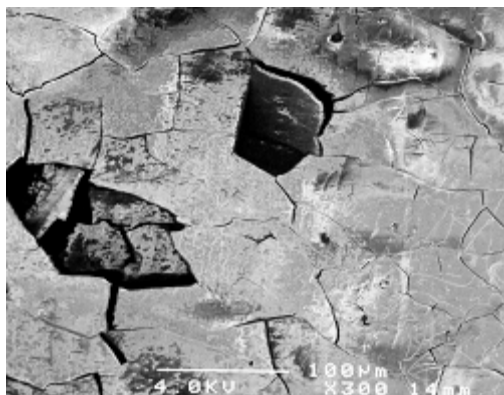


Figure IV-28. Typical morphology of aluminum with 48 μm thick Al_2O_3 film in 1.0 M LiTFSI/EC+DMC after 20 hours at 6.0 V

Future Plans

Iron Phosphate cells

- Examine the stability of $\text{LiFePO}_4/\text{NG}$ cells in non- LiPF_6 -containing electrolytes such as LiBOB, LiTFSI and derivative electrolytes.
- Evaluate HEV-designed $\text{LiFePO}_4/\text{NG}$ cells.
- Further elucidate the role of Carbon in iron phosphate's performance.
 - Examine the role of conductive additive preparation and morphology on cathode conductivity and performance.
 - Determine if the iron phosphate chemistry can meet HEV application requirements.
 - Determine the optimum amount of carbon in the iron phosphate system.
 - Simulate and investigate the effect of morphology of the carbon black additive to determine how it improves conductivity of the cathode.
- Create finite element models to simulate the pressing process to develop a guideline for electrode fabrication for optimized conductivity.
- Identify improved procedures for cell assembly, determine cell cycle life with HEV protocol, evaluate storage life at high temperature.
- Investigate the relationship between electrode thickness and electrochemical performance of composite LiFePO_4 cathodes using numerical modeling.
- Use soft X-rays to study LiFePO_4 cathodes, especially the effect of oxygen vacancies.

Aluminum Current Corrosion

- Determine the source of F^- for forming AlF_3^- type film?
- Establish role of H_2O in the corrosion behavior of Al, measure (H_2O) in tests already conducted.

New Binder

- Identify a new water-soluble binder (WSB) for both anode and cathode.
- Demonstrate HQ coating process with low-cost WSB in electrodes containing natural and artificial graphite.

IV.E. Li/Polymer Component Limitations

Objectives

- Determine the limitations on Li-ion transport in polymer electrolytes and composite electrodes.
- Develop composite polymer electrolytes that are low-cost, highly conducting, impart electrode-electrolyte interfacial stability, and yield long cycle life.
- Gain molecular-level understanding of ion transport mechanisms in single-ion conductors and gel electrolytes.
- Develop tools and methodologies for accurate prediction of structural and dynamic properties of solid polymer electrolytes (SPE), single-ion conductors (SIC), and gel electrolytes. Use these tools to understand ion complexation and transport mechanisms. Perform virtual design of novel electrolytes with high conductivity and transport number.
- Synthesize new battery electrolytes based on oligomeric bis(perfluoroalkylsulfonyl)imide anions having high ionic conductivity and high Li transference. Characterize solid polymer and gel electrolytes made from the target salts with respect to structure, transport and mechanical properties, reactivity with electrodes and current collectors, and performance in test cells.

Approach

To obtain a fundamental understanding of charge transport in polymers, they are characterized by methods such as neutron scattering, dielectric relaxation spectroscopy, and light scattering to obtain new insights into rate-limiting transport processes.

Next, surface-functionalized fumed silica fillers are used to determine the effects of filler type and concentration on interfacial stability and cell cycling. Electrochemical characteristics are correlated with mechanical properties and materials chemistry (e.g., silica-type or poly(ethylene oxide) [PEO]-type). Data collected include elastic and viscous moduli, ionic conductivity, transference number, Li cycling efficiency, Li-electrolyte interfacial resistance, and full-cell cycling capacity using 3V cathodes.

Theoretical efforts include developing *ab initio* quantum chemistry based force fields for SPEs, single ion conductors, and gel electrolytes. Next, molecular dynamics (MD) simulations and experimental results are used to obtain a detailed understanding of the transport mechanisms in these materials. Based upon that understanding, novel electrolytes are virtually designed and their

properties are predicted using MD simulations. Based on these results, the most promising electrolytes for experimental synthesis are recommended.

The surface interactions of polyelectrolyte single ion conductor materials are under investigation in order to understand their role in a variety of phenomena that limit the performance of lithium batteries, including dendrite initiation and growth at lithium metal anodes, interfacial polarization leading to limitations on power and energy as well as limitations on transport phenomena and capacity fade.

Finally, salts are being developed using variants of methodologies developed at Clemson University over the last 15 years.²⁰ The transport properties are then measured using impedance combined with restricted diffusion, direct current (DC) polarization, and concentration cell techniques.

Accomplishments

Polymer Electrolytes. Research continues on rheo-dielectric characterization of polymer electrolytes. Specifically, the rheological properties of comb-branched poly(trimethylene oxide) (PTMO) polymers containing LiTFSI have been measured and compared to the characteristics of PEO/LiTFSI mixtures. Zero shear viscosity measurements on the systems indicate a lower activation energy for Li-ion transport in the PTMO polymer matrix. These measurements, together with those of conductivity and salt diffusion, indicate that the mobility of Li⁺ ions in PTMO is substantially greater than that in PEO due to a decrease in the activation energy for the Li/polymer complex in the two systems.

The dielectric properties of PEO melts containing LiClO₄ under steady shear flow were measured using a custom rheo-dielectric instrument. The instrument also enabled measurement of the linear and non-linear rheological properties and the dielectric properties of the PEO/LiClO₄ mixtures. A significant increase in the zero-shear viscosity, η_0 , is observed upon addition of LiClO₄ to PEO. This is due to Li-mediated intermolecular bridging of the PEO chains. Significant shear thinning was observed under fast shear, suggesting the flow-induced break-up of the intermolecular bridges and the flow induced liberation of Li ions. The presence of liberated ions was detected directly by dielectric dispersion experiments under steady shear flow. The dielectric dispersion curves shift to higher frequencies, ω , with increasing shear rate, indicating an increase in ionic conductance.

Dispersion curves obtained at different shear rates collapse onto a single master curve when plotted against a reduced frequency $\lambda^{-1}\omega$, where λ is a shear rate-dependent normalizing factor. The shear rate dependences of λ^{-1} and η/η_0 are identical. This establishes the quantitative connection between shear thinning, observed in the rheological experiments, and the shear-induced increase in the electrical conductivity, observed in the dielectric experiments.

New Polymer Structures for Improved Performance. The introduction of a trimethylene oxide (TMO) link into the polymer chains clearly increases the polymer mobility. However, TMO appears to lower the dielectric constant of the medium resulting in increased ion pairing and a decrease in the concentration of free charges to carry current. Combination of large anions such as bis(trifluoromethanesulfonyl)imide (TFSI) and bis(perfluoroethylsulfonyl)imide (BETI) with

²⁰ D. DesMarteau, *J. Fluorine Chem.* 1995, **72**, 203–208.

TMO-containing polymers leads to better ion dissociation which, combined with increased chain flexibility, gives better transport (Figure IV-29). The synthesis of a comb polymer system that contains only TMO solvation units, even in the backbone, has been initiated. Studies are also under way on the curing chemistry of polymers for gel and “dry” polymer and polyelectrolyte systems.

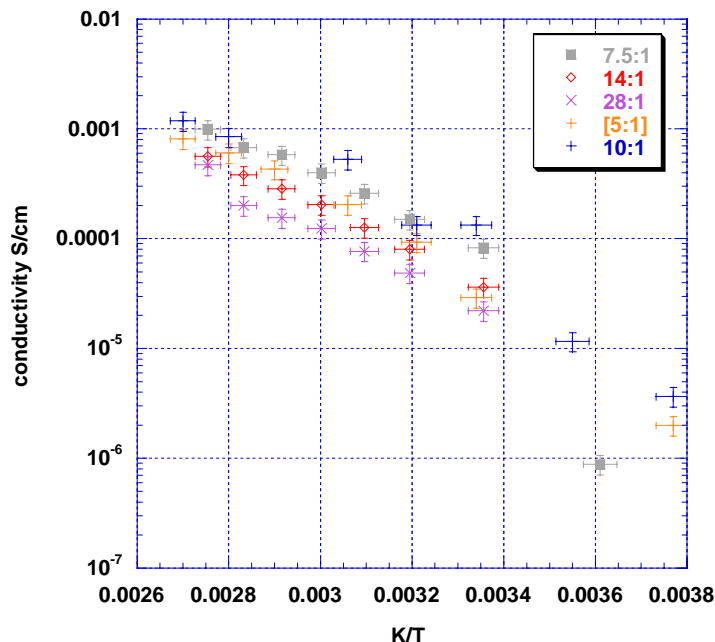


Figure IV-29. Conductivity of PTMO with LiBETI salt

Dendrite Initiation and Growth. Studies have been carried out on both symmetrical lithium/lithium and full Li/V₆O₁₃ cells using linear and comb-branch polymers, with varying levels of cross-linking and added filler material to vary the mechanical properties of the polymer electrolyte. Dendrite initiation is completely inhibited if the cell polarization is kept sufficiently low, e.g., less than 20 mV for 0.1 mA/cm².

Increase of the current density or a decrease in the temperature to values where the transport properties can no longer relax the concentration gradients quickly enough result in increases in the interfacial and concentration impedances. This leads to steadily increasing cell polarizations and surface roughening. The LiTFSI and LiBETI imide salts are able to sustain 0.1 mA/cm² indefinitely. However, salts with poorer transport properties, such as LiMethide and LiTriflate, cannot sustain these densities while a variety of salts (LiBF₄, LiPF₆, LiBOB and LiClO₄) appear to react with the lithium metal during cycling, and show large increases in interfacial impedances upon cycling. LiPF₆ appears to be particularly unsuitable as would be consistent with the reaction of PF₅ on the PEO-type polymer.

Higher current densities can be applied provided the duration of the polarization does not allow establishment of steady-state conditions. The polarization is minimized by use of thin cells (<50 μm), use of electrolytes with good transport properties, and minimization of the interfacial impedance. It has been noted that extended cycling at current densities above a critical value appears to lead to increases in the salt diffusion coefficient and interfacial impedance. This is consistent with

transport effects that lead to salt concentrations at the electrodes that differ from the bulk. These effects can be more effectively controlled by use of electrolytes with better transport and mechanical properties.

Composite Polymer Electrolytes. Recent efforts have been in four areas: (a) nanocomposite electrolytes consisting of lithium salt + fumed silica (FS) + mixtures of low- and high-molecular weight (MW) PEO solvents; (b) reactivity of aluminum current collectors in electrolytes containing FS; and (c) electrolytes containing FS with salts other than TFSI.

(a) The conductivity and rheology of P(EO)₂₀LiTFSI + 10% A200 fumed silica electrolytes with different mass ratios of PEO (MW=600K) to PEG-dM (MW=250): 100/0, 80/20, 67/33, 50/50, 33/67, and 20/80 have been measured. Conductivity increases with the amount of low-MW component but the heat of fusion as well as melting and crystallization temperatures decrease.

Surprisingly, the corresponding moduli of the blends are higher than the composite containing the high-MW component, and the elastic modulus and yield stress show a maximum in concentration with PEG-dM (Figure IV-30). These results are important since it was expected that the low-MW component would plasticize the high-MW PEO and produce a monotonic decrease in elastic modulus. Lithium dendrite formation was investigated via in situ microscopy at 65 and 80°C using mixed-MW P(EO)₂₀LiTFSI (PEO:PEG-dm; 50:50) electrolytes. Dendrites that have a current density-dependent morphology form in the electrolyte but the addition of fumed silica suppresses their growth considerably.

(b) The effect of fumed silica (FS) on aluminum corrosion was studied using low-MW PEO electrolyte (PEG-dM+LiTFSI; Li:O=1:20). The open circuit voltage (OCV) for cells with FS-based electrolytes was more stable than that for the baseline liquid electrolyte, and the corrosion current density was lower. In electrochemical impedance spectroscopy (EIS) measurements, the electrolytes containing FS have a large phase lag over a wide frequency range, which does not exist for the baseline liquid electrolyte. These phenomena may be interpreted as a film-coating behavior (Figure IV-31).

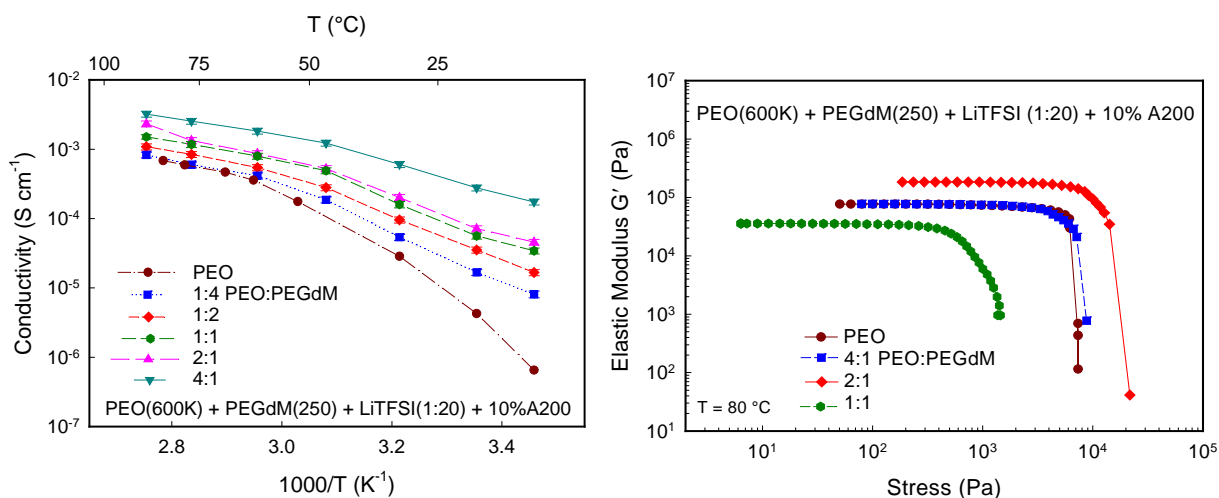


Figure IV-30. Conductivity and elastic modulus of mixed MW systems

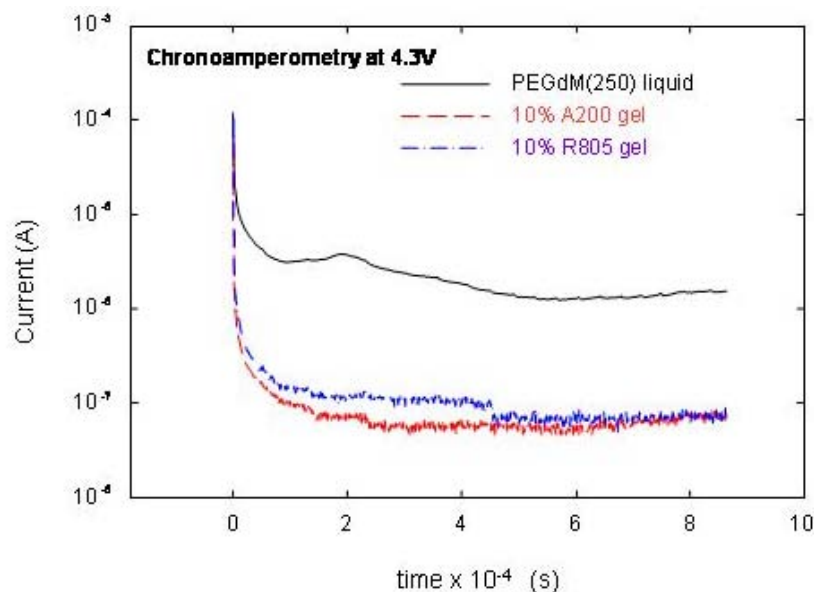


Figure IV-31. Fumed silica in low-MW PEGdM attenuates aluminum corrosion current

(c) Thermal stabilities of different lithium salts: LiBETI, LiBOB, and Li dianionic are also being studied by thermogravimetric analysis (TGA). The TGA measurements were done from room temperature to 600°C at a heating rate of $5^{\circ}\text{C}/\text{min}$ in nitrogen. Preliminary results indicate that the thermal stabilities of LiBETI and Li dianionic salts are better than that of LiBOB. The potential windows of these three lithium salts both in liquid (PEG-dM) and gel (PEG-dM+10% R805) states has been investigated. Fumed silica has no effect on the potential window; LiBETI and LiBOB have slightly higher potential windows (~ 5.3 V) than Li dianionic (~ 5.2 V).

Molecular Dynamics Simulations. The transport and mechanical properties of polymer and gel electrolytes and single-ion conductors (SICs) depend on numerous parameters that include the polymer structure, choice and amount of plasticizer, Li salt concentration, and choice of anion. Experimental investigation of this vast parameter space is expensive and is further complicated by a lack of fundamental understanding of property-structure relationships in general and cation transport mechanism in particular. Molecular dynamics (MD) is well suited for gaining a fundamental understanding of the mechanisms for Li conductivity and thereby guiding the search for novel electrolytes with improved transport properties.

Recent research has focused on developing state-of-the-art potentials, force field fitting tools, and methodologies for accurate prediction of structural and dynamic properties of solid polymer electrolytes (SPEs), SICs, and gel electrolytes. These tools are used to assist experimentalists in understanding the transport mechanisms and to perform virtual design and characterization of novel electrolytes. New quantum-chemistry-based potential energy functions have been developed for predicting properties of numerous polyethers and carbonates doped with LiTFSI. MD simulations using these force fields predict static and dynamic factors in good agreement with experiments. MD simulations of a SIC gel electrolyte based upon poly(epoxide ether) predict an ionic conductivity of 10^{-2} S/cm at 393 K, indicating that gel electrolytes and SICs of this type show promise for Li-ion batteries (Figure IV-32).

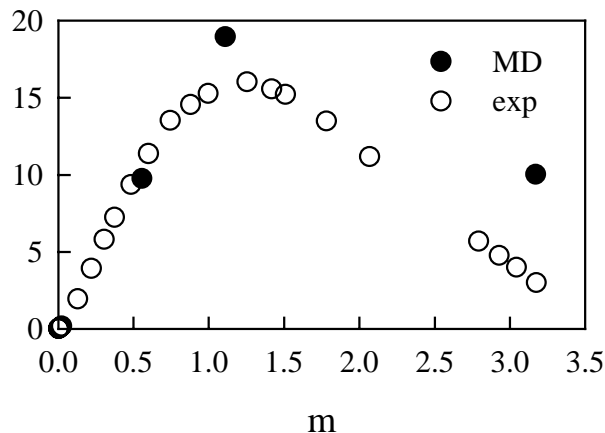


Figure IV-32. Conductivity vs concentration of DME/LiTFSI at 308 K

The influence of the PEO conformational (local) dynamics on Li and TFSI diffusion has also been investigated by varying barriers for PEO conformational transitions. It is found that local PEO dynamics are coupled not only with the Li mobility but also with the TFSI anion mobility. This result has important ramifications for the design of new electrolytes: i.e., one cannot increase only Li dynamics without also increasing the TFSI anion dynamics by selecting a polymer with more rapid local dynamics. MD simulations of poly(epoxide ether) with side chains of long ether repeat units (PEPE₅) doped with LiTFSI showed that Li is complexed primarily by ether oxygens from the side chains and not from the main chain. This data explains why the ionic conductivity (measured by Dr. Kerr's group) of a number of PEO-based comb branched copolymers doped with LiTFSI was independent of the chemistry of the groups connecting side chains to the main chain.

Additional research concentrated on prediction of structural and dynamic properties of two classes of materials: dry single ion conductors and ionic liquids. MD simulations have been performed on the PEPE-*m*-20-TFSILi, *m*=5,10,20 single ion conductors and the LiTFSI-EO_{*n*}-TFSILi ionic liquids for *n*=12,20,40 at 423 K. The main goal is to find the optimal length of the side chain or polyether connector in these materials. Conductivity has been estimated at 423 K and is shown in Figure IV-33. These data indicate that the most optimal number of ether oxygen units in a side chain is ~10–12 for the PEPE-*m*-20-TFSILi electrolyte, and ~20 for the LiTFSI-EO_{*n*}-TFSILi ionic liquid. A drop in conductivity with a decrease in the side chains from 10 to 5 ether oxygen repeat units in the PEPE-*m*-20-TFSILi electrolyte is associated with a sharp decrease of the fraction of “free” Li⁺ charge carriers from ~60% to ~30%. This is also accompanied by a slowing of the polymer and Li⁺ local dynamics.

MD simulations of the single ion conductors have also begun. These polymers have rather short side chains of five EO repeat units, with the TFSI anion attached to side chains every 2,4,8 repeat units. Due to short side chain length, these SICs are not expected to crystallize but could exhibit transport properties even better than those shown above. Initial estimates of transport properties from short simulations indicate conductivities of $\sim 1 \times 10^{-3}$ S/cm at 100°C.

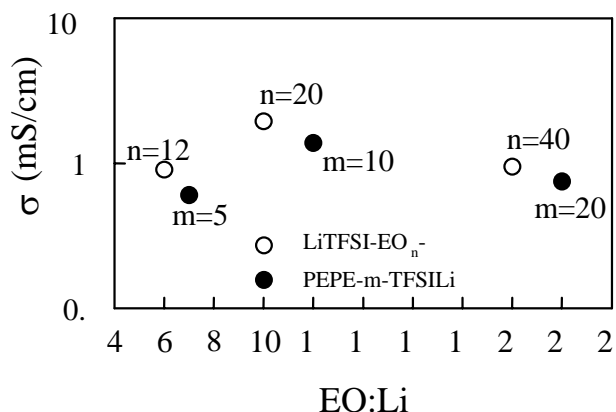


Figure IV-33. Conductivity of the PEPE-n-(20) and LiTFSI-EO_n-TFSILi electrolytes at 423 K

New Electrolytes. A dianionic salt of structure $\text{CF}_3\text{SO}_2\text{N}(\text{Li})\text{SO}_2(\text{CF}_2)_4\text{SO}_2\text{N}(\text{Li})\text{SO}_2\text{CF}_3$ was tested. Early indications are that half-cells prepared using a 1:1 EC:DEC solution of the salt with an LiFePO_4 cathode and lithium reference and counter electrodes undergo reversible galvanostatic cycling at voltages comparable to those for similar cells prepared using, e.g., LiTFSI. Voltammetry studies in a composite PEG-dm(250) electrolyte indicate a voltage window of 5.2 V, comparable to that of LiBETI in the same host.

A working hypothesis has been that the use of low-lattice-energy salts with large and/or oligomeric anions would provide a favorable combination of high ionic conductivity and low anion mobility. Transport studies focusing on salt diffusion and lithium transference indicate that the motion of oligomeric anions in polyether hosts is slow relative to that of monomeric anions but not slow enough to prevent salt polarization in cells under charging/discharging conditions. This finding has led to a focus on methods for immobilizing fluorosulfonimide anions in polyether hosts. In this regard, allyl-ether-modified salts were synthesized.

Substantial progress has been made synthesizing and characterizing polyether-based ionic melts consisting of fluorosulfonate and fluorosulfonimide anions linked to polyethers, with lithium cations solvated by the polyether chains. It should be noted that while these materials are not themselves intrinsic single-ion conductors, they should behave as single-ion conductors when used in a Li-ion battery for which both electrodes are blocking for anions but non-blocking for lithium. Preliminary conductivity data acquired on a material with lithium fluorosulfonate attached to a 350 MW PEG monomethyl ether chain, which still contained some excess unmodified PEG, were quite promising, with room-temperature conductivity $>10^{-4}$ S/cm (Figure IV-34).

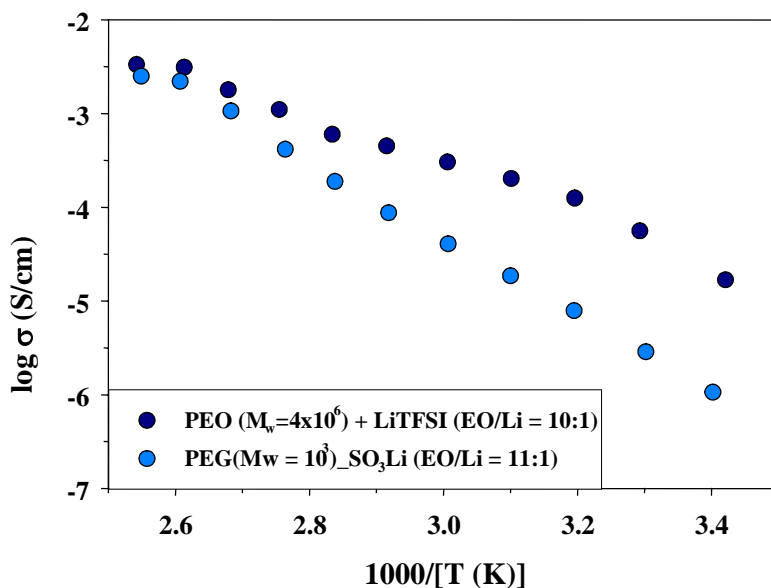


Figure IV-34. Ionic conductivity of SPEs

Future Plans

Polymer Electrolytes

- Investigate new polymers with better transport properties by introducing butanediol groups for more flexibility and sulfur donor atoms.
- Develop polymer structures with 4-volt stability.
- Optimize conductivity of the PEPEN-TFSI/Li⁺ single ion conductors and PEPEN-TFSI/Li⁺/EC gel electrolytes by varying the length and spacing of side chains.
- Determine appropriate wetting conditions by studying the gel/anode and gel/cathode interfaces.
- Determine the stability of the gel polymer with different solvents by slow-scan cyclic voltammetry and gas chromatography mass spectrometry (GCMS).
- Evaluate the effects of cross linking on gel formation (ultraviolet [UV], infrared [IR], and thermal).
- Study the possibility of increasing conductivity of polymer electrolytes by chain alignment.

Composite Polymer Electrolytes

- Understand the effect of unmodified and modified SiO₂ surfaces on PEO/LiTFSI.
- Determine the appropriate wetting conditions by studying the gel/anode and gel/cathode interfaces.
- Investigate the effect of processing conditions on the rheological and electrochemical properties of mixed MW composite polymer electrolyte (CPE).
- Study the effect of adding single-ion conducting fumed silica to mixed-MW CPE.

New and Improved Salts

- Characterize lithium fluorosulfonimide-PEG ionic liquids.
- Synthesize allyl ether epoxide salts for preparing single-ion conductors by ring-opening polymerization.
- Continue development of low-cost salt LiFSI [Lithium bis(fluorosulfomyl)].

- Evaluate the new Li salt, 4,5-dicyano-1,2,3-triazole lithium.

Selected Publications

1. C. Monroe and J. Newman, "The Effect of Interfacial Deformation on Electrodeposition Kinetics," *J. Electrochem. Soc.* **151**, A880 (2004)
2. C.P. Grey, W.S. Yoon, J. Reed, and G. Ceder, "Electrochemical Activity of Li in the Transition-Metal Sites of $\text{O}_3 \text{Li}[\text{Li}_{(1-2x)/3}\text{Mn}_{(2-x)/3}\text{Ni}_x]\text{O}_2$ " *Electrochem. Solid-State Lett.* **7**, A290 (2004).
3. C.W. Wang, Y.B. Yi, A.M. Sastry, J. Shim, and K. Striebel, "Particle Compression and Conductivity in Li-Ion Anodes with Graphite Additives," *J. Electrochem. Soc.* **151**, A1489 (2004)
4. F. Hu and M.M. Doeff, *J. Power Sources*, **129**, 296 (2004).
5. G.V. Zhuang, K. Xu, T.R. Jow, P.N. Ross, "Study of SEI Layer Formed on Graphite Anodes in PC/LiBOB Electrolyte Using IR Spectroscopy", *Electrochem. and Solid-State Lett.* **7**, A224–A227, 2004.
6. H.S. Lee, Z.F. Ma, X.Q. Yang, X. Sun, and J. McBreen, "Synthesis of a Series of Fluorinated Boronate Compounds and Their Use as Additives in Lithium Battery Electrolytes," *J. Electrochem. Soc.* **151**, A1429 (2004).
7. J. Katana Ngala, N.A. Chernova, M. Ma, M. Mamak, P.Y. Zavalij, M. Stanley Whittingham, *J. Mater. Chem.*, **14** 214–220 (2004).
8. J.-S. Kim, C.S. Johnson, J.T. Vaughey, M.M. Thackeray, S.A. Hackney, W.C. Yoon, and C.P. Grey, *Chem. Mater.*, **16**, 1996 (2004).
9. K.A. Cook and A.M. Sastry, 2004, "An algorithm for selection and design of hybrid power supplies for MEMS with a case study of a micro-gas chromatograph system," *Journal of Power Sources*, in review.
10. K.A. Cook and A.M. Sastry, 2004, "Influence of scaling effects on designing for power efficiency of a micro-preconcentrator," *Journal of Vacuum Science and Technology, B*, in review.
11. K.A. Striebel, J. Shim, E.J. Cairns, R. Kostecki, Y.J. Lee, J. Reimer, T.J. Richardson, P.N. Ross, X. Song, G.V. Zhuang, "Diagnostic analysis of electrodes from high-power Li-ion cells cycled under different conditions," *J. Electrochem. Soc.* **151**, A857–A866, 2004.
12. M. Dollé, J. Hollingsworth, T. Richardson, and M.M. Doeff, *Solid State Ionics*, in press, 2004.
13. S. Patoux and M.M. Doeff, *Electrochem. Commun.*, **6/8**, 767 (2004).
14. S.-W. Song, G.V. Zhuang, P.N. Ross, "Surface Film Formation on $\text{LiNi}_{0.8}\text{Co}_{0.15}\text{Al}_{0.05}\text{O}_2$ Cathodes Using Attenuated Total Reflection IR Spectroscopy," *J. Electrochem. Soc.* **151**, A1162–A1167, 2004.
15. W.S. Yoon, M. Balasubramanian, X.Q. Yang, Zugen Fu, Daniel A. Fischer, and J. McBreen "Soft X-ray Absorption Spectroscopic Study on the $\text{LiNi}_{0.5}\text{Mn}_{0.5}\text{O}_2$ Cathode Material during charge" *J. Electrochem Soc.* **151** A246 (2004).
16. Won-Sub Yoon, Clare P. Grey, M. Balasubramanian, Xiao-Qing Yang, Daniel A. Fischer, and James McBreen, "Combined NMR and XAS Study on Local Environments and Electronic Structures of Electrochemically Li-Ion Deintercalated $\text{Li}_{1-x}\text{Co}_{1/3}\text{Ni}_{1/3}\text{Mn}_{1/3}\text{O}_2$ Electrode System," *Electrochem. Solid-State Lett.* **7**, A53 (2004).
17. Y. Hu, M.M. Doeff, R. Kostecki, and R. Fiñones, "Electrochemical Performance of Sol-Gel Synthesized LiFePO_4 in Lithium Batteries," *J. Electrochem. Soc.* **151**, A1279 (2004).
18. Y. Matsumiya, N.P. Balsara, J.B. Kerr, and H. Watanabe, *Macromolecules*, **37**, 544–553, 2004.

19. Y.B. Yi, C.-W. Wang and A.M. Sastry, "Two-dimensional versus Three-dimensional Clustering and Percolation in Fields of Overlapping Ellipsoids," *J. Electrochem. Soc.* **8** 150 (2004).
20. Y.S. Meng, G. Ceder, C.P. Grey, W.-S. Yoon and Y. Shao-Horn, "Understanding the Crystal Structure of Layered $\text{LiN}_{0.5}\text{Mn}_{0.5}\text{O}_2$ by Electron Diffraction and Powder Diffraction Simulation," *Electrochem. Sol. St. Lett.*, **7**, A155–A58 (2004).

Appendix

Contributors

Battery Technology Development	
J. Barnes	Naval Surface Warfare Center West Bethesda, MD 20817-5700
J. Deppe	DOE Energy Storage Consultant 2522 Hobbits Ln Davidsonville MD 21035
A. Pesaran	National Renewable Energy Laboratory 1617 Cole Boulevard Golden, CO 80401-3393
I. Weinstock	Sentech Corp 7475 Wisconsin Ave. Bethesda, MD 20814

Applied Battery Research	
Program Manager: Gary Henriksen Argonne National Laboratory Argonne, IL 60439-4837	
More Accurate Life Prediction	
J. Belt, J. Christophersen, K. Gering, C. Ho, G. Hunt, C. Motloch, and T. Murphy	Idaho National Engineering and Environmental Laboratory Idaho Falls, ID 83415-3830
D. Abraham, I. Bloom, D. Dees, G. Henriksen, Y. Hyung, A. Jansen, J. Knuth, J. Liu, B. Potter, and L. Putty	Argonne National Laboratory Argonne, IL 60439-4837
H. Haskins	USABC Consultant
E. Thomas	Sandia National Laboratories Albuquerque, NM 87185-0613
V. Battaglia, E. Cairns, S. Jeong, M. Kerlau, J. Kerr, R. Kostecki, F. McLarnon, K. McCarthy, J. Newman, J. Reimer, T. Richardson, P. Ross, A. Sierra, X. Song, V. Srinivasan, S. Wilcke, and V. Zhuang	Lawrence Berkeley National Laboratory Berkeley CA 94720-8168
E. Gunen and J. Prakash	Illinois Institute of Technology Department of Chemical and Environmental Engineering, Chicago, IL 60616

Applied Battery Research	
R. Haasch, S. Maclaren, E. Sammann, and R. Twisten	Center for Microanalysis of Materials University of Illinois at Urbana-Champaign
Understand and Enhance Abuse Tolerance	
H. Case, C. Crafts, L. Davis, D. Doughty, C. Durant, B. Hance, D. Johnson, J. Langendorf, G. Nagasubramanian, P. Roth, and B. Sanchez	Sandia National Laboratory Mail Stop 0613 Albuquerque, NM 87185
K. Amine, I. Belharouak, G. Henriksen, Y. Hyung, A. Jansen, J. Liu, W. Lu, D. Vissers	Argonne National Laboratory Argonne, IL 60439
E. Gunen and J. Prakash	Illinois Institute of Technology Department of Chemical and Environmental Engineering, Chicago, IL 60616
C. P. Grey	State University of New York at Stony Brook, Department of Chemistry Stony Brook, NY
Y. Xia and M. Yoshio	Saga U/ONRI
M. Balasubramanian, K. Chung, J. Hanson, H. Lee, J. McBreen, X. Yang, and W. Yoon	Brookhaven National Laboratory P.O. Box 5000, MSD Bldg. 555, Upton, NY 11973-5000
Cell Level Cost Reduction	
K. Amine, D. Andrekus, I. Belharouak, I. Bloom, D. Chaiko, Z. Chen, D. Dees, G. Henriksen, A. Jansen, J. Liu, P. Nelson, G. Nielsen, S. Niyogi, B. Oh, D. P. Redey, J. Vaughey, D. Vissers, and Q. Wang	Argonne National Laboratory Argonne, IL 60439
J. Christophersen, K. Gering, C. Ho, C. Motloch, and T. Murphy	Idaho National Engineering and Environmental Laboratory Idaho Falls, ID 83415-3830
M. Winter	Graz University of Technology, Austria
Y. Marcus	Hebrew University of Jerusalem
J. Allen, M. Ding, T. Jow, K. Xu, and S. Zhang	Army Research Laboratory Adelphi, MD 20783
S. Kobayashi	Tokyo Institute of Technology

Understand and Enhance Low Temperature Performance	
J. Christophersen, K. Gering, C. Ho, C. Motloch, and T. Murphy	Idaho National Engineering and Environmental Laboratory Idaho Falls, ID 83415-3830
D. Abraham, K. Amine, D. Dees, R. Gerald, G. Henriksen, A. Jansen, A. Kahaian, J. Vaughey, and M. Stoll (ANL/LANL)	Argonne National Laboratory Argonne, IL 60439
V. Battaglia	Lawrence Berkeley National Laboratory Berkeley CA 94720-8168

Long-Term Battery Research	
Program Manager:	Dr. John Newman Lawrence Berkeley National Laboratory Berkeley CA 94720-8168
LiNiCoMnO₂ and Spinel Systems: Performance and Limitations	
T. Devine, M. Doeff, S. Ki Jeong, R. Kostecki, J. Lei, K. McCarthy, F. McLarnon, J. Newman, T. Richardson, P. Ross, J. Shim, A. Sierra, V. Srinivasan, K. Strieble, H. Yang, V. Zhuang	Lawrence Berkeley National Laboratory Berkeley CA 94720-8168
C. P. Grey	State University of New York at Stony Brook, Department of Chemistry Stony Brook, NY
G. Ceder and Y. Shao-Hornm	Massachusetts Institute of Technology Cambridge, MA 02139-4307
J. Goodenough and S. Schougaard	University of Texas at Austin Austin, TX 78712
Jim McBreen, K. Y. Chung, H. S. Lee, X. Q. Yang, and W. Yoon	Brookhaven National Laboratory Upton, NY 11973
S. Whittingham	Chemistry and Materials Research Center State University of New York at Binghamton Binghamton, NY 13902-6000
C. Johnson and M. Thackeray	Argonne National Laboratory Argonne, IL 60439
T. R. Jow and K. Xu	Army Research Laboratory Adelphi, MD 20783

New, High Energy, Materials	
M. Doeff, J. Reed, T. Richardson, V. Srinivasan, and K. Striebel	Lawrence Berkeley National Laboratory Berkeley CA 94720-8168
G. Ceder	Massachusetts Institute of Technology Cambridge, MA 02139-4307
K. Zaghib	Hydro-Québec, IREQ Varenes, QC, J3X 1S1
C. P. Grey	State University of New York at Stony Brook, Department of Chemistry Stony Brook, NY
M. Anderson, K. Walz and W. Zeltner	University of Wisconsin – Madison
R. Benedek, C. Johnson, J. Kim, M. Thackeray, and J. Vaughney	Argonne National Laboratory Chemical Technology Division Argonne IL 60439
S. Whittingham	Chemistry and Materials Research Center State University of New York at Binghamton Binghamton, NY 13902-6000
J. Goodenough and S. Schougaard	University of Texas at Austin Austin, TX 78712
H. Bryngelsson and K. Edström	Uppsala University, Sweden
S. Hackney	Michigan Technological University Houghton, MI 49931-1295
LiFePO₄ System: Performance and Limitations	
K. Zaghib	Hydro Quebec Varenes, J3X 1S1 Quebec Canada
T. Devine, M. Doeff, R. Kostecki, G. Lau, K. McCarthy, F. McLarnon, J. Newman, T. Richardson, A. Sierra, J. Shim, V. Srinivasan, K. Striebel, J. Wilcox, X. Zhang, and V. Zhuang,	Lawrence Berkeley National Laboratory Berkeley CA 94720-8168
K. Cook, A.M. Sastry, C.W. Wang, and Y.B. Yi	The University of Michigan Department of Mechanical Engineering and Applied Mechanics, Ann Arbor, MI 48109-2125
K. Kepler	Farasis Energy Inc 23575 Cabot Blvd. Suite 206 Hayward, CA 94545

Li/Polymer Component Limitations	
N. Balsara, Y. Han, J. Kerr, G. Liu, Y. Matsumiya, J. Newman, L. Odusanya, C. Reeder, K. H. Shin, M. Singh, X.G. Sun, and J. Xie,	Lawrence Berkeley National Laboratory Berkeley CA 94720-8168
P. Fedkiw, S. Khan, Y. Li, A. Sanchez, and X. Zhang	Department of Chemical Engineering North Carolina State University, Raleigh, NC 27695
H. Watanabe	Institute of Chemical Research, Kyoto University
O. Borodin and G. D. Smith	Department of Materials Science and Engineering University of Utah Salt Lake City, UT
G. L. Baker	Department of Chemistry Michigan State University East Lansing, MI 48824-1322
L. Curtis	Argonne National Laboratory Argonne, IL 60439
W. Halley	University of Minnesota School of Physics and Astronomy Minneapolis, MN 55455
S. Creager, D. DesMarteau, O. Geiculescu, P. Hallac, and R. Rama	Department of Chemistry Clemson University Clemson, SC 29634-0973.

This document highlights work sponsored by agencies of the U.S. Government. Neither the U.S. Government nor any agency thereof, nor any of their employees, makes any warranty, express or implied, or assumes any legal liability or responsibility for the accuracy, completeness, or usefulness of any information, apparatus, product, or process disclosed, or represents that its use would not infringe privately owned rights. Reference herein to any specific commercial product, process, or service by trade name, trademark, manufacturer, or otherwise does not necessarily constitute or imply its endorsement, recommendation, or favoring by the U.S. Government or any agency thereof. The views and opinions of authors expressed herein do not necessarily state or reflect those of the U.S. Government or any agency thereof.

A Strong Energy Portfolio for a Strong America

Energy efficiency and clean, renewable energy will mean a stronger economy, a cleaner environment, and greater energy independence for America. Working with a wide array of state, community, industry, and university partners, the U.S. Department of Energy's Office of Energy Efficiency and Renewable Energy invests in a diverse portfolio of energy technologies.

For more information contact:
EERE Information Center
1-877-EERE-INF (1-877-337-3463)
www.eere.energy.gov